THE UNIVERSITY OF CHICAGO

STRUCTURAL AND FUNCTIONAL CHARACTERIZATION OF THE MULTIPASS TRANSLOCON

A DISSERTATION SUBMITTED TO
THE FACULTY OF THE DIVISION OF THE BIOLOGICAL SCIENCES
AND THE PRITZKER SCHOOL OF MEDICINE
IN CANDIDACY FOR THE DEGREE OF
DOCTOR OF PHILOSOPHY

GRADUATE PROGRAM IN BIOCHEMISTRY AND MOLECULAR BIOPHYSICS

BY

MELVIN YAMSEK

CHICAGO, ILLINOIS

DECEMBER 2023

To my family.

TABLE OF CONTENTS

LIST OF FIGURES

LIST OF TABLES

ACKNOWLEDGEMENTS

First, I'd like to thank my P.I., Dr. Robert J. Keenan. While certain parts of my projects seemed to go very smoothly for me during my Ph.D., the road to getting a cryo-EM structure with programmed ribosomes proved to be extremely challenging, with lots of repeated failure. Bob was always patient and encouraging. Even when nothing seemed like it was going the right way, he always seemed to have a way to move forward. Cryo-EM had just started to become a big thing (winning the 2017 Nobel prize!) when I joined, and he was motivated to provide a successful environment for me. He often told me to take control and do everything I needed to do while troubleshooting. Thanks, Bob, for supporting me this entire time!

Next, I'd like to thank each and every member of the Keenan Lab that I've had the pleasure of working with throughout my Ph.D. Particularly Frank Zhong and Arunkumar Sundaram, who worked very closely with me when assembling the story on the Multipass Translocon. Overall, the entire project has been very collaborative and basically everyone in the lab has worked together on it at one point or another. Andrei Anghel and Phil McGilvray played a major role in training me during my rotation and as a new grad student in the lab. I had never done a western blot, worked with Hek293 cells, or done anything cryo-EM related, and they were both extremely helpful when teaching me new techniques. I'd also like to give a big thanks to Amanda DiGuilio for bringing useful cell culture techniques including CRISPR to the lab. She was always a big help for the lab, and an incredible friend. Plus, thanks to all other lab members that I've worked with: Ben Chang, Przemek Grygier, Roshan Jha, Szymon Kordon, Madeline Rollins, Miguel

Saucedo, Natasha Santhanam, JoJo Tang, Matt Wohlever, and Ben Zalisko. I wish you all the best of luck in your future endeavors!

I'd like to thank my family for their encouragement me throughout my entire Ph.D. It's been tough being the only one away, but every time I visit, I am refreshed with a new mindset and energy to push on. I'd especially like to thank my Mom and Dad who have always been there for me. Especially when things got tough, I knew that I could always lean on them. They kept by my side and showed their unconditional love and support. I'd also like to thank my siblings – Mike & Melody, Laura & Dan, and Connor – for always keeping things fun and exciting. Plus, we got to welcome two new lives into the world – Lily and Oliver – I hope you guys like science! Also, my extended family. I always look forward to a Mulvany family vacation every two years and would like to give the biggest hug to GiGi who started the family and unfortunately struggled with Alzheimer's in the last few years of her life. It was an absolute honor knowing her, and I smile looking at the wonderful family she created. Plus, Christmas time with the Yamseks for lasagna and Fireball shots (thanks, Grandma!) is something I look forward to every year. And of course, I must thank my cat Waffles, who never fails to brighten my day with her welcome-home-headbutts, and always encourages me to take a break with a game of fetch. I would also like to give a recognition to Pedals, my parent's beloved English cream golden retriever, who tragically passed away way too young earlier this summer from canine lymphoma.

I'd also like to thank everyone who made a significant impact during my undergraduate career. When I was the only freshman in sophomore level organic chemistry, Ali Najafi was the one who encouraged me to join a research lab. Dr. Jared

Anderson kindly gave me a project in his lab starting my freshman year of undergrad and encouraged me to apply for a summer research fellowship program. He was ultimately the one who convinced me to pursue a research career instead of going to pharmacy school! Kevin Clark taught me my way around a lab and how to carefully design experiments. Kevin was also very patient and helpful with me as I was writing my very first scientific proposal, which I cannot stress how much that has benefited me since. I'd also like to thank Dr. Don Ronning for bringing me into his lab after Dr. Anderson moved to Iowa State University. I learned so much about biochemistry and structural biology from him. Plus, he was very helpful when I was stressing about which graduate school to select. It's safe to say now that I made the right decision. Mike Banco was very patient and helpful… even when I accidentally shot my first looped crystal across the room! Dr. Mike Harris hosted me as an REU fellow – it was great to be back in Cleveland for the summer! Also, I can't forget about my good friend Rodney Park, who was right by my side during most of my undergraduate research experience. We made many good memories together, ranging from various antics in analytical chem lab, to falling down a mountain together in Utah.

I'd also like to thank the entire BMB cohort, especially Craig DeValk, Cole Ladd, and Chris Katanski. I always felt comfortable going to you for support knowing that you'd have something supportive to say. And I had a lot of fun being in BMB, especially since we had a lot of good events ranging from journal clubs, retreats, and many dean's council activities. Having a strong community was something that I actively sought out for my graduate school experience, so I'm glad that I was able to find that at UChicago. Furthermore, the department itself is extremely collaborative science-wise. It's been really

nice to be able to walk down the hall and be able to easily ask for advice or to share a reagent or piece of equipment.

I'd also like to thank the University of Chicago's Advanced Electron Microscopy Facility – James Fuller, Tera Lavoie, Joe Austin, and Josh Fisher. The Covid-19 pandemic started during my fourth year right as I was gaining more experience and independence with cryo-EM as a technique, and the facility worked with me to ensure that I could be trained. Luckily, I was given the opportunity to work on merging a couple of datasets that Phil had collected while we were all quarantining. James was extremely helpful and patient with me while I learned the ropes.

Ultimately, my Ph.D. was fueled by people who believed in me and my science. I'd like to thank the organizers (Catherine Will, Phoebe Rice, Ben Glick) of the MCB Training grant who funded me for two years. I'd also like to thank Chip Ferguson for helping me fine-tune my research in progress talks – sorry I got hit by an SUV that one time and never actually got to deliver it! I'm also very grateful to have been awarded the NSF GRFP fellowship, which financially supported me for another three years.

There are many others who need to be thanked: my committee members Dr. Engin Özkan, Dr. Eduardo Perozo, and Dr. Minglei Zhao who helped improve my research and offered me useful advice; the BMB office Shani Charles, Lisa Anderson, Amy Murphy, Bulent Yagcier, Alicia Sharfner, Shay Purba, Giovanni Tolentino Ramos; the molecular biosciences administrators Sue Levison and Stephanie Laine Nazaire; the Thermo Fisher store room including Jess Krupinski and Eileen Leahy; lab assistants Dorian and Gayle; the DNA sequencing facility. Also, the many friends I've made since moving to Chicago. You know who you are!

ABSTRACT

All cells contain hydrophobic lipid bilayers, or membranes, which act as a barrier to the outside of the cell. Additionally, eukaryotic cells contain additional internal membrane-bound compartments known as organelles. Within these membranes exist a diverse set of proteins that play important roles for cellular function and comprise about a third of the proteome. Because these membrane proteins reside and function within a hydrophobic membrane, the cell must complete the challenging task of trafficking them from the cytosol and inserting them into the correct cellular membrane. This process of membrane protein targeting and insertion is known as membrane protein biogenesis. In eukaryotes, most membrane proteins are inserted co-translationally, where they are first targeted to the endoplasmic reticulum and dock to the protein conducting channel Sec61 for their biogenesis. However, it has recently become more evident that the cell contains additional membrane protein biogenesis factors that can facilitate the insertion of more complicated membrane proteins. Here, I present research focusing on the structure and function of a translocon specializing in multipass membrane protein biogenesis. More specifically, this translocon is termed the “Multipass Translocon” and is comprised of three subcomplexes that assemble to Sec61 and the ribosome during multipass membrane protein biosynthesis. These studies reveal the mechanisms by which substrate directs the co-translational assembly of the Multipass Translocon and highlights the importance of the Multipass Translocon for multipass client protein biosynthesis. Additionally, I describe my ongoing efforts to capture structures of multipass folding intermediates within the Multipass Translocon. Overall, this work characterizes the translocon as a dynamic

assembly that co-translationally adapts its subunit composition to meet the various biosynthetic requirements of its diverse client proteins.

CHAPTER 1. Introduction and Background

1.1 Cellular Membranes and Membrane Proteins

The fundamental unit of life is the cell, which is characterized by aqueous cytoplasm enclosed in a membrane bilayer. In eukaryotes, membranes also enclose intracellular compartments to form organelles and vesicles. The membrane bilayer is semi-permeable, acting as a barrier to protect a cell from its surroundings, while also allowing certain molecules to pass through. Cellular membranes contain both lipids and proteins.

The membrane bilayer, also known as the phospholipid bilayer, is made of up of two layers of phospholipids. Phospholipids are amphipathic, containing a hydrophilic head group and a hydrophobic tail (Nicolson, 2014; Singer & Nicolson, 1972). In the bilayer, the hydrophobic tails point inwards while the hydrophilic head groups assemble on the outside of the sheet to interact with the surrounding aqueous environment. The cell membrane also contains other lipids, such as sphingolipids and steroids such as cholesterol (Jiang & Li, 2022).

Membrane proteins are another major component of the membrane and make up about a third of all human proteins (Fagerberg et al., 2010; Wallin & Heijne, 1998). They can be divided up into two major classes: integral membrane proteins and peripheral membrane proteins. Peripheral membrane proteins are loosely held to the membrane through electrostatic interactions with the lipid head groups or are post-translationally modified with lipid that can insert into the membrane bilayer (Ferguson, 1991; Paulick & Bertozzi, 2008). Most membrane proteins are integral membrane proteins (Von Heijne, 2007), also known as transmembrane proteins, which is the major topic for this work.

These proteins cross the lipid bilayer and perform many important functions in the cell, acting as ion and small molecule transporters, receptors, adhesion molecules, and enzymes. Transmembrane proteins often contain hydrophobic α-helical membrane-spanning regions known as transmembrane domains (TMDs), in addition to external hydrophilic regions that interact with aqueous environment. Another class of transmembrane proteins are β-barrels, which are mostly found in the outer membranes of bacteria and mitochondria and is not addressed in this work (Gouaux, 1997; Schulz, 1996).

Integral membrane proteins are diverse, and differ widely in their biophysical properties, topology (Figure 1 A), and subcellular localizations. For example, membranes can be either singlepass, containing a single TMD in the membrane, or multipass, with two or more TMDs inserted into the membrane. They also vary based on their topology. Type I membrane proteins contain an N-terminal signal peptide that gets cleaved off by the signal peptidase complex, leaving the N-terminus of the matured protein in the lumen (N-exo). Type II membrane proteins have an N-cyto topology. Type III membrane proteins are characterized by short (less than ~ 60 amino acids) N-terminus preceding the first TMD and are N-exo. Additionally, there are tail-anchored membrane proteins which contain a TMD close (approximately 65 amino acids) to the C-terminus and are N-cyto. Furthermore, some membrane proteins are short with small cytosolic and luminal regions.

1.2 The Ribosome

Ribosomes are macromolecular machines involved in protein translation. They use messenger RNA (mRNA) as a template to synthesize the correct sequence of amino

acids for a protein. The ribosome subunits are named according to their sedimentation coefficient, Svedbergs (S). The eukaryotic 80S ribosome contains a large 60S ribosomal subunit and a small 40S ribosomal subunit. Overall, the ribosome contains both protein (47 proteins in the 60S subunit and 33 proteins in the 40S subunit) and ribosomal RNA (rRNA; 3 rRNA in the 60S subunit and 1 rRNA in the 40S subunit) (Moraleva et al., 2022). Furthermore, multicellular eukaryotes contain additional rRNA components known as expansion segments which may coordinate ribosome binding to proteins in the ER (Knorr et al., 2019; Ramesh & Woolford, 2016). The large ribosomal subunit contains the peptidyl transferase center, which covalently links amino acids to the growing nascent peptide chain. It also contains the ribosomal exit tunnel where the nascent polypeptide departs. The small ribosomal subunit harbors the mRNA tunnel and decoding center. Here, transfer RNA (tRNA) recognizes triplet codons and deliver the corresponding amino acid to the peptidyl transferase center. The tRNA binding positions within the ribosome are referred to as aminoacyl- (A-), peptidyl- (P-), and exit (E-) sites.

Many of the experiments in this thesis use translationally-stalled ribosomes. This is accomplished using *in vitro* translation, where the mRNA is truncated and the stop codon is replaced with a Met-Leu-Lys-Val stalling sequencing (Shao et al., 2013; Shao & Hegde, 2014; Tsuboi et al., 2012). During translation, the nascent chain is covalently linked to the terminal valine tRNA through an aminopeptidyl-tRNA bond and the ribosome becomes stalled. Notably, the length of the ribosomal exit tunnel is approximately 30-35 amino acids long (Voss et al., 2006). Therefore, many of the truncated products described in this thesis are stalled 40 amino acids beyond the point of interest (the TMDs). Additionally, ribosomes can be translationally stalled when the mRNA forms significant

secondary structure, during stretches of rare codons, or during translation of a poly-A tail during translation of poly-lysine sequences (Arthur et al., 2015; Doma & Parker, 2006; Letzring et al., 2013).

1.3 Membrane Protein Biogenesis

Integral membrane proteins are first translated by ribosomes in the cytosol but must be correctly targeted and inserted their designated cellular membrane to perform their proper function. While bacterial membrane proteins are first targeted to the plasma membrane, this work focuses on eukaryotic membrane proteins, which are first inserted into the endoplasmic reticulum (ER) before being trafficked to their final designated cell membrane. However, as an exception, mitochondrial membrane proteins are synthesized in the cytosol prior to mitochondrial targeting by the Translocase of the Inner/Outer Membrane (TIM/TOM) complexes (Chacinska et al., 2009; Pfanner & Geissler, 2001). Because membrane proteins are so diverse in their properties, multiple membrane protein biogenesis pathways exist. Membrane protein biogenesis is generally characterized by four stages: targeting, insertion, folding, and assembly (Figure 1B). Failure to properly insert can lead to aggregation, which can be toxic for the cell, and activate quality control pathways (Chiti & Dobson, 2006; Kopito, 2000).

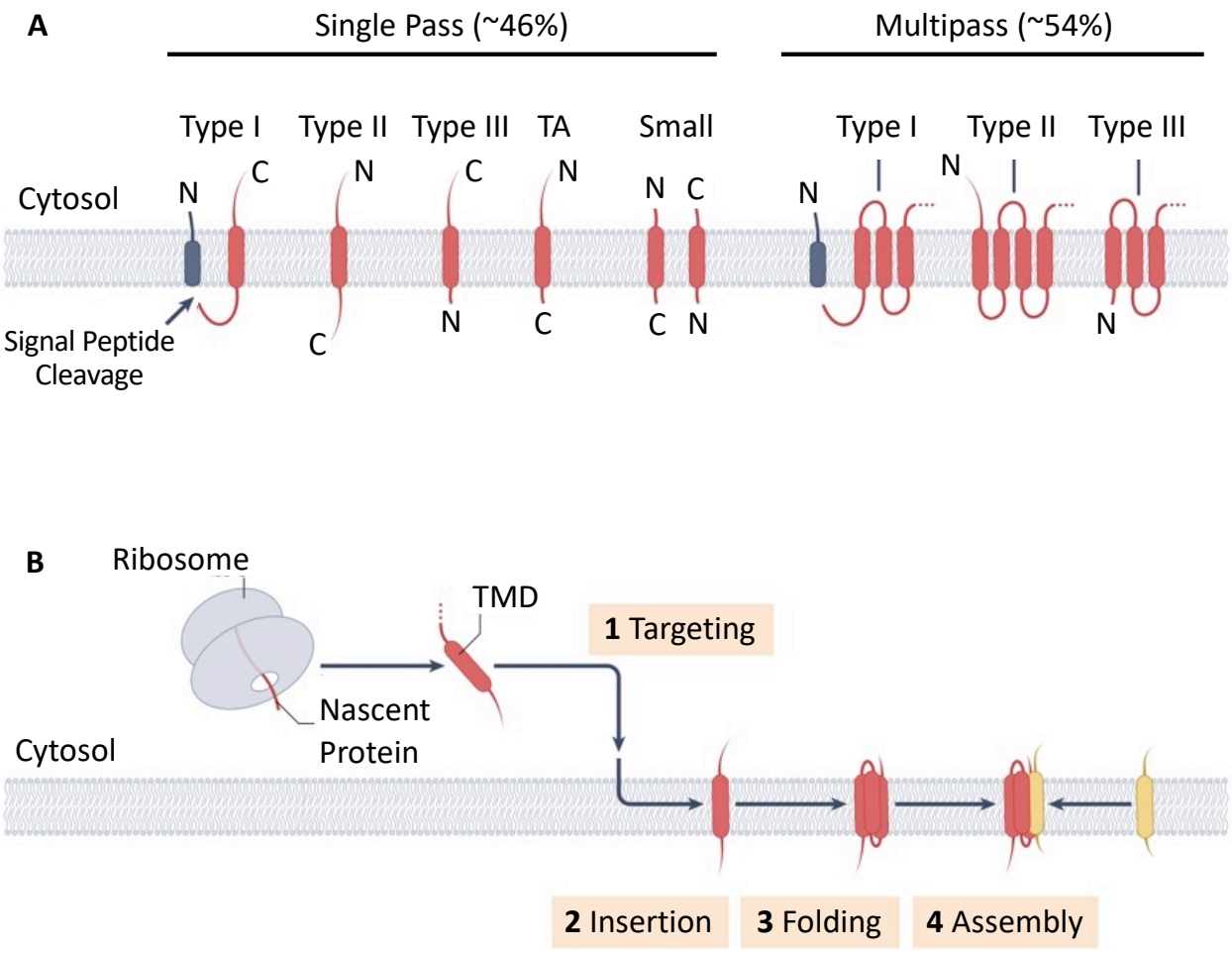

Figure 1. Overview of Membrane Protein Biogenesis

(A) The major classes of integral membrane proteins. (B) The four steps of membrane protein biogenesis. (Hegde & Keenan, 2022)

1.4 Co-Translational Membrane Protein Biogenesis

The co-translational membrane protein insertion pathway is the best understood. During translation by the ribosome, a hydrophobic N-terminal signal sequence (around 7-9 amino acids; (Almagro Armenteros et al., 2019)) or TMD (around 15-25 amino acids (Krogh et al., 2001)) emerges from the ribosomal exit tunnel. This hydrophobic sequence is recognized by the signal recognition particle (SRP), which binds substrates co-

translationally and protects them from escaping into the cytosol (Halic et al., 2004; Voorhees & Hegde, 2015). SRP contains a hydrophobic groove lined with many methionine residues that allows it to recognize diverse hydrophobic sequences (Halic et al., 2004; Keenan et al., 1998; Von Heijne, 1985; Voorhees & Hegde, 2015). From there, SRP is targeted to the SRP receptor in the ER membrane, which interacts with a protein-conducting channel known as Sec61, and promotes release of the ribosome-nascent chain complex (Hwang Fu et al., 2017; Luirink, 2004).

The Sec61 (SecY in bacteria and archaea) complex is used for secretion of soluble proteins and insertion of hydrophobic TMDs into the membrane. The Sec61 complex is a conserved heterotrimeric protein conducting channel known as Sec61αβγ in eukaryotes. Sec61's central channel is located within Sec61α, which is the largest subunit with 10 TMDs. The main function of the central channel is to translocate proteins across the membrane. Sec61α also contains a short plug helix and a lateral gate that opens and allows passage of TMDs into the membrane (Li et al., 2016; Osborne et al., 2005; Tanaka et al., 2015; Voorhees et al., 2014; Voorhees & Hegde, 2016). The lateral gate is commonly referred to as the front of Sec61, at the interface between helices 2b and 7. Importantly, the lateral gate functions to recognize sufficiently hydrophobic sequences, often TMDs, for lateral insertion into the lipid bilayer. Sec61α is made up of an N-terminal and C-terminal halves that surround an hour-glass shaped central channel (Van den Berg et al., 2004; Voorhees et al., 2014). These two halves are connected by a hinge (a luminal loop between TMDs 5 and 6) which allows the lateral gate to open. When Sec61 opens, the N-terminal half undergoes a rigid body movement with respect to the C-terminus, resulting in the opening of the channel at the lateral gate. Sec61β is an N-cyt tail anchored

protein that assembles near the N-terminus of Sec61α. Sec61γ contains two alpha helical segments. The C-terminal helix traverses the membrane and contacts both halves of Sec61α, while the N-terminal helix lies perpendicular to the membrane and contacts the C-terminus of Sec61α. While their roles are less understood, it has been shown that Sec61βγ assembly to Sec61α increases translation efficiency (Nishiyama et al., 1993; Pohlschröder et al., 1997). Additionally, several Sec61 inhibitors which inhibit protein translocation exist. While these inhibitors are structurally distinct, all inhibitors bind to a partially opened lateral gate and stabilize the plug domain such that it remains closed (Itskanov et al., 2023)

Once a ribosome translating the nascent membrane protein is delivered to its target by SRP, it docks to Sec61 and causes the channel to enter a primed state (Park et al., 2014; Pfeffer et al., 2015; Voorhees et al., 2014; Voorhees & Hegde, 2016). Interactions with the ribosome cause Sec61's lateral gate to open slightly while the plug still remains in the channel. The signal peptide or TMD binds to and parts the lateral gate, which displaces the plug helix and creates an open channel across the membrane (Li et al., 2016; Mandon et al., 2009; Voorhees & Hegde, 2016). For single pass membrane proteins, as translational elongation occurs, the soluble domains will pass through the channel while the hydrophobic TMD is recognized by the lateral gate and partitions laterally into the lipid bilayer (Hessa et al., 2005; White & Vonheijne, 2005).

While the mechanism for co-translational single pass membrane protein insertion has been well-characterized, multipass membrane protein insertion is a bit more complicated. Multipass membrane protein TMDs are often much more hydrophilic because many are channels or receptors, so their TMDs often contain polar or charged

amino acids (Hessa et al., 2007). Because exposed hydrophilic side chains within the membrane are recognized by the ER-associated degradation pathway, multipass membrane proteins must also be shielded from the membrane before folding into their final form. Folding of multipass membrane proteins is further complicated by the fact that one TMD may need to pack against another TMD that has not yet been synthesized or inserted into the membrane. Additionally, the hydrophilic TMDs may be less recognizable as an insertable TMD by Sec61's lateral gate. Up until recently, the recognized model for multipass membrane protein insertion has depicted sequential insertion of TMDs through Sec61 (Blobel, 1980; Patterson et al., 2015; Shao & Hegde, 2011); however, the work described in this dissertation presents data showing that Sec61 is not the only membrane protein insertion factor residing in the ER.

1.5 Eukaryotic Translocon Accessory Factors

Although the ribosome-Sec61 complex provides a foundation for understanding co-translational membrane protein insertion, the process is much more complicated. Membrane proteins have diverse biophysical properties which must be accounted for during their biogenesis. Additionally, many membrane proteins are modified, including events such as signal peptide cleavage or glycosylation, during their biogenesis. Therefore, other proteins, called translocon accessory factors, assemble to the ribosome-Sec61 complex to facilitate the insertion requirements of broader membrane proteins. While the function of many of these accessory factors is not well-understood, they seem to assemble in a substrate-dependent manner (Conti et al., 2015). Together, the

ribosome-Sec61 complex along with the translocon accessory factors make up the translocon.

The Translocon Associated Protein (TRAP) complex is a heterotetrameric complex, formerly known as the signal sequence receptor (SSR) that assembles to Sec61 with or without ribosomes (Hartmann et al., 1993). Three of the TRAP monomers (α, β, δ) are single-pass membrane proteins while TRAPγ contains four TMDs. While TRAP's role remains largely unknown, research has shown that enhances the ability of weakly hydrophobic signal peptides to initiate co-translational translocation through Sec61 (Fons et al., 2003; Görlich et al., 1992). A recent cryo-EM structure has been solved, revealing how the mammalian TRAP complex interacts with a translating ribosome and Sec61 (Jaskolowski et al., 2023). Key interactions with the ribosome include a TRAPα anchor with the ribosomal protein uL29 and rRNA, plus an interaction between some positively-charged amino acids in TRAPγ and rRNA. Additionally, TRAPα contacts Sec61α on its luminal side.

The Oligoaccharyltransferase (OST) complex is a membrane protein complex that catalyzes asparagine-linked glycosylation for proteins traversing the secretory pathway. Glycosylation is one of the most common post-translational modifications of proteins (Zafar et al., 2011), and defects in glycosylation have been linked to decreased protein stability and disease (Jayaprakash & Surolia, 2017; Lee et al., 2015; Shrimal et al., 2013). N-glycosylation is also important for protein topology because is constrains it to the lumen and prevents retrotranslocation (Welply et al., 1983). Glycan Transfer occurs at an Asn-X-Ser/Thr concensus sequence, where X is any amino acid, excluding proline (Tai & Imperiali, 2001). Glycosylation occurs at OST's catalytic site located in the ER lumen

(Hanover & Lennarz, 1980; Welply et al., 1983), where a preassembled oligosaccharide is transferred to an asparagine by an N-glycosidic bond (Helenius & Aebi, 2004; Mohorko et al., 2011; Shrimal et al., 2015). The catalytic subunit SST3 (staurosporine and temperature sensitive 3) of OST is present in two paralogous forms in higher eukaryotes– STT3A and STT3B (Kelleher et al., 2003). STT3A glycosylates proteins co-translationally and catalyzes the majority of all N-glycosylation events (Ruiz-Canada et al., 2009). STT3B glycosylates acts as a proofreader for sites missed by STT3A and acts post-translationally (Cherepanova & Gilmore, 2016; Kelleher et al., 2003; Ruiz-Canada et al., 2009).

While Sec61 is often involved in co-translational translocation with docking of the ribosome, it can also accommodate post-translational translocation when it engages with a fully synthesized client protein. In mammals, these precursor proteins are post-translationally inserted because they are too short to interact with SRP and the ribosome (Schlenstedt et al., 1990). Sec63 and Sec63 assemble with Sec61 as the core machinery to activate its post-translational mode (Deshaies et al., 1991; Panzner et al., 1995). Sec62 binds both Sec61 and Sec61, plus has the ability to bind ribosomes (Müller et al., 2010). Sec63 is a three TMD protein containing a luminal J-domain that allows chaperones such as BiP to facilitate in substrate translocation into the lumen by a ratcheting mechanism (Brodsky et al., 1995). In the current model for Sec61 post-translational translocation, Sec63 binding primes the lateral gate by partial opening (Itskanov & Park, 2019; Wu et al., 2019). Sec62 further widens the lateral gate and displaces the plug domain away from the central channel (Itskanov et al., 2021).

The Translocating-chain Associated Membrane Protein (TRAM) contains eight TMDs and is an essential accessory factor for the biogenesis of many secreted membrane proteins (Görlich et al., 1992; Görlich & Rapoport, 1993; Tamborero et al., 2011). TRAM has been crosslinked to both soluble proteins with signal sequences and membrane proteins with TMDs (Do et al., 1996; Görlich et al., 1992; Heinrich et al., 2000; Krieg et al., 1989; McCormick et al., 2003; Saurí et al., 2007; Voigt et al., 1996). It has also been proposed that TRAM stimulates the biogenesis of membrane proteins containing more hydrophilic and/or TMDs (Heinrich et al., 2000; Meacock et al., 2002).

The Ribosome Associated Membrane Protein (RAMP4) is a small, 66 amino acid, tail-anchored protein that interacts with the ribosome and Sec61 (Görlich & Rapoport, 1993; L. Wang & Dobberstein, 1999). RAMP4 is upregulated during ER stress, and RAMP4 overexpression in cells experiencing ER stress decreased membrane protein aggregation and degradation (Yamaguchi et al., 1999). Furthermore, RAMP4 deletion has been shown to induce the unfolded protein response (Hori et al., 2006). Other studies have shown that RAMP4 binds hydrophobic client proteins and is recruited to the ribosome during membrane protein biogenesis before the TMD emerges from the ribosomal exit tunnel (Pool, 2009; Schroder, 1999).

Importantly, this is not a complete list of all the eukaryotic translocon accessory factors. However, it does highlight the vast amount of additional machinery the cell contains to accommodate the diverse needs of membrane proteins.

1.6 The Oxa1 Superfamily

In addition to Sec61, the ER membrane contains at least three other insertion factors. These include TMCO1, EMC, and the GET1-GET2 complex, which are all members of the Oxa1 superfamily, discussed in further detail below. Oxa1 superfamily members arose long before the emergence of eukaryotes before the divergence of bacteria and archaea. Its members mediate membrane protein biogenesis and are located in bacterial (YidC) (Dalbey et al., 2014; Pross et al., 2016) and archaeal (Mj0480) (Borowska et al., 2015) plasma membranes, the inner mitochondrial membrane (Oxa1) (Hell et al., 2001), chloroplast thylakoid membrane (Alb3 and Alb4) (P. Wang & Dalbey, 2011) and the eukaryotic ER (TMCO1) (Anghel et al., 2017; McGilvray et al., 2020). Its members share a common N-out/C-in topology and feature a cytosolic-facing coiled coil between the first and second TMDs (Anghel et al., 2017). All Oxa1 superfamily members feature a hydrophilic vestibule in a conserved three-TMD core, which may be play a role in TMD insertion. The hydrophilic vestibule is thought to thin the membrane bilayer, allowing Oxa1 insertases to lower the energetic penalty associated with translocating hydrophilic segments across the bilayer. Because Oxa1 superfamily proteins lack a membrane-spanning channel, this insertion activity is often restricted to fewer than 50 amino acids (Wu & Rapoport, 2021).

1.7 Post-Translational Membrane Protein Biogenesis

Some membrane proteins (approximately 700) only contain a TMD close (approximately 65 amino acids) to the C-terminus, and are therefore known as tail-anchored membrane proteins (Kutay et al., 1993). These proteins must be post-

translationally targeted because the TMD at the C-terminus precludes recognition until it leaves the ribosomal exit channel. A couple of pathways for post-translational membrane protein insertion are discusses in further detail below.

1.8 The Guided Entry of Tail-Anchored Proteins (GET) Pathway

The GET pathway is involved in the post-translational biosynthesis of proteins with moderate to high hydrophobicity. In this pathway, as the nascent chain of a tail-anchored membrane protein releases from the ribosome, it is captured by the TMD-binding chaperone SGTA, plus GET4-GET5, forming a 'pre-targeting' complex (Mariappan et al., 2010; Mateja et al., 2015; Mock et al., 2015; Shao et al., 2017; F. Wang et al., 2010), which facilitates transfer of the tail-anchored protein to the soluble chaperoning factor GET3 (Mateja et al., 2015; Shao et al., 2017; F. Wang et al., 2010). The extended cytosolic domains of GET2 capture GET3 and direct it towards the GET1-GET2 complex (Schuldiner et al., 2008; Zalisko et al., 2017). This allows the GET1 cytosolic domains to interact with GET3, inducing a conformational change and releasing the tail-anchored substrate (Mariappan et al., 2011; Stefer et al., 2011). Next, the tail-anchored protein is inserted into the lipid by the ER-resident GET1-GET2 complex (F. Wang et al., 2014). Notably, GET1 is a member of the Oxa1 superfamily (Anghel et al., 2017), so the TMD and hydrophilic tail can engage with the GET1 hydrophilic vestibule for insertion into the membrane.

1.9 The ER Membrane Protein Complex (EMC)

EMC is an assembly of eight or nine different proteins, depending on the species. It contains 14 TMDs, plus large cytosolic and luminal domains (Bai et al., 2020; Chitwood & Hegde, 2019; Volkmar & Christianson, 2020). Recent structures of EMC have revealed a hydrophilic vestibule containing conserved positively-charged amino acids, plus a hydrophobic crevice within the cytosolic face (Bai et al., 2020; Miller-Vedam et al., 2020; O'Donnell et al., 2020; Pleiner et al., 2023). Importantly, one of EMC's subunits (EMC3) is a member of the Oxa1 superfamily.

Many tail-anchored proteins contain TMDs of low hydrophobicity that cannot be efficiently inserted by the GET pathway, suggesting there is an alternative insertion route (Mateja et al., 2015; Rao et al., 2016). EMC has recently been characterized to be involved in the biogenesis of low- to moderately- hydrophobic proteins. Herein, purified EMC has been shown to be sufficient for tail-anchored protein insertion of a moderately hydrophobic tail-anchored protein (Guna et al., 2018). Furthermore, a recent study has carefully examined the path of tail-anchored membrane protein insertion using mutagenesis and site-specific crosslinking (Pleiner et al., 2023). EMC has also been shown to be involved in co-translational insertion of Type III (N-exo) signal anchors and multipass membrane proteins (Chitwood et al., 2018). Notably, Type III membrane proteins also contain a relatively short hydrophilic segment that must be translocated across the membrane along with the TMD.

In the current model (Pleiner et al., 2023), the flexible hydrophobic loops in the cytosolic region of EMC capture a tail-anchored protein or the first TMD of a Type III multipass membrane protein. This interaction allows their C- or N- terminal domain to

probe the positively-charged hydrophilic vestibule, which acts as a selectivity filter. TMDs lacking positive charge are easily translocated through EMC, while charge repulsion by the hydrophilic vestibule facilitates rejection of mistargeted mitochondrial tail-anchored proteins (which are enriched for positive charges in their C-terminal tails (Costello et al., 2017; Horie et al., 2002; Rao et al., 2016)) by EMC. Additionally, this positively- charged selectivity filter helps to maintain the correct topology of proteins by enforcing the "positive-inside" rule, where the positively-charged soluble domain remains in the cytosol (Heijne & Gavel, 1988).

1.10 TMCO1 and the Multipass Translocon

This thesis focuses on the Multipass Translocon, which is involved during the biosynthesis of multipass membrane proteins. Briefly, this translocon contains three subcomplexes that selectively assemble to the translocon during multipass membrane protein biosynthesis. These subcomplexes include the "Protein Associated with Translocon" Complex (PAT Complex; CCDC47 and Asterix) "GET and EMC-Like" (GEL Complex; TMCO1 and OPTI), and "Back of Sec61" (BOS; TMEM147, NOMO, Nicalin) (Sundaram, Yamsek, Zhong et al., 2022). TMCO1 (Transmembrane and Coiled-Coil Domains 1) was recently characterized as a eukaryotic Oxa1 superfamily member (Anghel et al., 2017).

CHAPTER 2. Substrate-Driven Assembly of a Translocon for Multipass Membrane Proteins

2.1 Overview

Previous work by McGilvray *et al.* described an ER translocon involved in multipass membrane protein biogenesis. Herein, TMCO1-containing ribosome-nascent-chain complexes were immunoprecipitated and mass spectrometry was used to identify associating factors. Furthermore, cryo-EM and crosslinking experiments showed that many of these identified proteins (CCDC47, NOMO, Nicalin, and TMEM147) were shown to associate with the ribosome and Sec61. Additionally, mRNA sequencing on TMCO1-ribosome-bound transcripts revealed selective translocon engagement with multipass membrane proteins. This work led to additional questions about the Multipass Translocon, including why the Multipass Translocon is selective for multipass proteins, how the Multipass Translocon is recruited during multipass biosynthesis, and how it functions during multipass membrane protein biogenesis.

Early on, my research focused on looking at the functional aspect of the Multipass Translocon. Herein, I selected multipass client proteins from the TMCO1 mRNA sequencing data and used *in vitro* translation as a tool to screen the proper insertion of many multipass client proteins in wild-type versus knockout membranes. Ultimately, I found a significant insertion and glycosylation defect in knockout TMCO1 membranes for the 5-TMD containing protein YIPF1. This initial observation allowed us to further study the functional role of the Multipass Translocon. Briefly, this work showed that the Multipass Translocon is made up of three obligate heterocomplexes that assemble to the ribosome during multipass membrane protein biosynthesis. The Multipass Translocon is

recruited to ribosomes translating multipass membrane proteins once more than one TMD has been inserted into the membrane. Additionally, the Multipass Translocon is important for maintaining proper protein topology and stability.

A version of this work was published as Sundaram, A.[#], Yamsek, M.[#], Zhong, F.[#], Hooda, Y., Hegde, R. S., & Keenan, R. J. (2022). Substrate-driven assembly of a translocon for multipass membrane proteins. *Nature*, *611*(7934), Article 7934. ([#] = Equal Contribution, Listed Alphabetically) (https://doi.org/10.1038/s41586-022-05330-8)

2.2 Contributions

A.S., M.Y. and F.Z., who contributed equally, are listed alphabetically. A.S. and F.Z. performed the interaction analysis in cells; A.S., M.Y. and F.Z. performed the *in vitro* interaction analyses; M.Y. and A.S. carried out the *in vitro* and cell-based glycosylation assays; F.Z. and Y.H. performed the flow cytometry experiments; R.S.H. and R.J.K. provided funding and guidance. R.J.K. conceived the study and wrote the manuscript with input from all authors.

2.3 Abstract

Most membrane proteins are synthesized on endoplasmic reticulum (ER)-bound ribosomes docked at the translocon, a heterogeneous ensemble of transmembrane factors operating on the nascent chain (Gemmer & Förster, 2020; Rapoport et al., 2017). How the translocon coordinates the actions of these factors to accommodate its different substrates is not well understood. Here we define the composition, function and assembly of a translocon specialized for multipass membrane protein biogenesis3. This ‘multipass

translocon' is distinguished by three components that selectively bind the ribosome–Sec61 complex during multipass protein synthesis: the GET- and EMC-like (GEL), protein associated with translocon (PAT) and back of Sec61 (BOS) complexes. Analysis of insertion intermediates reveals how features of the nascent chain trigger multipass translocon assembly. Reconstitution studies demonstrate a role for multipass translocon components in protein topogenesis, and cells lacking these components show reduced multipass protein stability. These results establish the mechanism by which nascent multipass proteins selectively recruit the multipass translocon to facilitate their biogenesis. More broadly, they define the ER translocon as a dynamic assembly whose subunit composition adjusts co-translationally to accommodate the biosynthetic needs of its diverse range of substrates.

2.4 Introduction

The ER translocon is built around the Sec61 complex (Görlich & Rapoport, 1993). This essential factor binds ribosomes, houses a membrane-spanning channel for polypeptide translocation, and a contains a lateral gate that opens towards the lipid bilayer for transmembrane domain (TMD) insertion (Li et al., 2016; Van den Berg et al., 2004; Voorhees et al., 2014; Voorhees & Hegde, 2016). The ER also contains members of the Oxa1 superfamily of TMD insertases (Anghel et al., 2017), including the guided entry of tail anchored protein (GET) complex (Schuldiner et al., 2008), the ER membrane protein complex (EMC) (Jonikas et al., 2009) and TMCO1 (Xin et al., 2010). We recently discovered that affinity purification of TMCO1 strongly enriches for ribosome–Sec61 complexes that are translating multipass membrane proteins (McGilvray et al., 2020).

This ‘multipass translocon’ also contains CCDC47 and a three-protein complex comprising TMEM147, nicalin and NOMO (Dettmer et al., 2010) (hereafter termed the BOS complex). Using cryogenic electron microscopy, these factors were visualized behind Sec61 (McGilvray et al., 2020), where the oligosaccharyl transferase complex (OST) ordinarily resides (Pfeffer et al., 2014). How the multipass translocon is recruited to this site in place of OST, why it is selective for multipass membrane proteins, and what its functions are during protein biogenesis are all poorly defined.

2.5 The Multipass Translocon is Distinguished by Three Obligate Heterocomplexes

As previously shown, affinity purification of epitope-tagged TMCO1 from cells co-purified ribosomes that contained the Sec61 complex, CCDC47 and the BOS complex3 (Figure 2a,b). These ribosomes also contained Asterix (also known as WDR83OS), the partner of CCDC47 in the recently defined PAT complex (Chitwood & Hegde, 2020; Meacock et al., 2002), and C20Orf24 (also known as RAB5IF), a recently proposed binding partner of TMCO1 (Lewis & Hegde, 2021). Like the PAT and BOS complex subunits, TMCO1 and C20Orf24 were mutually dependent on each other, so we named the latter OPTI (obligate partner of TMCO1 insertase; Figure 2c and Figure 3a). OPTI is homologous to GET2 and EMC6, binding partners of the Oxa1 superfamily members GET1 and EMC3, respectively (Bai et al., 2020; Lewis & Hegde, 2021; McDowell et al., 2020; Miller-Vedam et al., 2020; O’Donnell et al., 2020; Pleiner et al., 2020). TMCO1 and OPTI are hereafter termed the GEL complex (Figure 3b).

TMCO1-purified ribosomes contained the TRAP complex, but did not contain OST (Figure 2b). This is consistent with the observation that the PAT, GEL and BOS

complexes occupy positions that overlap with OST, but on a different side of Sec61 to the TRAP complex. Affinity purification using tagged subunits of the PAT or BOS complexes similarly recovered ribosomes that contain the PAT, GEL, BOS, Sec61 and TRAP complexes, but not OST. Notably, the co-purification of all of these complexes is seen only in the ribosome fraction, with little or no association observed in the ribosome-free fraction (Figure 2b). Although the subunits within each multipass translocon complex are mutually dependent on each other, loss of any one complex does not impact the overall abundance of the others (Figure 2c). However, because they make (limited) contact with each other at the translocon (Figure 3b), recruitment of each complex to the ribosome is partially dependent on the other two, as discussed later. Thus, the multipass translocon contains the PAT, GEL and BOS complexes co-assembled on ribosomes containing the Sec61 and TRAP complexes, but lacking OST (Figure 2d). Earlier work analyzing ER membranes engaged in protein secretion defined a core translocon containing only the Sec61 and TRAP complexes, and a secretory translocon that additionally contains the OST complex (Pfeffer et al., 2014).

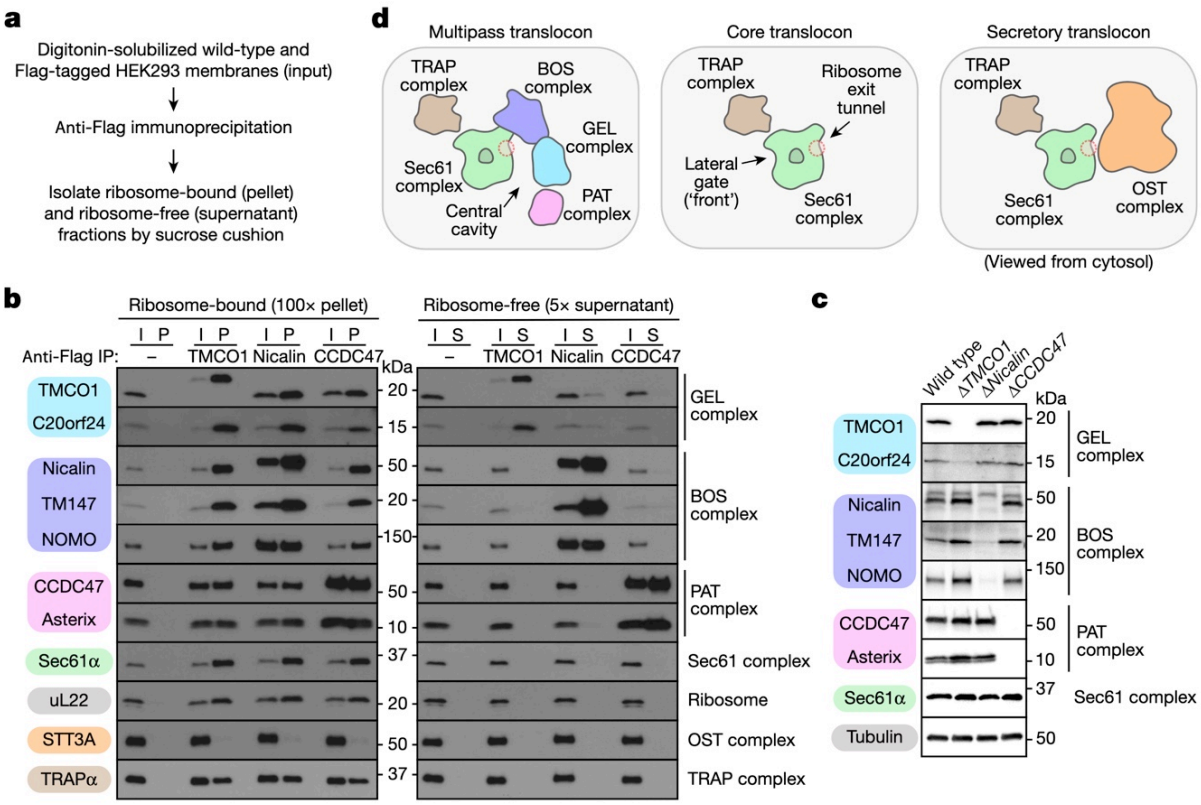

Figure 2. The Multipass Translocon is Distinguished by Three Obligate Heterocomplexes

(a) Experimental strategy. Nuclease-treated membranes from wild-type or stably integrated Flag-tagged (TMCO1, Nicalin (also known as NCLN) and CCDC47) HEK293 cells were digitonin-solubilized, immunoprecipitated and sedimented through a sucrose cushion to isolate the ribosome-bound and ribosome-free fractions for analysis. **(b)** Analysis of input (I), ribosome-bound (pellet (P)) and ribosome-free (supernatant (S)) fractions by SDS–PAGE and immunoblotting. uL22 and STT3A are used here as markers for the ribosome and OST, respectively. IP, immunoprecipitation. **(c)** Whole-cell lysates from the indicated wild-type and knockout HEK293 cell lines were analyzed by SDS–PAGE and immunoblotting. **(d)** Subunit organization and key architectural features of the compositionally distinct multipass, core and secretory translocons, viewed from the cytosol.

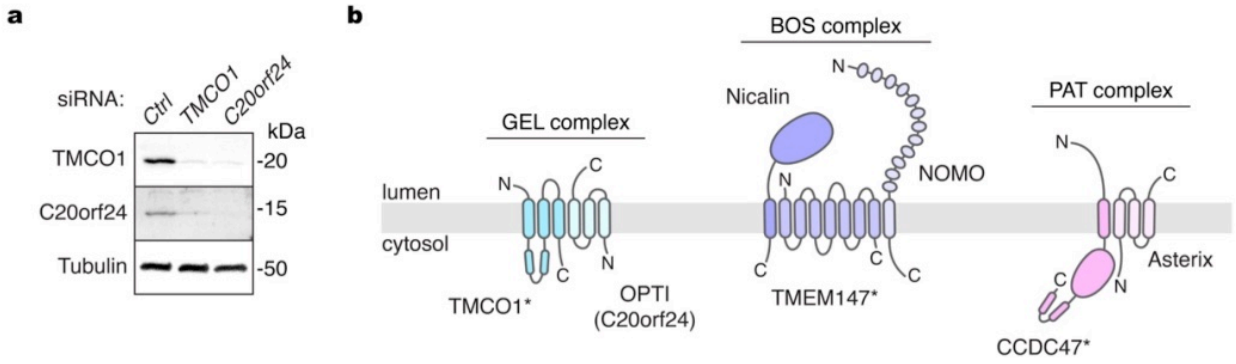

c

	Fungi	Metazoa	Protista	Viridiplantae	
TMCO1	5	450	72	135	GEL complex
OPTI	5	446	29	167	
CCDC47	539	461	23	168	PAT complex
Asterix	402	407	18	128	
TM147	0	398	31	153	BOS complex
Nicalin	3	526	31	153	
NOMO	1	468	53	124	
Sec61α1	695	755	200	315	Sec61 complex
Sec61β	388	384	69	338	
Sec61γ	516	470	136	265	
TRAPα	515	522	12	190	TRAP complex
TRAPβ	2	464	56	198	
TRAPγ	0	471	2	0	
TRAPδ	0	388	0	0	

Figure 3. Three Obligate Complexes of the Multipass Translocon

(a) Whole cell lysates from siRNA depleted HEK293 cells were analyzed by SDS-PAGE and immunoblotting; 'Ctrl' is a non-targeting control siRNA. **(b)** Nomenclature, subunit topology and number of transmembrane domains for three obligate heterocomplexes of the multipass translocon. Subunits that directly contact the ribosome in the assembled state are indicated with an asterisk. Within the translocon, CCDC47 and TMEM147 contact different regions of Sec61, while interactions between the PAT, GEL and BOS complexes are limited to small portions of TMCO1 that contact CCDC47, TMEM147 and Nicalin. **(c)** Distribution of the multipass translocon components in eukaryotes (OrthoDB v10.1).

2.6 Substrate-Directed Assembly of the Multipass Translocon

To understand the relationship between these translocons, we analyzed a series of translocation intermediates assembled at ER membranes by *in vitro* translation (Figure 4a). Both early and late intermediates of the single-spanning membrane protein ASGR1

were associated with the secretory translocon, but not the multipass translocon (Figure 4b). The five-TMD protein YIPF1 (Shakoori et al., 2003), chosen because its mRNA is enriched with the affinity-purified multipass translocon (McGilvray et al., 2020), behaved differently. Although early intermediates of YIPF1 contained the secretory translocon, this was markedly reduced with concomitant gain of multipass complexes at later stages (Figure 4b). A similar result was observed using a series of intermediates of the eight-TMD protein TRAM2 (Figure 5a,b). The key step when this switch begins corresponds to the point when two TMDs have been membrane inserted and the third is inside the ribosome exit tunnel. Thus, OST is exchanged for the PAT, GEL and BOS complexes specifically at the point when the substrate can be minimally defined as a multipass membrane protein.

Unexpectedly, the PAT, GEL and BOS complexes were not required for substrate-triggered displacement of OST from the translocon. Even in ER membranes lacking the complexes, OST was effectively displaced by YIPF1 and TRAM2 intermediates with at least two membrane-inserted TMDs (Figure 4c and Figure 5c). These results indicate that the presence of multiple TMDs in the membrane impairs OST binding to its site behind Sec61. This might be explained by a shift in the position of the inserted TMDs relative to Sec61 (Sadlish et al., 2005). Notably, the ribosome exit tunnel is offset from the central channel of Sec61 towards its back side (Figure 2d). As a consequence, an insertion intermediate ending with a TMD whose N terminus faces the lumen (N(exo)) TMD and a 30–40-amino-acid downstream tether to the truncation point might favor the back side of Sec61 due to tension in the nascent chain (Figure 4d). If such a TMD associates with preceding TMDs (such as TMDs linked by short loops), the presence of multiple TMDs

behind Sec61 would hinder OST binding. Consistent with this idea, an earlier structural analysis provisionally assigned an N(exo) TMD (followed by a 32-amino-acid tether) to a site behind Sec61 adjacent to OST (Braunger et al., 2018). As additional TMDs cannot be accommodated at the OST–Sec61 interface, a multipass insertion intermediate ending in this TMD–tether configuration would not be compatible with OST binding. However, the multipass complexes would be able to bind such an intermediate because there is more space between Sec61 and the multipass components (McGilvray et al., 2020) (Figure 4d). Indeed, structural and photocrosslinking analysis of a rhodopsin intermediate with three membrane-inserted TMDs in the multipass translocon revealed the third TMD in its N(exo) topology behind Sec61 and connected to the downstream tether inside the ribosome exit tunnel (Smalinskaitė et al., 2022). YIPF1 and TRAM2 intermediates with two membrane-inserted TMDs are probably in the same configuration, albeit with one fewer N-terminal TMD.

Similar behavior was observed with KDELR1, a seven-TMD N(exo) protein with the opposite topology to YIPF1 and TRAM2, whose N termini face the cytosol (N(cyt)) (Figure 6a). The first targeted intermediate of KDELR1 engaged the core translocon (Figure 6b). Further elongation resulted in a mixture of secretory and multipass translocons until TMD2 and TMD3 were inserted. At this point, OST binding was reduced, with a concomitant increase in recruitment of the multipass components. OST displacement was largely independent of the multipass components (Figure 6c). Thus, N(cyt) and N(exo) substrates trigger displacement of OST from the translocon by a similar mechanism, except offset by one TMD.

Surprisingly, displacement of OST was insufficient for assembly of the multipass translocon, because an early YIPF1 intermediate did not recruit the multipass components even in ER membranes lacking OST (Figure 4c). To further define the trigger(s) for multipass translocon assembly, we analyzed variants of the minimal recruitment intermediate containing only the first two TMDs of YIPF1 followed by a 42-amino-acid downstream tether (Figure 4e). At this length, a mixture of secretory and multipass translocons are observed, making it a sensitive reporter of changes to this balance. The second TMD proved to be strictly required because its replacement with a hydrophilic linker abolished multipass translocon assembly (Figure 4f). Conversely, introducing TMD2 of YIPF1 downstream of the native ASGR1 TMD was sufficient to trigger recruitment of the multipass translocon complexes (Figure 7a). In the two-TMD YIPF1 intermediate, increasing the hydrophobicity of both TMDs slightly (but reproducibly) reduced multipass translocon assembly in favor of secretory translocon retention (Figure 4f and Figure 7b). This is consistent with the finding that TMD hydrophilicity is a key requirement for interaction with the PAT complex (Chitwood & Hegde, 2020), and perhaps other multipass translocon components. Thus, a shift in translocon composition can be triggered in two non-mutually exclusive ways: accumulation of multiple TMDs behind Sec61 to disfavor OST binding and direct TMD engagement of the multipass complexes to favor their recruitment and retention.

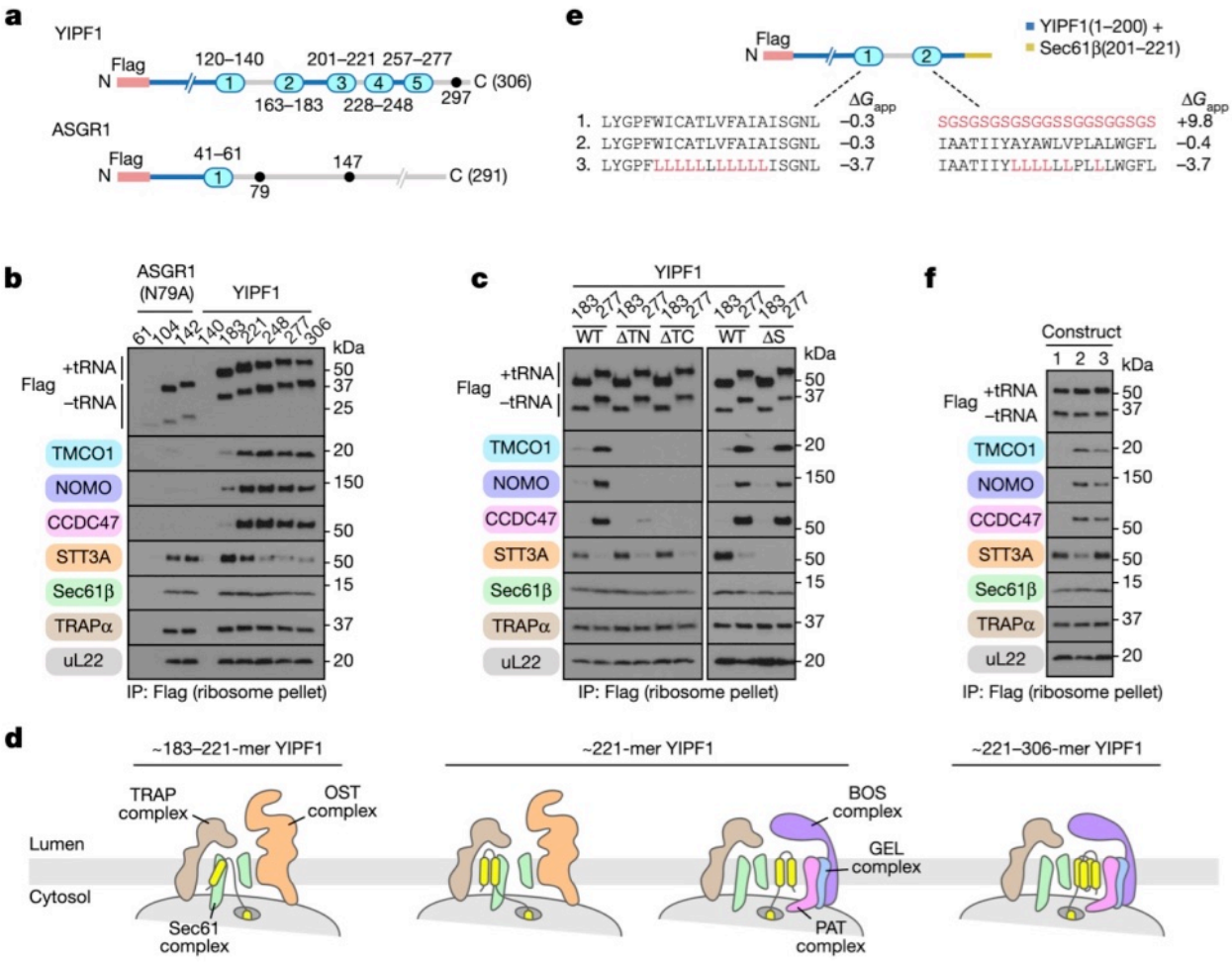

Figure 4. Substrate-Directed Assembly of the Multipass Translocon

(a) Templates used to generate truncated, Flag-tagged constructs for affinity purification of stalled (no stop codon) ribosome–nascent chain complexes. All stalled intermediates are appended with Met-Leu-Lys-Val. Luminal loops (grey) and native N-glycosylation acceptor sites (black circles) are indicated. **(b)** Stalled, Flag-tagged ASGR1(N79A) and YIPF1 constructs truncated at the indicated positions were translated in rabbit reticulocyte lysate (RRL) in the presence of wild-type HEK293 rough microsomes, and the membrane-associated fraction was isolated by sedimentation. Following anti-Flag immunoprecipitation of the digitonin-solubilized membranes, stalled ribosome–nascent chain complexes were isolated by sedimentation and analyzed by SDS–PAGE and immunoblotting. Note the earliest intermediates (ASGR1 61-mer and YIPF1 140-mer) do not target to the membrane as their first TMD remains buried inside the ribosome exit tunnel, thus serving as a control for nonspecific binding. **(c)** Stalled, Flag-tagged YIPF1 constructs truncated at positions 183 and 277 were translated in RRL in the presence of wild-type (WT), double-knockout (TMCO1/Nicalin (ΔTN) and TMCO1/CCDC47 (ΔTC)) or STT3A-knockout (ΔS) rough microsomes and analyzed as in b. **(d)** Diagram of translocon composition at different stages of

(Figure 4 Continued) YIPF1 synthesis, based on data in b & c. **(e)** Series of two-TMD YIPF1 templates containing different TMD1 and TMD2 sequences. The calculated apparent free energy of membrane insertion (Hessa et al., 2007) (ΔGapp) for each TMD is indicated. **(f)** Stalled, Flag-tagged YIPF1 constructs as in e were analyzed as in b; quantification for n = 5 biological replicates is shown in Figure 7b.

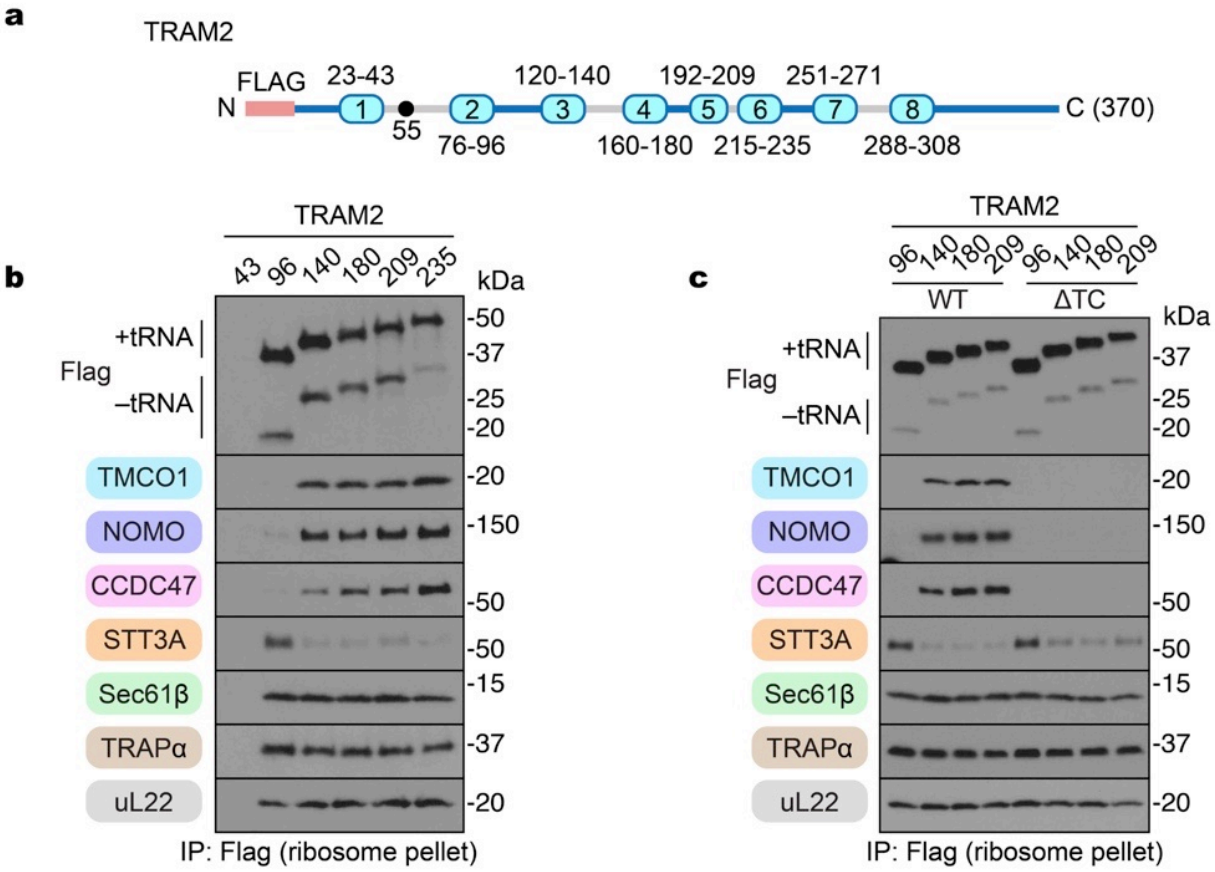

Figure 5. Translocon Dynamics During TRAM2 Synthesis

(a) Template used to generate truncated, Flag-tagged TRAM2 constructs, as in Figure 4a. **(b)** Stalled, Flag-tagged TRAM2 constructs truncated at the indicated positions were analyzed as in Figure 4b. Note that the 140-mer intermediate (and beyond) is glycosylated at position 55. **(c)** Stalled, Flag-tagged TRAM2 constructs truncated at the indicated positions were translated in RRL in the presence of WT and double knockout (TMCO1/CCDC47, 'ΔTC') rough microsomes, and analyzed as in (b).

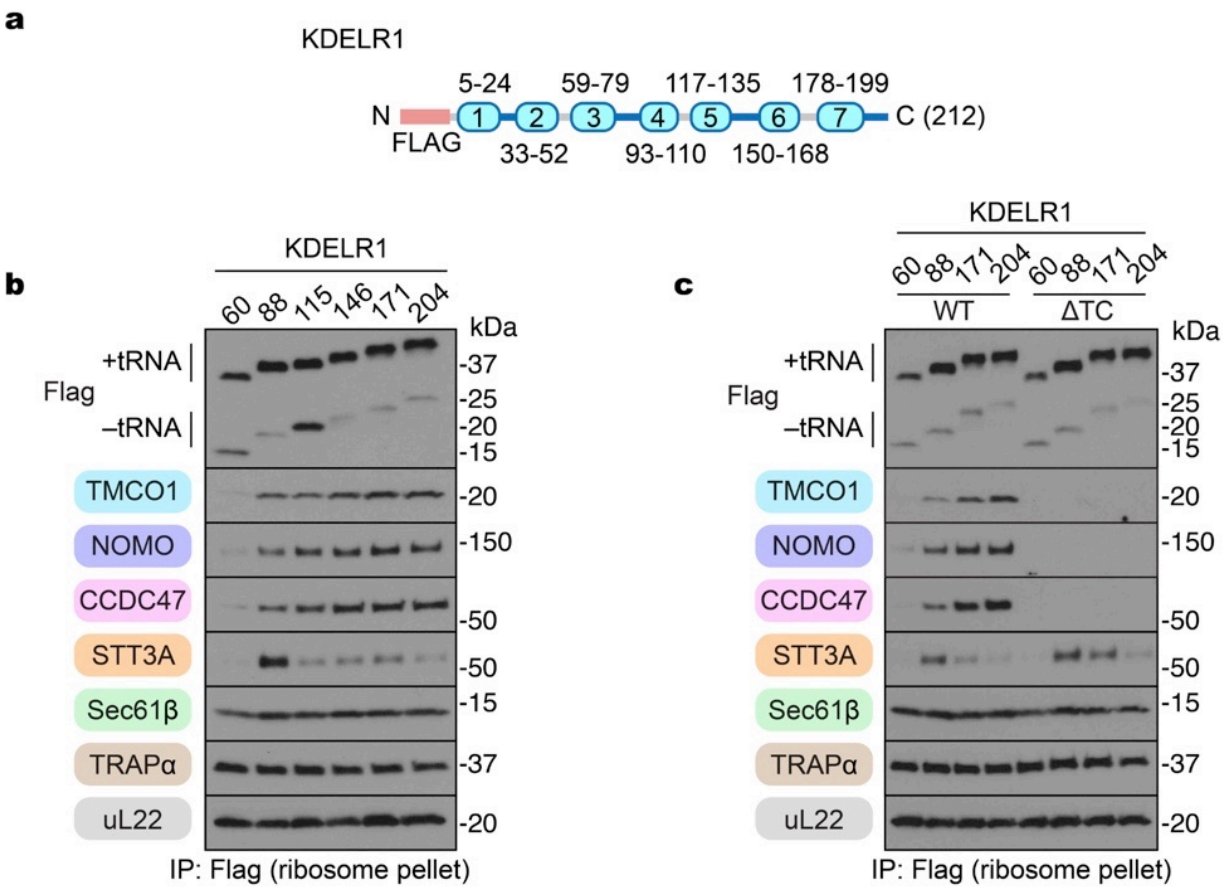

Figure 6. Translocon Dynamics During KDELR1 Synthesis

(a) Template used to generate truncated, Flag-tagged KDELR1 constructs, as in Figure 4a. **(b)** Stalled, Flag-tagged KDELR1 constructs truncated at the indicated positions were analyzed as in Figure 4b. **(c)** Stalled, Flag-tagged KDELR1 constructs truncated at the indicated positions were translated in RRL in the presence of WT and double knockout (TMCO1/CCDC47, 'ΔTC') rough microsomes, and analyzed as in (b).

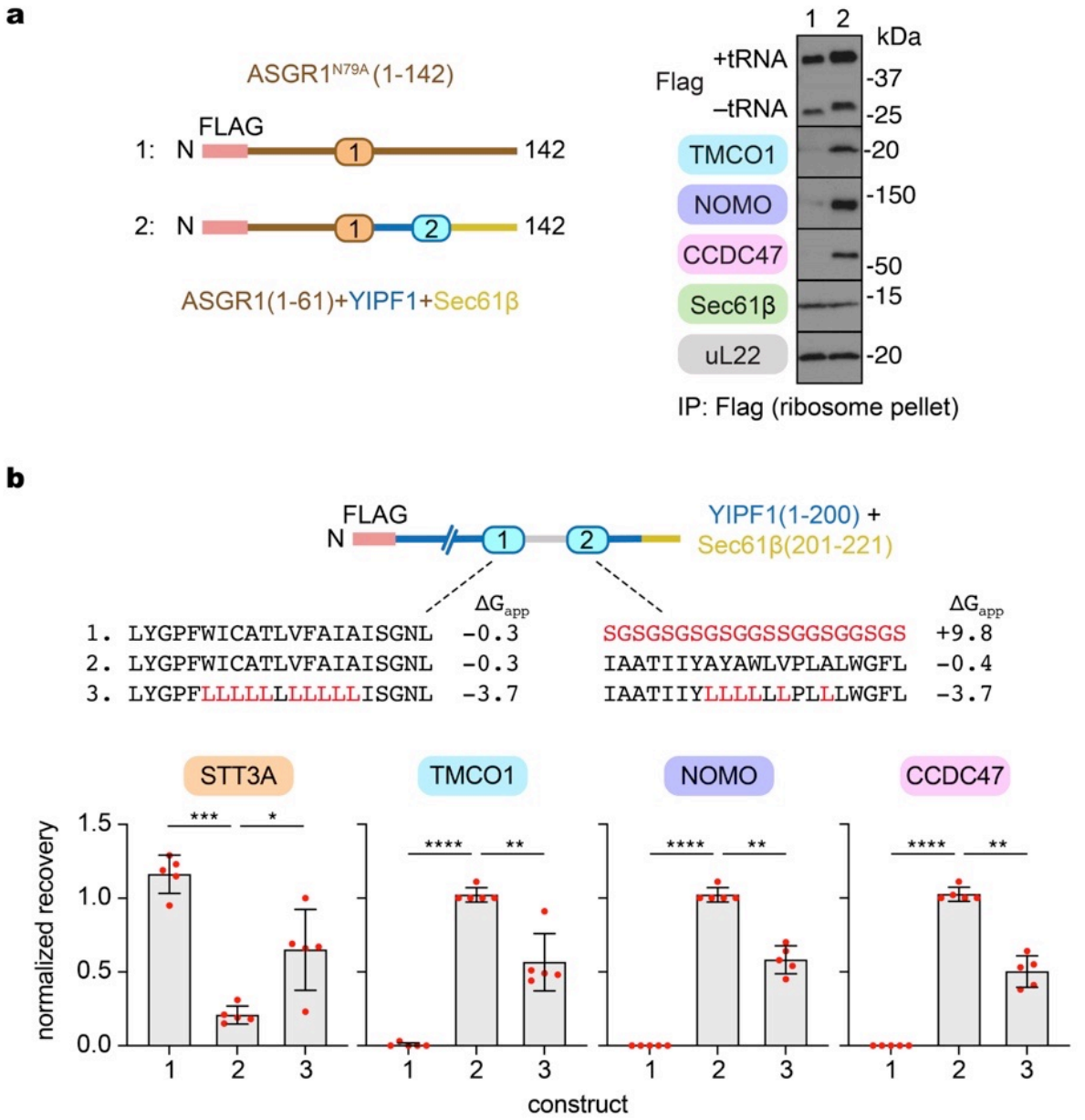

Figure 7. Additional Characterization of Substrate Features that Direct Assembly of the Multipass Translocon

(a) The indicated ASGR1- derived intermediates were translated in RRL in the presence of wild-type HEK293 rough microsomes, and the membrane-associated fraction was isolated by sedimentation. Following anti-Flag immunoprecipitation of the digitonin-solubilized membranes, stalled RNCs were isolated by sedimentation and analyzed by SDS-PAGE and immunoblotting. **(b)** Quantification of STT3A, TMCO1, CCDC47 and NOMO recruitment to stalled 2-TMD YIPF1 constructs as in Figure 4f, for n = 5 biological replicates. Data are mean ± S.D. Analysis was performed using an RM one-way ANOVA with the Geisser-Greenhouse correction and Tukey's multiple comparisons test as implemented in GraphPad Prism 9.4.0.

(Figure 7 Continued) *, $p < 0.0332$; **, $p < 0.0021$; ***, $p < 0.0002$; ****, $p < 0.0001$; p values are given in Supplementary Table 2.

2.7 Internal Loop Translocation at the Secretory Translocon

Although most co-translationally modified glycosylation sites in multi pass membrane proteins occur early, at a point when OST would still be at the translocon, at least some sites occur in long loops translocated after multiple TMDs have been inserted (Cherepanova et al., 2019). These loops presumably begin translocating through the Sec61 complex when the preceding TMD engages the lateral gate of Sec61 in the N(cyt) orientation. To test whether internal loop translocation occurs at the secretory translocon, we analyzed biogenesis intermediates of EAAT1, an eight-TMD protein (Canul-Tec et al., 2017) with a glycosylated luminal loop after TMD3 (Figure 8a). As with YIPF1 and TRAM2, the earliest targeted insertion intermediate is part of the secretory translocon, after which OST is displaced when TMD2 is inserted (Figure 8b). This EAAT1 153-mer intermediate is largely associated with the core translocon presumably because its tether length or TMD hydrophobicity limits binding to the multipass components. With elongation to a point when TMD3 has emerged from the ribosome exit tunnel, a mixture of secretory and multipass translocons are observed. Notably, the reappearance of OST at the translocon coincides with the onset of glycosylation (Figure 8b). At later lengths OST again departs, concomitant with increased recruitment of the multipass translocon components (Figure 8b). At each point, OST displacement occurs independently of the multipass components (Figure 8c). We posit that TMD3 engagement of the lateral gate favors repositioning of the preceding TMDs to the front side of Sec61, allowing OST to rebind at the back side (Figure 8d). Thus, translocon subunit composition is responsive

to the nascent chain and is influenced by both the positions (relative to Sec61) and interactions of preceding TMDs.

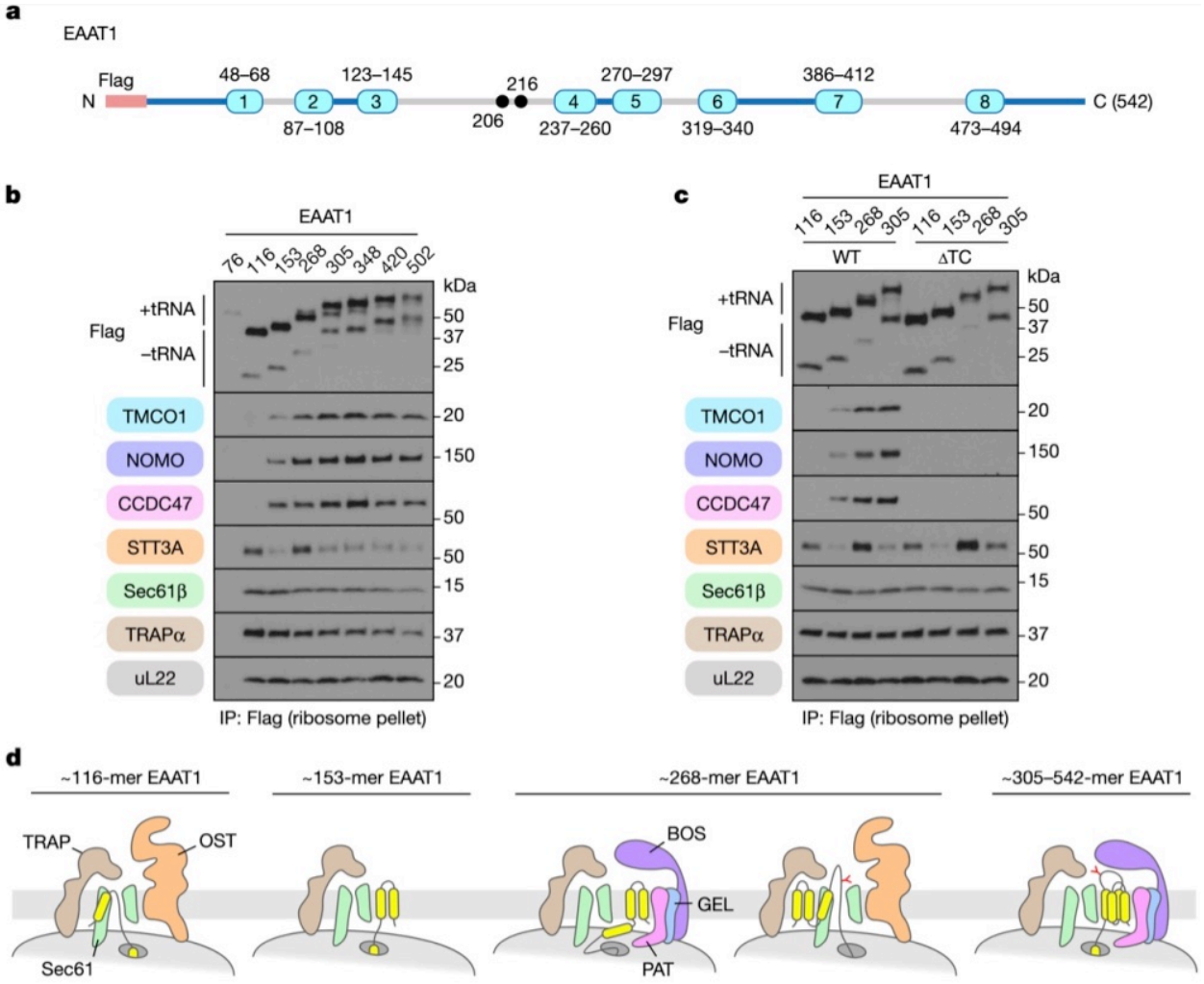

Figure 8. Internal Loop Translocation at the Secretory Translocon

(a) The template used to generate truncated, Flag-tagged EAAT1 constructs, as in Figure 4a. **(b)** Stalled, Flag-tagged EAAT1 constructs truncated at the indicated positions were analyzed as in Figure 4b. The appearance of additional EAAT1 bands in later intermediates (EAAT1(268) onwards) is due to glycosylation in the TM3–TM4 luminal loop. **(c)** Stalled, Flag-tagged EAAT1 constructs truncated at the indicated positions were translated in RRL in the presence of wild-type and double-knockout (TMCO1/CCDC47 (ΔTC)) rough microsomes, and analyzed as in B. **(d)** Diagram of translocon composition at different stages of EAAT1 synthesis, based on data in b & c. Glycosylation of the EAAT1 acceptor site(s) is indicated.

2.8 Multipass-Translocon-Dependent Topogenesis

To analyze the consequence of multipass translocon assembly for membrane protein biogenesis, we examined the insertion of YIPF1. The single N-linked glycosylation site in this substrate is close to the carboxy terminus and is necessarily modified post-translationally (Figure 9a). It therefore serves as a reporter of topogenesis errors occurring anywhere preceding it. The fraction of glycosylated YIPF1 was substantially reduced when it was inserted into ΔTMCO1 microsomes compared to microsomes from wild-type cells (Figure 9b). Notably, equal percentages of YIPF1 were recovered from these two reactions after carbonate extraction, indicating comparable levels of membrane insertion. As glycosylation itself is unimpaired in these microsomes (see below), the defect in YIPF1 glycosylation is likely to be a consequence of altered topology. Consistent with this idea, protease protection analysis of YIPF1 showed a reduction of around 40% of protected fragments in ΔTMCO1 microsomes (Figure 9c).

Using glycosylation as a proxy for proper YIPF1 topogenesis, we observed similarly strong defects in microsomes lacking the PAT, GEL or BOS complexes, and even stronger effects in double-knockout microsomes (Figure 9d,e). The YIPF1 defects could not be overcome by adding more microsomes to the reaction, consistent with an intrinsic biogenesis defect (Figure 10a,b). ASGR1 biogenesis (as judged by glycosylation) and translocation of another single-spanning membrane protein TMED2 (as judged by signal peptide cleavage) were unaffected in the same set of knockout microsomes (Figure 9d). Thus, loss of the multipass translocon components impairs YIPF1 topogenesis without affecting SRP-dependent targeting, Sec61-mediated translocation and insertion, OST-mediated glycosylation or signal peptidase-dependent signal peptide cleavage. It is

noteworthy that loss of any one multipass translocon complex reduces ribosome recruitment of the others (Figure 10d). For this reason, it is difficult from these data to assign the YIPF1 topogenesis defect to any one factor. Nonetheless, it is clear that the multipass translocon is functionally important for biogenesis of the multipass protein YIPF1.

Analysis of YIPF1 in cultured cells showed glycosylation defects in multipass translocon mutants similar to the *in vitro* results, indicating similar topogenesis defects in both systems (Figure 9f,g). The consequence of this defect is promiscuous degradation of YIPF1 tagged with red fluorescent protein (RFP) as determined using a flow cytometry assay (Figure 9h). In this setup, RFP–YIPF1 is translated in tandem with green fluorescent protein (GFP) but separated by the ribosome-skipping viral 2A sequence. Instability of newly made YIPF1 can be monitored as a reduction in RFP signal relative to the signal from GFP, which is necessarily translated at equal levels. The fluorescence ratio for the YIPF1 reporter was reduced in cells on knockdown of genes encoding components of the PAT, GEL or BOS complexes, consistent with impaired biogenesis (Figure 9i and Figure 10e). A similar effect was seen for reporters of two unrelated multipass membrane proteins (EAAT1 and the G-protein-coupled receptor AGTR2), but not for ASGR1 (Figure 9j). Thus, the multipass translocon is not only recruited to nascent multipass membrane proteins as monitored *in vitro*, but also facilitates their biogenesis in cells.

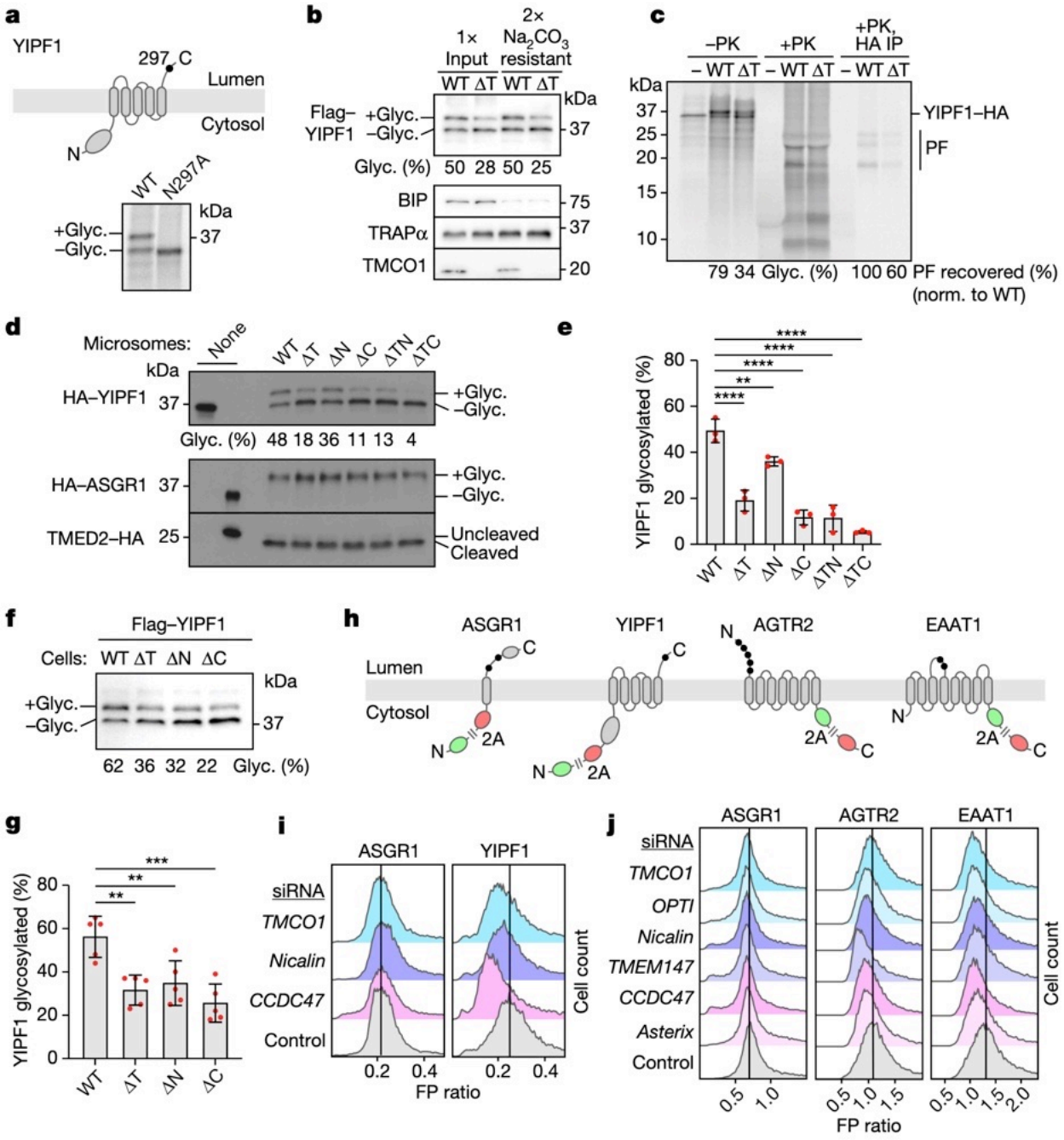

Figure 9. Multipass-Translocon-Dependent Topogenesis

(a) Top: YIPF1 harbors a single N-glycosylation site (black circle) near its C terminus. Bottom: [^{35}S]methionine-labelled wild-type and mutant (N297A) YIPF1 were translated in RRL in the presence of rough microsomes, isolated by sedimentation, and analyzed by autoradiography. **(b)** Flag–YIPF1 was translated in RRL with wild-type or TMCO1-knockout (ΔT) rough microsomes, isolated by sedimentation, and analyzed either directly (input) or after alkaline sodium carbonate extraction. YIPF1, TMCO1, BIP (ER luminal) and TRAPα (ER integral) were visualized by immunoblotting. The proportion of glycosylated (Glyc.) YIPF1

(Figure 9 Continued) is indicated. **(c)** [^{35}S]methionine-labelled, C-terminally haemagglutinin (HA)-tagged YIPF1 was translated in RRL with wild-type or ΔT rough microsomes, isolated by sedimentation, and analyzed by autoradiography before (−PK) or after (+PK) proteinase K treatment. The PK-treated sample was also analyzed after immunoprecipitation using the HA tag. Full-length YIPF1–HA, its protease-protected fragments (PF), and the proportion of recovered PF are indicated. **(d)** HA–YIPF1, HA–ASGR1 and TMED2–HA were translated in RRL with wild-type, single-knockout (TMCO1 (ΔT), Nicalin, (ΔN) or CCDC47 (ΔC)) or double-knockout (TMCO1/Nicalin (ΔTN) or TMCO1/CCDC47 (ΔTC)) rough microsomes, isolated by sedimentation, and analyzed by immunoblotting. **(e)** Quantification of YIPF1 glycosylation for n = 3 biological replicates, as in d. The data are shown as the mean ± s.d. **(f)** Flag–YIPF1 was transiently transfected into wild-type or knockout cells, and total lysates were analyzed by immunoblotting. **(g)** Quantification of YIPF1 glycosylation as in f, for n = 5 biological replicates. The data are shown as the mean ± s.d. **(h)** Reporter constructs to monitor protein stability in cells. **(i, j)** Stably integrated HEK293 reporter lines were treated with the indicated short interfering RNA (siRNAs), induced with doxycycline, and analyzed by flow cytometry. The histograms show FP ratios for each siRNA–reporter pair; the vertical black line indicates the mode of the control population. Statistical analyses in e & g were performed by ordinary one-way analysis of variance (ANOVA) with Dunnett's multiple comparison test (single pooled variance) in GraphPad Prism 9.4.0. **P < 0.0021; ***P < 0.0002; ****P < 0.0001; P values are given in Supplementary Table 1.

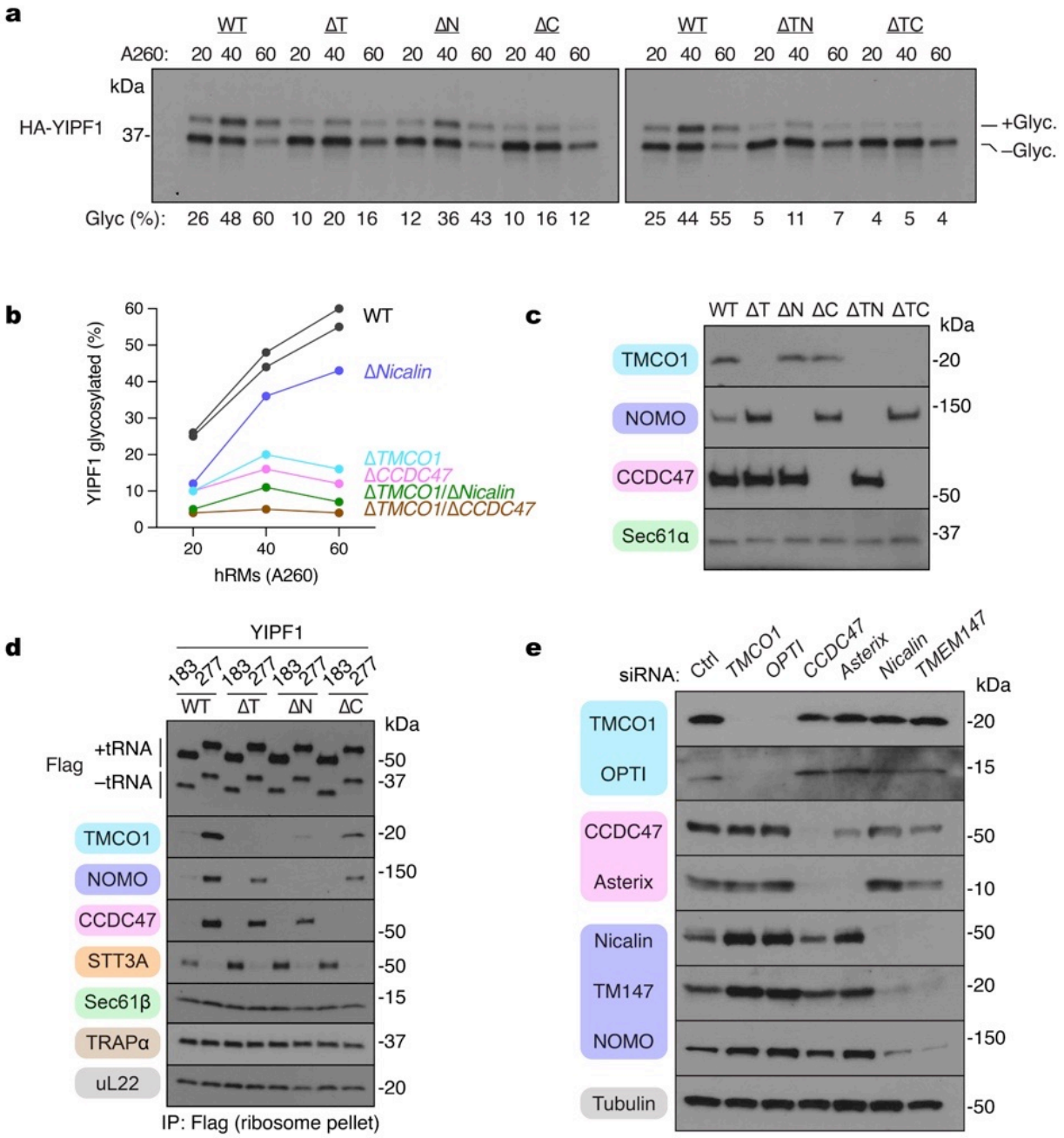

Figure 10. Additional Characterization of the *In Vitro* System and Validation of siRNA Knockdowns

(a) HA-YIPF1 was translated in RRL in the presence of WT, single- (TMCO1, ΔT; Nicalin, ΔN; CCDC47, ΔC) or double knockout (TMCO1/Nicalin, ΔTN; TMCO1/CCDC47, ΔTC) rough microsomes at different concentrations (determined by absorbance at 260 nm), isolated by sedimentation, and analyzed by SDS-PAGE and immunoblotting. The percentage of glycosylated YIPF1 is indicated below the gel. **(b)** Plot of the data in a. **(c)** Membranes prepared from the indicated wild-type, single- or double-knockout HEK293 cell lines were analyzed by SDS-PAGE and immunoblotting. **(d)** Stalled, Flag-tagged YIPF1 constructs

(Figure 10 Continued) truncated at position 183 and 277 were translated in RRL in the presence of wild-type (WT) or single knockout rough microsomes, and the membrane-associated fraction was isolated by sedimentation. Following anti-Flag immunoprecipitation of the digitonin-solubilized membranes, stalled RNCs were isolated by sedimentation and analyzed by SDS-PAGE and immunoblotting. **(e)** Whole cell lysates from HEK293 cells treated with the indicated siRNAs were analyzed by SDS-PAGE and immunoblotting; 'Ctrl' is a non-targeting control siRNA.

2.9 Discussion

We have defined the modular composition of the multipass translocon, established its role in multipass protein topogenesis, and revealed how nascent substrates drive translocon remodeling to facilitate their successful maturation. The multipass translocon components are most broadly distributed in metazoans (Figure 3c). This mirrors the marked increase in membrane proteome complexity that accompanied evolution of multicellular organisms (Attwood et al., 2017). The most notable example of this expansion is seen with the seven-TMD G-protein-coupled receptors, with about nine hundred family members encoded in the human genome but only three in Saccharomyces cerevisiae (Fredriksson & Schiöth, 2005). The multipass translocon may have evolved to increase the efficiency of multipass protein biogenesis, particularly in metazoans.

Demand for multipass protein synthesis in other organisms might be satisfied by more broadly conserved components of the biogenesis machinery. In eukaryotes lacking some or all of the multipass components, the widely conserved EMC (Wideman, 2015)may play a more central role in multipass protein biogenesis (Chitwood et al., 2018; Miller-Vedam et al., 2020; Shurtleff et al., 2018; Tian et al., 2019). Fungi, which lack recognizable homologues of the GEL and BOS complexes, may use their conserved PAT

complex components during multipass protein synthesis at Sec61. Prokaryotes lack PAT and BOS components, but GEL complex homologues in archaea (Borowska et al., 2015; Lewis & Hegde, 2021) and the Oxa1 superfamily insertase YidC in bacteria (Nagamori et al., 2004; Serdiuk et al., 2019; Zhu et al., 2013) may facilitate multipass protein biogenesis with SecY. In other cases, the TMD chaperone and insertase functions of the multipass components may be encoded by still unknown membrane factors.

Accommodating the diversity of secretory and membrane proteins during biogenesis requires the ER translocon to coordinate multiple transmembrane factors that operate on the nascent chain. These factors include TRAM family members (Görlich et al., 1992; Voigt et al., 1996), RAMP4 (Görlich & Rapoport, 1993; Pool, 2009), signal peptidase (Evans et al., 1986; Liaci et al., 2021), chaperones (Chevet et al., 1999; Dudek et al., 2005), putative RNA-binding proteins (Cui et al., 2012) and others. For multipass membrane proteins, the signals directing translocon composition proved to be multifactorial, and included negative selection (for example, by disfavoring the binding of OST on the basis of TMD number and position) and positive selection (for example, by binding to specific factors such as the PAT complex). This is analogous to the interplay between cytosolic factors at the ribosome exit tunnel during synthesis of soluble proteins (Kramer et al., 2019). Our findings provide a framework for dissecting how other biogenesis factors are coordinated at the ER translocon.

CHAPTER 3. Progress Toward a Cryo-EM Structure of a YIPF1-programmed Multipass Translocon

3.1 Overview

The work presented in McGilvray *et al.* characterized the cryo-EM structure of the Multipass Translocon isolated from cultured Hek293 microsomes. Briefly, this structure contained the ribosome and Sec61 along with five accessory factors: TMCO1, CCDC47, Nicalin, NOMO, and TMEM147. While this structural characterization was an important first step, the resolution is limited in the membrane regions and a few of the TMDs are not completely resolved. A likely explanation for the limited resolution is because these natively isolated complexes are trapped in various stages of translation, with the ribosomes translating hundreds of different substrates. Therefore, the work presented in this chapter describes my progress toward obtaining a cryo-EM structure of the Multipass Translocon programmed with a multipass membrane protein stalled at a single point.

3.2 Contributions

I performed all the experiments, plus the cryo-EM processing written in this chapter. Robert Keenan built the model into the cryo-EM density, which were further adjusted by myself. The University of Chicago Advanced Electron Microscopy Facility assisted with the loading of the grids and aligning the microscopes. James Fuller compiled RELION-4.0.1 onto the lab's beagle3 computing cluster account.

3.3 Introduction

One goal for the Multipass Translocon is to obtain higher resolution structural information that will allow us to visualize additional components more clearly. By stalling ribosomes with a substrate at a single point, it is likely that the complex will be less dynamic. First, by programming ribosomes with a multipass substrate, we will enrich the sample for the Multipass Translocon. Second, even when a multipass substrate is recruited to the Multipass Translocon, it is possible that the subcomplexes are still moving in a substrate- or length-dependent manner. Therefore, by stalling one substate at a single point, we expect these dynamics to be limited. Third, it is possible that the interactions between the multipass client protein and the Multipass Translocon can help to stabilize the complex. These explanations may therefore lead to a less dynamic complex, potentially allowing us to achieve higher resolution and visualize more density within the Multipass Translocon (Murata & Wolf, 2018).

Additionally, we hope that the trapped intermediates can provide mechanistic insight into Multipass Translocon-dependent insertion. By visualizing the contacts between the multipass substrate and the Multipass Translocon, we can design experiments to investigate the mechanism. Furthermore, the ultimate goal is to be able to trap multipass substrates at different lengths throughout its biosynthesis and reconstruct a cryo-EM model at each point. From there, a molecular movie can be made to show how multipass membrane proteins interact with the Multipass Translocon during their biosynthesis. Furthermore, it may reveal certain signals that are required for the recruitment of other translocons, such as the Core and Secretory Translocon.

Recently, a collaborating lab has solved a couple of structures of the Multipass Translocon containing programmed ribosomes (Smalinskaitė et al., 2022). Briefly, this paper showed the substrate-mediated recruitment of the PAT complex to Sec61, focusing on the type III multipass membrane protein rhodopsin, a 7-TMD GPCR. The earliest PAT complex recruitment was observed when Rhodopsin was stalled 70 amino acids beyond the first TMD (Rho^{ext}). Rho^{ext} contains one TMD in the membrane while the second TMD and stalling sequence remain in the cytosol and ribosomal exit tunnel. Briefly, the first cryo-EM structure containing Rho^{ext} programmed ribosomes featured CCDC47 wedged between the ribosome and the N-terminal half of Sec61α, thereby constraining Sec61 in the closed conformation. The second cryo-EM structure was isolated with ribosomes programmed with a Rho-4TMD intermediate, containing three TMDs emerged from the ribosome and the fourth TMD inside the ribosomal exit tunnel. While this longer multipass intermediate also showed increased density for the GEL complex, it also contained visible density for the third Rhodopsin TMD adjacent to Sec61. Site-specific crosslinking experiments confirmed this interaction, while also revealing contacts between TMD1 and Asterix, plus TMD2 and TMCO1. While these structures contain clear density for the ribosome, Sec61, and the PAT complex, density for the other subcomplexes of the Multipass Translocon (GEL and BOS) is limited. Also, only one of the substrate's TMDs was visualized in the structure.

3.4 Preparation of Programmed Multipass Translocon Particles for Cryo-EM.

In an effort to increase the number of multipass client protein TMDs present in the cryo-EM structure, I sought to obtain a structure of the Multipass Translocon containing

a substrate that has more than three TMDs inserted into the membrane. Using *in vitro* translation (IVT), ribosomes were programmed with truncated 4xFlag-YIPF1-Terminal-Valine(306) (stalled 58 residues after the 4th TMD; YIPF1 contains 5 total TMDs as shown in Figure 4A) in the presence of WT Cas9 microsomes. Following IVT, the Multipass Translocon was isolated by pulling down on YIPF1's N-terminal flag tag. The particles were directly eluted from the resin and immediately frozen onto grids for imaging on the microscope (Figure 11A and B). As expected, this complex contained high levels for the Multipass Translocon subcomplexes and low levels of the Secretory Translocon when compared to various truncations of the singlepass membrane protein ASGR1 (Figure 4A), as visualized by western blot (Figure 11C). Particles were monodispersed on the grids and (Figure 12A and B) and several cryo-EM datasets were collected and combined on the sample.

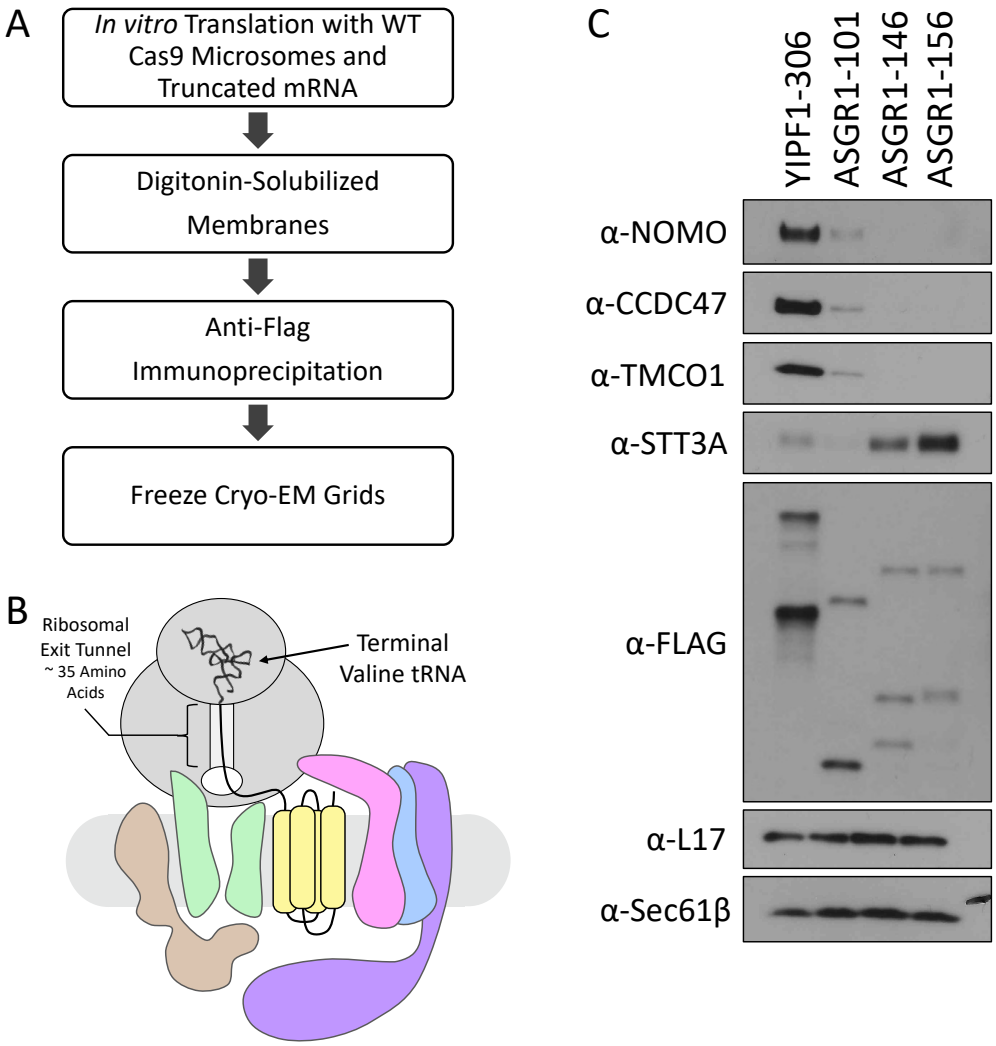

Figure 11. Preparation of Programmed Multipass Translocon Particles for Cryo-EM

(A) Flowchart for isolating programmed particles for Cryo-EM. Using *in vitro* translation (IVT), ribosomes were programmed with truncated 4xFlag-YIPF1-Terminal-Valine(306) in the presence of WT Cas9 microsomes. Following IVT, membranes were pelleted and solubilized in digitonin prior to anti-Flag immunoprecipitation. Particles were directly eluted from the resin and immediately frozen onto Quantifoil R1.2/1.3 200 mesh gold grids with 2 nm carbon. **(B)** Schematic of YIPF1-306 Programmed Multipass Translocon Particles. Four out of the five TMDs are emerged from the ribosome while one of the TMDs remains in the exit tunnel. **(C)** Western blot for 4xFlag-YIPF1-programmed ribosome immunoprecipitation alongside various single-pass membrane protein (4xFlag-ASGR1)-programmed ribosome immunoprecipitations. Schematics for 4xFlag-YIPF1 and 4xFlag-ASGR1 constructs are shown in Figure 4A.

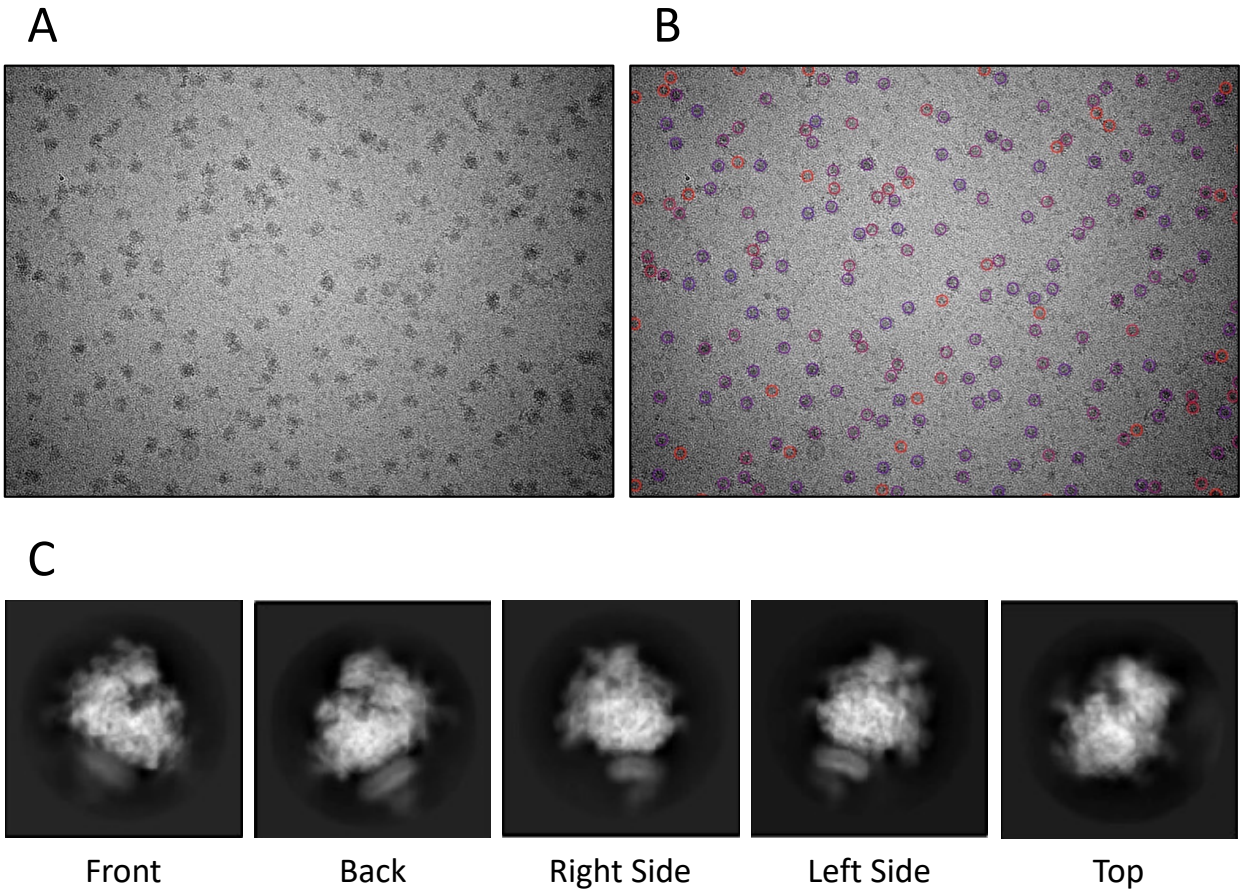

Figure 12. Cryo-EM Micrographs and Initial 2D Classification

(A) Representative cryo-EM micrograph imaged at 53,000X magnification on a Titan Krios. The micrographs contain monodispersed YIPF1-programmed stalled ribosomes. Particles were frozen on Quantifoil R1.2/1.3 200 mesh gold grids coated with 2 nm carbon. **(B)** Particles selected from Topaz, colored by figure of merit where Red = −3 and Blue = 5. **(C)** Representative 2D class averages for the YIPF1-programmed Multipass Translocon.

3.5 Cryo-EM Data Processing on the YIPF1-Terminal-Valine(306) Sample

All data processing was performed in RELION-4.0.1. The cryo-EM data processing workflow is outlined in Figure 13. Following Topaz particle picking and 2D classification (Figure 12C), the initial 3D refinement contained 1,113,500 particles. Initial 3D classification on the entire complex produced 7 similar classes (83.6%) that contained

density for the Multipass Translocon, one class (5.7%) that lacked the small 40S ribosomal subunit, and one poorly-aligned class (10.7%). Careful refinement on 928,794 particles was done in four rounds of 3D refinement, post-processing, and CTF-refinement, followed by a final Bayesian polishing step once the estimated final resolution had stabilized. Focused classification with signal subtraction on the Multipass Translocon (excluding significant ribosome density) identified a subset of 232,563 particles containing the Multipass Translocon. Further focused classification with signal subtraction on the BOS complex resulted in a class with 145,202 particles. This class was reverted to its original, ribosome-containing state (Map 1) and refined again, focused on the Multipass Translocon region (Map 2).

The overall resolution of the programmed Multipass Translocon was 3.36 Å for Map 1 and 3.38 Å for Map 2 (Table 1), with local resolutions around 3 Å for most of the ribosome, up to around 5-8 Å for the micellular and luminal regions (Figure 14).

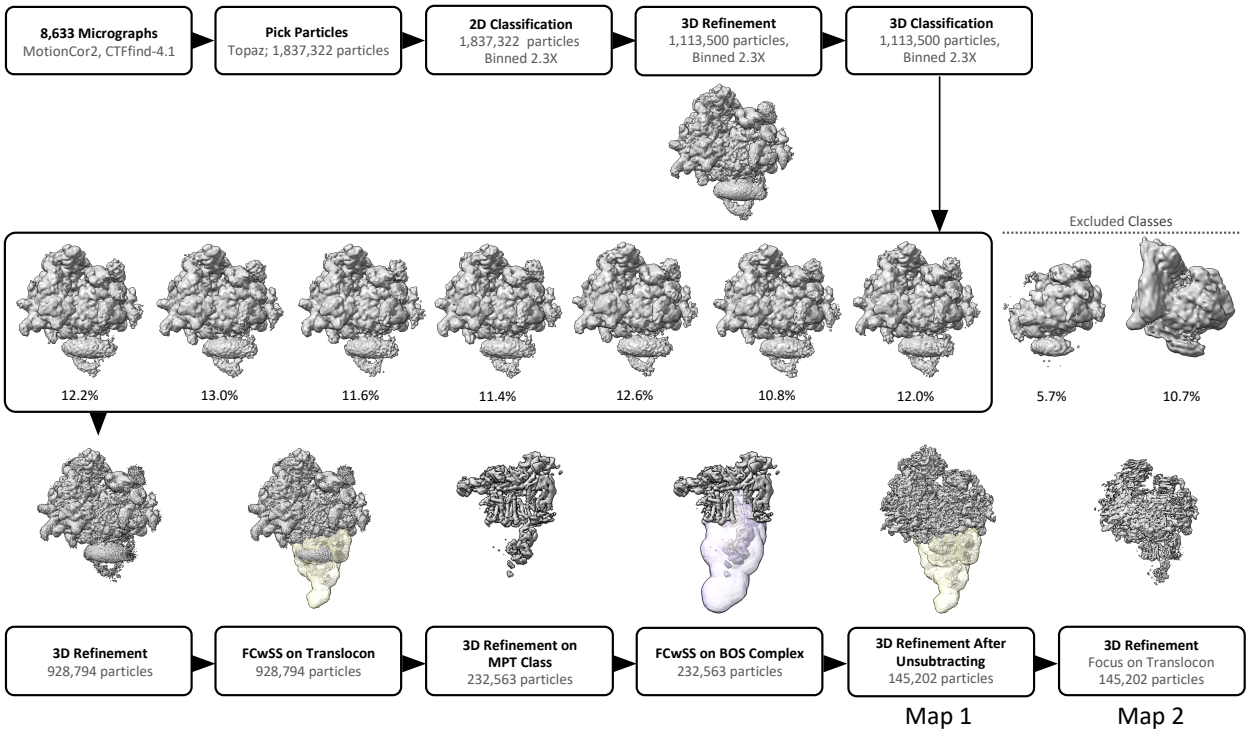

Figure 13. Cryo-EM Data Processing Workflow

All data processing was performed in RELION-4.0.1. Resulting structures were visualized using ChimeraX.

Table 1: Cryo-EM Data Collection and Processing		
Magnification	53,000X	
Voltage (kV)	300	
Electron Exposure (e^{-}/Å^2)	60	
Defocus Range (μm)	−0.9 to −1.9	
Pixel Size (Å)	0.84	
Symmetry	C1	
Micrographs Used	8,633	
Initial Particle Images (No.)	1,837,322	
Final Particle Images (No)	145,202	
	Map 1	**Map 2**
Map Resolution (Å)	3.36	3.38
FSC Theshold	0.143	0.143
Map Resolution Range (Å)	3.36 to 7.80	3.36 to 8.91

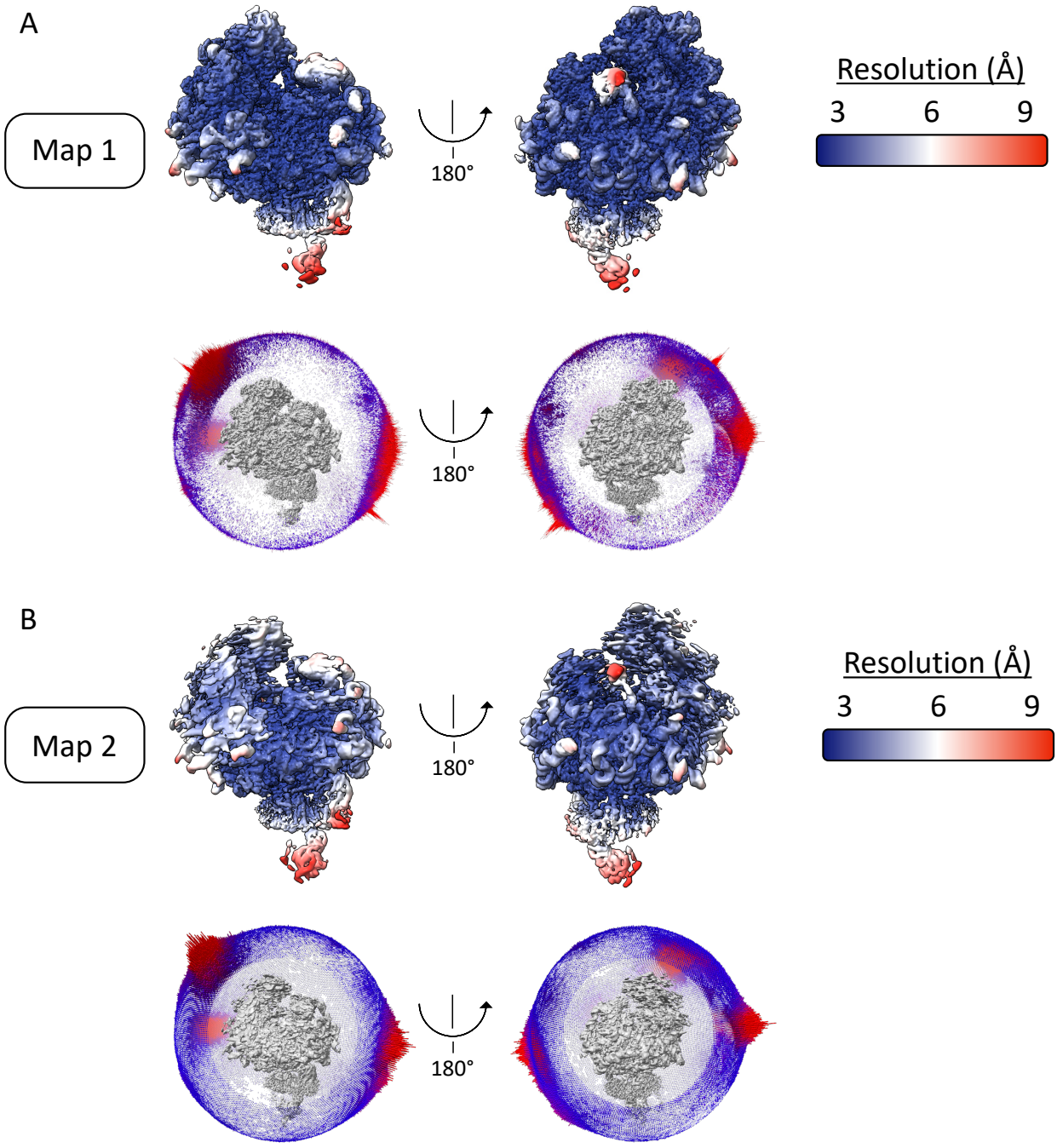

Figure 14. Cryo-EM Resolution Estimates

Two maps were used for the final analysis: **(A)** Global map calculated with unsubtracted particles and **(B)** Multipass Translocon-focused map calculated with unsubtracted particles. Top, Maps are colored by local resolution as estimated by RELION; Bottom, angular distribution of particles.

3.6 Structure of the Multipass Translocon Programmed with YIPF1

Overall, the map contained clear density for the ribosome (Figure 15A), and density for the Multipass Translocon subcomplexes was markedly improved compared to previous structures (Gemmer & Förster, 2020; McGilvray et al., 2020; Smalinskaitė et al., 2022). The translating nascent chain can be clearly seen in the ribosomal exit tunnel; however, the density cuts off near Sec61. As previously observed, CCDC47's coiled coil wedges between the ribosomal exit tunnel and Sec61 is in the closed conformation (Figure 15C; McGilvray et al., 2020; Smalinskaitė et al., 2022). Asterix density is still not fully resolved, but two of the three TMDs can be seen spanning the membrane, along with additional cytosolic density. TMCO1 density shows almost complete coverage of the three TMDs, plus the cytosolic coiled coil (Figure 15D). OPTI density also shows two out of the three TMDs completely spanning the membrane and the third TMD being mostly complete (Figure 15D). Notably, many of the secondary structural elements are visible in nicalin (Figure 15H), and up to three of the twelve NOMO immunoglobulin domains are visible in NOMO (Figure 15G). Furthermore, TRAP density was markedly improved compared to previous structures, discussed in further detail below.

One of the aims of this project was to be able to visualize how a multipass client protein interacts with the Multipass Translocon during biosynthesis. The resulting structure contains density for what appears to be two putative YIPF1 TMDs (Figure 15E). One of them lies adjacent to TMCO1, while the other one lies nearby, between Sec61 and TMCO1. Because TMCO1 is part of the Oxa1 superfamily (Figure 15F), this TMD placement near TMCO1 suggests that TMCO1 is acting as an insertase. While it currently remains a challenge to assign the TMDs due to lack of side chain density, this data is

consistent with our hypothesis that TMDs are inserted through the thinned lipid bilayer caused by TMCO1's hydrophilic groove and are chaperoned during folding by the surrounding Multipass Translocon components.

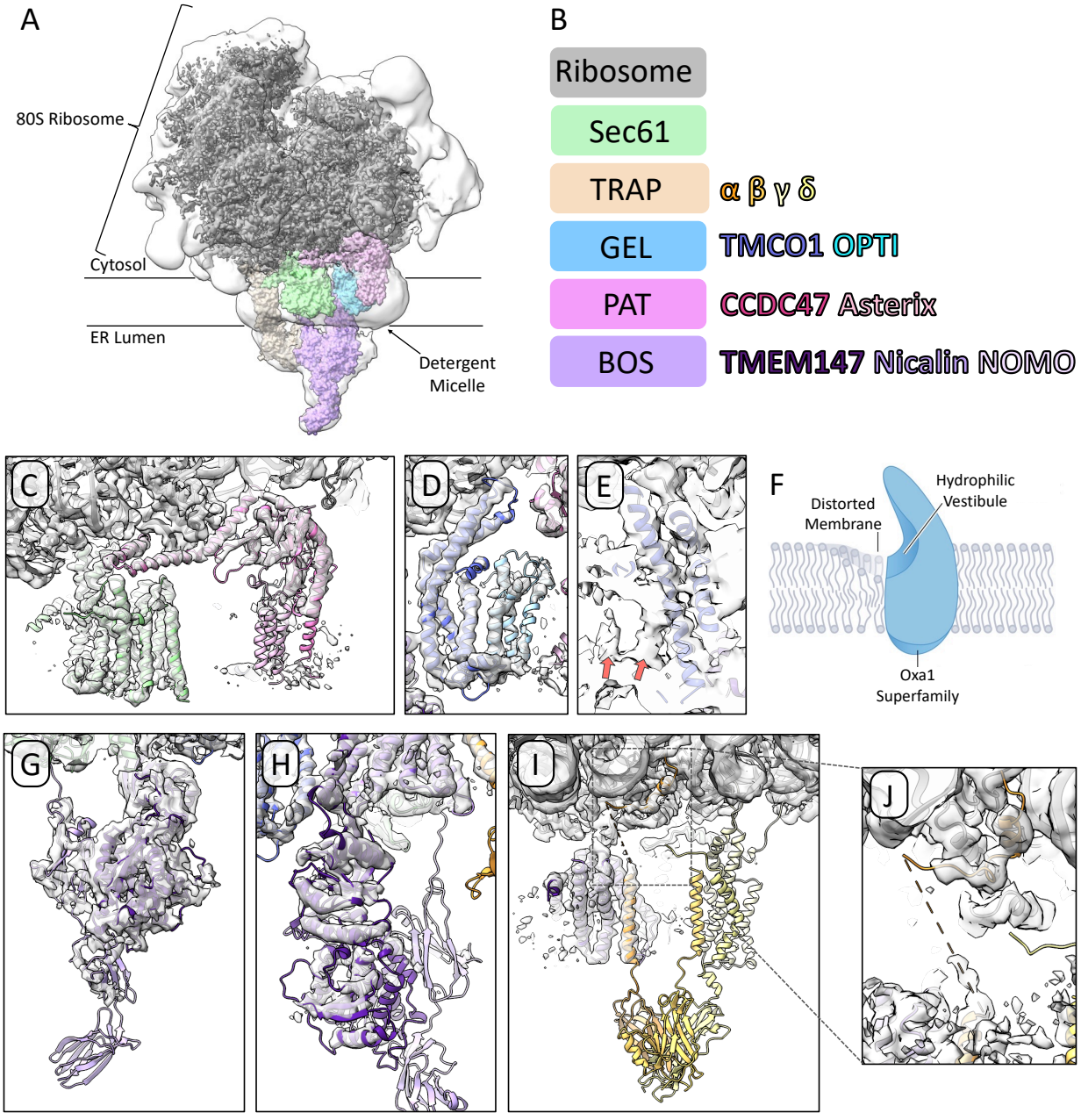

Figure 15. Structure of the Multipass Translocon programmed with YIPF1

For each subfigure, the cytosolic region is on top while the luminal region is on the bottom. **(A)** Overall density for the Multipass Translocon. Map #1 was lowpass

(Figure 15 Continued) filtered and shown at a lower threshold (transparent) to highlight luminal density and the micelle. Color schemes are shown in B. **(B)** Color scheme for the Multipass Translocon. Sec61 (green), the BOS complex (Nicalin = dark purple, TMEM147 = purple, NOMO = light purple), the GEL complex (TMCO1 = dark blue, OPTI = cyan), the PAT complex (CCDC47 = magenta, Asterix = light pink), and the TRAP complex (α = dark orange, β = orange, γ = light yellow, δ = yellow) (**C)** View of Sec61 and the PAT complex. **(D)** View of the GEL complex. **(E)** Putative substrate density for YIPF1 is visible near TMCO1's hydrophilic groove, pointed out by red arrows. **(F)** TMCO1 is part of the Oxa1 superfamily, which features a cytosolic-facing hydrophilic groove and a locally thinned membrane (Hegde & Keenan, 2022). **(G, H)** Close-up view of the BOS complex luminal domains. **(I)** View of TRAPα TMD adjacent to TMEM147 of the BOS complex. **(J)** Close-up view of TRAPα C-terminal latch helix adjacent to uL29 in the large ribosomal subunit.

3.7 TRAP Location in Core Translocon Versus the Multipass Translocon

Another notable feature of the structure is the presence of an additional TMD near TMEM147 of the BOS complex. Based on the location with the TRAPα luminal domain directly below it, it appears to be density for the TRAPα TMD (Figure 15I). The previously-observed TRAPα anchor (Jaskolowski et al., 2023) is also seen bound to uL29 in the large ribosomal subunit (Figure 15J). Notably, the location of this TRAPα TMD is shifted in the Multipass Translocon where it resides behind TMEM147, compared to its location in the Core Translocon where it resides behind Sec61 (Figure 16A). TMEM147 of the BOS complex overlaps with the location of the TRAPα TMD behind Sec61 in the Core Translocon (Figure 16A). Additionally, the other TRAP complex TMDs and luminal domains are also shifted back about 25 Å in the Multipass Translocon structure (Figure 16B). When the Multipass Translocon is overlaid with the Core Translocon, there is substantial overlap between the luminal domains of the BOS complex and the luminal domain of TRAPα (Figure 16C). Therefore, it is possible that the Multipass Translocon pushes TRAPα out of the way when it moves in.

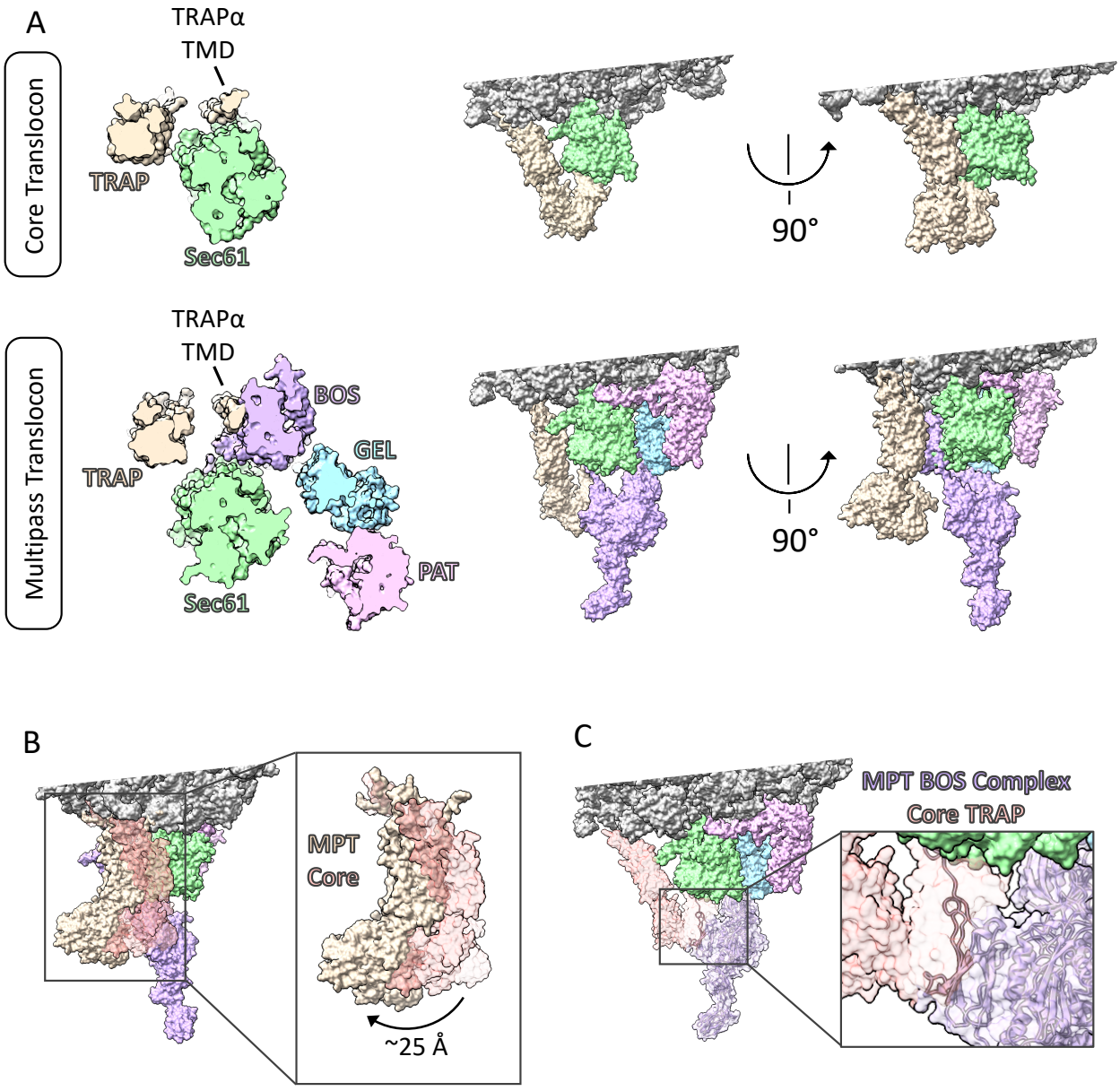

Figure 16. TRAP Location in the Core Translocon Versus the Multipass Translocon

(A) Views of the Core Translocon (top row) and the Multipass Translocon (bottom row). The translocons were aligned to the C-terminus of Sec61 (amino acids 242-465). Cytosolic view of the translocons (left image), front-facing view of the translocons (middle image), and side-facing view of the translocons (right image). **(B)** TRAP moves backward by about 25 Å in the Multipass Translocon (opaque beige) compared to its location in the Core Translocon (translucent red). **(C)** TRAP location from the Core translocon (translucent red) overlaid with the Multipass Translocon. The BOS complex is shown in translucent purple along with its

(Figure 16 Continued) secondary structural elements to highlight that TRAPα overlaps significantly with NOMO of the BOS complex.

3.8 Assembly of the Multipass Translocon in TRAPα Knockdown Membranes

To investigate the role that TRAPα plays within the Multipass Translocon, a TRAPα knockdown line was generated (Figure 17A and B). A recruitment experiment was carried out by immunoprecipitating the single pass membrane protein 4xFlag-ASGR1 truncated at position 112 with an “MLKV” stalling sequence (Figure 4A). Western blot analysis revealed an increase in the amount of Multipass components that assemble to the translocon in the TRAPα knockdown microsomes (Figure 17C). Notably, a significantly higher amount of NOMO, part of the BOS complex, was assembled, suggesting that the TRAPα knockdown allows for easier assembly of the BOS complex due to the lack of steric hinderance. When the multipass membrane protein 4xFlag-YIPF1 (Figure 4A), stalled at early (position 183) and late (position 277), was immunoprecipitated (Figure 17D), a similar result was observed. Higher levels of the Multipass Translocon assembled at the early intermediate with one TMD inserted into the membrane; however, for the later intermediate when multiple TMDs are already inserted, this effect is much more subtle.

In an effort to look at recruitment signals, ipomoeassin-F (IpomF) was added to the recruitment experiments. IpomF is a Sec61 inhibitor that binds to a partially opened lateral gate and stabilizes the plug domain such that it remains closed (Itskanov et al., 2023). When the above recruitment experiments were conducted in the presence of IpomF during translation, there was a significant reduction in the levels of STT3A (part of the OST complex of the Secretory Translocon) for both single pass ASGR1 and early intermediates of YIPF1 which resembles a single pass membrane protein (Figures 4A

and 17C,D). However, no significant change in STT3A levels was observed for the later multipass membrane proteins whether or not IpomF was added. These data could indicate that having an open Sec61 channel is required for signaling of the Secretory translocon, discussed in further detail below.

While these TRAP movements and initial experiments are interesting, what it means for multipass protein biogenesis remains unclear. While TRAP has been implicated to enhance the ability of proteins with weakly hydrophobic signal peptides to initiate co-translational translocation through Sec61 (Fons et al., 2003; Görlich et al., 1992) and as a chaperone to promote secretion and reduce ER stress (Jaskolowski et al., 2023), its role remains largely unknown. It has recently been shown that not all Multipass Translocons in the ER membrane contain the TRAP complex (Gemmer & Förster, 2020), suggesting that during synthesis of at least some substrates, TRAP may not be required. Preliminary IVT experiments showed similar YIPF1 glycosylation levels in WT and ΔTRAPα membranes; however, it remains possible that TRAP is important for the proper function of the Multipass Translocon. Therefore, the functional role of TRAP within the Multipass Translocon is yet to be determined.

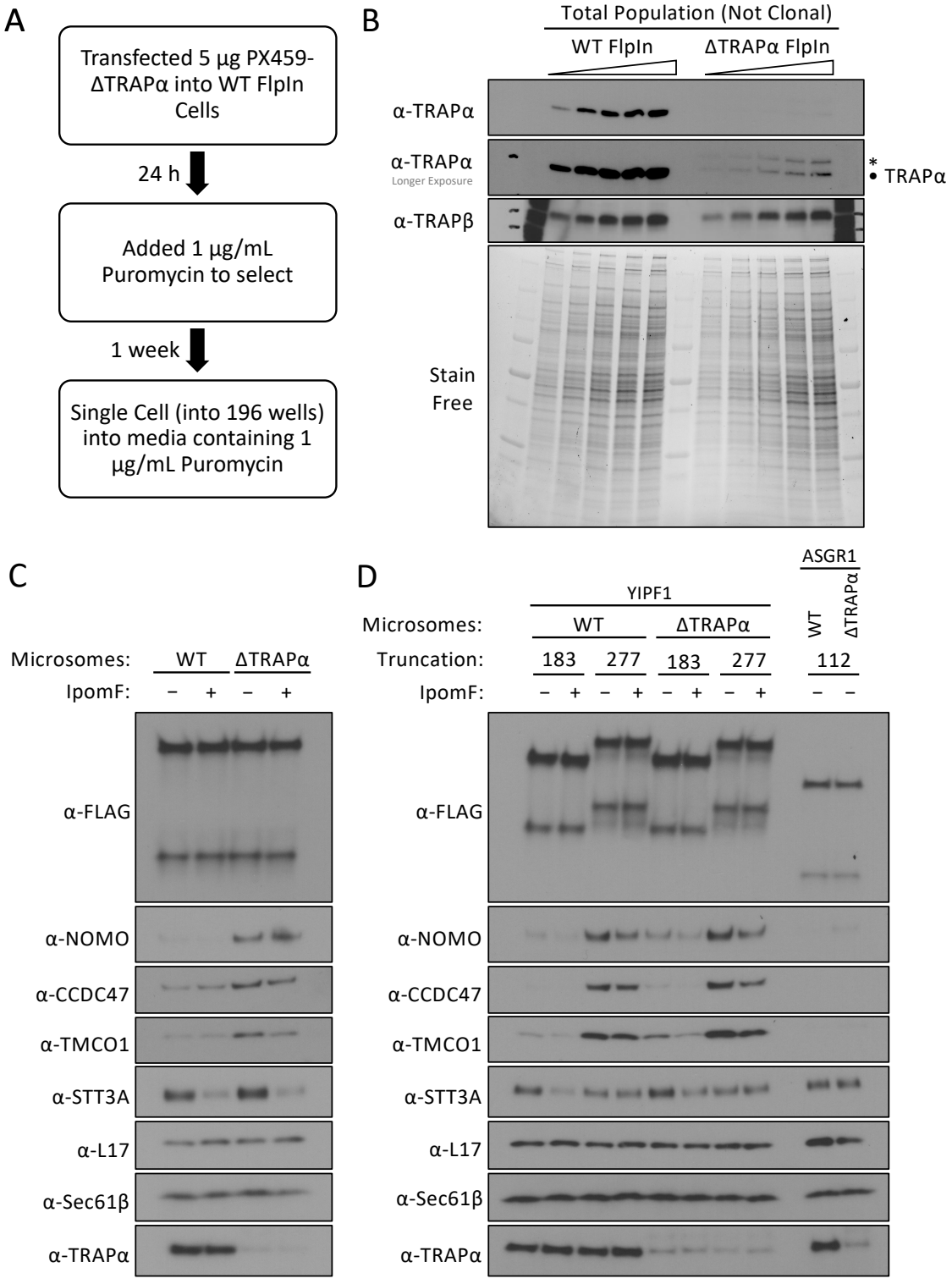

Figure 17. Assembly of the Multipass Translocon in TRAPα Knockdown Membranes

(A) Flowchart for generating TRAPα knockdown (ΔTRAPα) Hek293 single clonal cell line. A pX459 plasmid containing a TRAPα gRNA sequence and a puromycin

(Figure 17 Continued) resistance gene was transfected into WT FlpIn cells. After 24 hours, 1 µg/mL of puromycin was added as a selection reagent. Following one week of selection, cells were singe-cell sorted into two separate 96-well plates. Cells were allowed to grow up for about weeks and the knockouts were confirmed by DNA sequencing and western blotting. **(B)** Whole cell lysates from ΔTRAPα knock down FlpIn HEK293 cells were analyzed by SDS-PAGE and immunoblotting. The amount loaded was serial diluted to ensure equal loading. The asterix is an unknown higher molecular weight TRAPα band. **(C)** 4xFlag-ASGR1 was truncated at position 112 and an "MLKV" stalling sequence was added. It was translated in a rabbit reticulocyte lysate system in the presence of WT FlpIn or ΔTRAPα knock down FlpIn Hek293 microsomes. Where indicated, IpomF was added to a final concentration of 2 µM. Membrane-associated fraction was isolated by sedimentation. After anti-Flag immunoprecipitation of digitonin-solubilized microsomes, the stalled ribosome-nascent chain complexes were analyzed by SDS-PAGE and immunoblotting. **(D)** 4xFlag-YIPF1 was truncated at the indicated positions and immunoprecipitated as in C. ASGR1 samples stalled at position 112 are also included for reference.

3.9 Discussion

This work resulted in a cryo-EM structure of the Multipass Translocon programmed with the multipass membrane protein 4xFlag-YIPF1-Teminal-Valine(306) (Figure 4A). Density for many of the subcomplexes of the Multipass Translocon were improved compared to other previously reported structures (Gemmer & Förster, 2020; McGilvray et al., 2020; Smalinskaitė et al., 2022). Additionally, what appears to be putative substrate density in the central cavity of the Multipass Translocon is visible.

A major limitation with this structure is that the resolution for the two identified substrate TMDs is not sufficiently high to be able to confidently assign them to YIPF1. However, it is interesting that the putative substrate TMDs reside next to or nearby TMCO1. Because TMCO1 is a member of the Oxa1 superfamily and contains a hydrophilic groove which thins the membrane, it is possible that these two TMDs are part of a hairpin (for example, TMDs 1 and 2, or TMDs 3 and 4) that has been inserted by

TMCO1. This observation is very similar to what was observed in Smalinskaitė *et al*., where the TMDs of a multipass membrane protein are observed behind Sec61 in relation to its lateral gate. This, along with the data demonstrating that select type III multipass membrane proteins are Sec61 independent, helps to support a role for TMCO1 as an insertase. Although YIPF1 is a Type II membrane protein instead of a Type III membrane protein, it is proposed that the first two TMDs may be translocated through Sec61. The substrate then moves to the backside of Sec61, where the latter three TMDs are inserted (Sundaram*, Yamsek*, Zhong* et al., 2022). Further investigation is required to definitively assign the TMDs of this putative substrate density. Additionally, crosslinking may be carried out to verify its identity, as done previously (Smalinskaitė et al., 2022).

Another major observation of this structure was the movement of the TRAP complex in the Multipass Translocon relative to the Core Translocon (Jaskolowski et al., 2023). In the YIPF1-Terminal-Valine(306) structure presented in this thesis, there is density for the TRAPα TMD adjacent to TMEM147, in addition to the TRAPα C-terminal latch helix that makes contacts with uL29 of the large ribosomal subunit. Furthermore, when the two translocons are overlaid on the C-terminal half of Sec61, TRAP undergoes a significant movement in the Multipass Translocon. Overall, the TRAP complex is moved backward in relation to Sec61's lateral gate by approximately 25 Å. More specifically, the TRAPα TMD is observed on the back side of Sec61 in the Core Translocon (Jaskolowski et al., 2023), whereas it is located towards the back of TMEM147 in the Multipass Translocon. Interestingly, there is a significant steric clash between the luminal domains of TRAPα of the Core Translocon and the BOS complex (specifically NOMO) of the Multipass Translocon.

Preliminary data in which TRAPα was knocked down showed that components of the Multipass Translocon, especially NOMO, are more readily recruited in TRAPα knockdown microsomes. Notably, the Core Translocon TRAPα location and the first immunoglobulin-like domain of NOMO in the Multipass Translocon overlap significantly. Therefore, it appears that knocking down TRAPα can allow the Multipass Translocon to be recruited to the translocon more easily. While this effect is overall weak, it's possible that this observation would be more clear in the complete TRAPα knockout. Interestingly, this effect was more significant in recruitment experiments conducted on the single pass membrane protein ASGR1. Therefore, it's possible that TRAP helps to regulate Multipass Translocon recruitment by preventing it from assembling with the translocon non-specifically (i.e. with proteins that are not multipass). However, it has also recently been shown that not all Multipass Translocons contain the TRAP complex (Gemmer & Förster, 2020), which brings up the question about whether TRAP is necessary for multipass membrane protein biosynthesis. Overall, it is difficult to assign an actual biochemical role for TRAP and more research must be conducted to determine TRAP's role in the Multipass Translocon, in addition to the significance of TRAP relocation between the Core and Multipass Translocons.

When the Sec61 inhibitor IpomF was added to recruitment experiments, a significant reduction in the levels of STT3A was observed for both singlepass ASGR1 and early intermediates of YIPF1, which resembles a singlepass membrane protein. Sec61 inhibitors lock the lateral gate in a partially open state while stabilizing the plug domain in a closed conformation (Itskanov et al., 2023). The current model for Type II multipass protein (such as YIPF1) translocation through the Multipass Translocon posits that the

early TMDs are translocated and inserted through an open Sec61 channel. Once two or more TMDs are inserted into the membrane, the TMDs move to the back side of Sec61 where the Secretory Translocon is displaced and the Multipass Translocon is recruited (Sundaram*, Yamsek*, Zhong* et al., 2022). The Multipass Translocon keeps Sec61 in the closed conformation with the help of CCDC47 which wedges between the ribosome and Sec61 (Smalinskaitė et al., 2022). Therefore, when IpomF is added to recruitment experiments for singlepass membrane proteins or early multipass membrane proteins, Sec61's lateral gate is going from an open to partially-open state with a closed plug domain. Notably, OST makes contacts to Sec61 via its DC2 subunit. While this interaction seems to be stable in both opened and closed Sec61 states (Braunger et al., 2018), it is possible that an open Sec61 channel more strongly recruits OST and the Secretory Translocon. In the later YIPF1 truncation where multiple TMDs are inserted into the membrane, Sec61 is presumably in the closed position and there was no significant change in STT3A levels with and without IpomF. While this data is very preliminary, it could be a hint as to what the signals are for Secretory Translocon recruitment. However, these signals must be further evaluated in more detail.

CHAPTER 4. Future Directions

The data presented in Sundaram, Yamsek, Zhong *et al*. demonstrates that the Multipass Translocon is selectively recruited during multipass membrane protein biosynthesis. Furthermore, it shows that the translocon is dynamic, where the subunit composition adapts to accommodate the various biosynthetic requirements for a wide range of translational substrates. Multiple structures, including the 4xFlag-YIPF1-Terminal-Valine(306) structure described in this thesis, have now shown transmembrane density behind Sec61 (Braunger et al., 2018; Smalinskaitė et al., 2022). Notably, the Sec61 channel is closed in the Multipass Translocon structures, suggesting that proteins are not translocated through the channel. Furthermore recent work has shown that select Type III multipass membrane proteins are inserted independently of Sec61 (Smalinskaitė et al., 2022). In these experiments, addition of the Sec61 inhibitor IpomF had no noticeable effect on the insertion and glycosylation of Type III multipass membrane proteins with short loops. Therefore, a potential model for insertion of Type III membrane proteins is that the first TMD is inserted through EMC prior to docking to the Multipass Translocon which facilitates insertion of the subsequent TMDs. We speculate that other multipass membrane proteins (Type I and Type II) often only require an open Sec61 channel for the first one or two TMDs, and then are inserted on the back side of Sec61. Although multipass membrane proteins rarely contain long internal luminal loops, these proteins would require translocation through Sec61. Therefore, future work will focus on the mechanism of multipass membrane protein insertion, folding, and chaperoning on the back side of the Multipass Translocon.

Ultimately, one goal of our work is to obtain a complete picture of the synthesis of multipass membrane protein biogenesis. To accomplish this, we would attempt to obtain a molecular movie of multipass membrane protein biosynthesis. Herein, several cryo-EM datasets could be collected on a substrate stalled at various points during its translation. If the substrate is well-behaved and we are able to visualize density for the nascent chain for each structure, that will enable us to see interactions between the substrate and translocon. Such information would provide critical insights into how the Multipass Translocon is inserting latter TMDs. Additionally, it would allow us to see how the Multipass Translocon interacts during the folding of a multipass client protein.

While the YIPF1-Terminal-Valine(306) structure features improved density for much of the Multipass Translocon, ultimately it lacks definitive density for the multipass client protein. Several routes can be taken in an effort to improve these results. First, crosslinking can be carried out to verify the identity of the observed TMDs (as in Smalinskaitė et al., 2022). In addition to observed TMD verification, crosslinking may provide information as to Multipass Translocon component interactions with specific TMD's, allowing us to elucidate the mechanistic detail of TMD insertion. Additionally, different substrates can be screened in order to reduce the dynamics of the Multipass Translocon. First, it is likely that some client proteins interact with the Multipass Translocon more strongly than others, thereby allowing us to visualize the nascent chain. Second, the Multipass Translocon also features a large basket-like luminal domain made up of the TRAP and BOS complexes which could be involved in chaperoning client proteins with luminal domains. If this is true, it's possible that selecting a multipass client protein with a luminal domain could help improve the structure. Lastly, selecting a

substrate that contains a fully folded domain would potentially allow for a more stable structure. While previous data suggested that the Multipass Translocon dissociates from the ribosome once a domain is fully folded (Chitwood & Hegde, 2020), it's possible that if the client protein is able to fold, it may be less dynamic, allowing us to visualize its TMDs.

Another, more subtle, observation within the YIPF1-Terminal-Valine(306) cryo-EM structure is the presence of what appears to be lipid density in the micellular region. It is well-known that many proteins require lipids for their function (Chavent et al., 2018; Sych et al., 2022; Yen et al., 2018). Therefore, it's possible that digitonin-solubilizing the complex can lead to a less stable structure. Therefore, our lab is currently focusing on obtaining a high resolution cryo-electron tomography (cryo-ET) structure of a programmed Multipass Translocon in native ER microsomes. While cryo-ET is often limited in its capacity for obtaining high resolution information, there are several advantages of attaining the structure in its native lipid environment. First, it limits the potential for artifacts caused by digitonin solubilization into a micelle. Second, the sample preparation time is significantly decreased, which can potentially limit the dynamics in the sample and increase density for unresolved features such as the multipass client protein. Overall, we hope that cryo-ET in native membranes will allow us to visualize multipass folding intermediates in context with the Multipass Translocon.

A major question that remains is the role of each subcomplex of the Multipass Translocon. Recent data has demonstrated that the PAT complex acts as a chaperone to shield hydrophilic TMDs from the membrane (Chitwood & Hegde, 2020). More specifically, Asterix contains a highly conserved and amphiphilic domain that was shown to be involved in binding partially hydrophilic substrates (Smalinskaitė et al., 2022).

Additionally, CCDC47 wedges between Sec61 and the ribosomal exit tunnel to lock Sec61 in the closed conformation (Smalinskaitė et al., 2022). Further investigation is necessary to determine the full role of the PAT complex both independent of the Multipass Translocon and within the context of the Multipass Translocon.

Because TMCO1 is a member of the Oxa1 superfamily, it is likely that the GEL complex functions as an insertase (Anghel et al., 2017). A major feature of the Oxa1 superfamily is a cytosolic-facing hydrophilic groove which is thought to facilitate insertion by deforming the membrane. By thinning the membrane, insertases may lower the energetic penalty associated with translocating hydrophilic segments across the bilayer. Notably, other members of the Oxa1 superfamily (Oxa1 of the mitochondria, Alb3 of the chloroplast, and bacterial YidC in the plasma membrane) have been implicated in membrane protein insertion (Hell et al., 2001; Moore et al., 2000; Samuelson et al., 2000). Additionally Hrd1, which is a protein that retrotranslocates misfolded ER-luminal proteins, interacts with Der1 to form a large cytosolic-facing hydrophilic cavity (Wu & Rapoport, 2021). Therefore, it has been proposed that this hydrophilic cavity thins the membrane, which allows substrate hairpins to be retrotranslocated from the ER lumen.

While very little is known about the BOS complex, we speculate that it may be involved in post-translational chaperoning. One study has shown that depleting TMEM147 levels results in mistargeting of the lamin B receptor, and that TMEM147 forms interactions with both lamin B receptor and the sterol reductase DHCR7 (Christodoulou et al., 2020). Another study similarly showed that TMEM147 forms an interaction with CHRM3 in the ER, which decreases CHRM3 trafficking to the cell membrane (Rosemond et al., 2011). Another interesting feature of the BOS complex is the presence of conserved

residues on the luminal side of nicalin. Therefore, it's possible that the BOS complex may be involved in chaperoning the luminal components of multipass membrane proteins during their biosynthesis.

Because multipass membrane proteins vary widely in biophysical properties, topology, and loop length between TMDs, it is likely that the Multipass Translocon plays varying roles dependent on the client protein's characteristics. To investigate this question, we are currently working on ribosomal profiling experiments. Previously, we have performed RNA-sequencing on Multipass Translocons. Using a similar strategy, we have taken this one step further to examine the exact location on mRNA sequences at which the Multipass Translocon is recruited. Herein, the various subcomplexes of the Multipass Translocon were independently immunoprecipitated and the ribosome-protected mRNA footprints were isolated and sequenced. These results will provide additional information for when the Multipass Translocon components recruited. For example, many solute carriers contain two bundles of helices with a long loop in between the bundles. Because the Multipass Translocon is limited in the amount of space within its central cavity, it is likely that following insertion and folding of the first bundle, it moves out of the central cavity. Then, it's possible that the Multipass Translocon dissociates for the insertion of the early TMDs within the next bundle and is re-recruited at later TMDs in that bundle. Analysis of these sequences will allow us to better characterize the features that require the multipass translocon. One can imagine that certain clients may require the Multipass Translocon in its entirety while other clients may require only a subset of the Multipass Translocon. Furthermore, profiling data will enable to examine dynamics for the order of recruitment of the Multipass Translocon.

CHAPTER 5. Materials and Methods

5.1 Protocols Related to CHAPTER 2. Substrate-Driven Assembly of a Translocon for Multipass Membrane Proteins

5.1.1 Antibodies and siRNAs

Antibodies to human Sec61β (1:10,000 dilution), TRAPα ((Fons et al., 2003); 1:5,000) and TMCO1 ((Anghel et al., 2017); 1:5,000) were described previously. Other antibodies were obtained from the following commercial sources: rabbit anti-nicalin (A305-623A-M; 1:1,000) and rabbit anti-CCDC47 (A305100A; 1:2,000) from Bethyl Laboratories; mouse anti-HA (326700; 1:1,000), goat anti-NOMO (PA5-47534; 1:1,000), rabbit anti-TMEM147 (PA5-95876; 1:1,000), rabbit anti-Asterix (PA5-66788; 1:5,000), rabbit anti-C20Orf24 (PA5-43332; 1:1,000) and rabbit anti-Sec61α (PA5-21773; 1:1,000) from Invitrogen; rabbit anti-uL22 from Abgent (AP9892b; 1:1,000); mouse anti-tubulin (ab11304; 1:1,000) and mouse anti-HRP (ab6728; 1:1,000) from Abcam; mouse anti-Flag (F1804; 1:1,000), rabbit anti-Flag (F7425; 1:1,000), rabbit anti-peroxidase (SAB3700863; 1:10,000) and goat anti-peroxidase (A5420; 1:20,000) from Sigma; mouse anti-STT3A (H00003703-M02; 1:1,000) from Novus Biologicals; mouse anti-BiP/GRP78 (610979; 1:1,000) from BD Biosciences. siRNAs were purchased from Thermo Fisher: negative control (4390843), TMCO1 (s29085), C20Orf24 (s31821), Asterix (s28089), CCDC47 (s32576), Nicalin (s32411) and TMEM147 (s20404).

5.1.2 Constructs

pcDNA5 GFP–P2A–RFP–ASGR1 and pcDNA5 AGTR2–GFP–P2A–RFP fluorescent reporter constructs were described previously (Chitwood et al., 2018). pcDNA5 EAAT1–

GFP–P2A–RFP was constructed by Gibson cloning full-length human EAAT1 (amplified from a HEK293 cDNA library) into a modified pcDNA5/FRT/TO vector encoding a C-terminal GFP–P2A–RFP tag. pcDNA5 GFP–P2A–RFP–YIPF1 was generated by Gibson cloning a gBlock (IDT) into a modified pcDNA5/FRT/TO vector encoding an N-terminal GFP–P2A–RFP tag. Full-length constructs for *in vitro* translation (IVT) were generated by Gibson cloning gBlock (IDT) (YIPF1, ASGR1 and TMED2) or PCR fragments (EAAT1, KDELR1 and TRAM2) into a modified pSP64 vector encoding the desired N- or C-terminal Flag or HA tags. The 221-residue Flag–YIPF1(1–200)–Sec61β series was generated by Gibson cloning DNA fragments (Twist Biosciences) into a Flag–YIPF1 SP64 vector. The 142-residue Flag–ASGR1(1–61)– YIPF1(TM2)–Sec61β construct was generated by Gibson cloning into the parent Flag-ASGR1 SP64 vector. ASGR1(N79A) and YIPF1(N297A) substitutions were introduced using the QuikChange II Site-Directed Mutagenesis Kits (Agilent). A full-length Flag–YIPF1 construct was Gibson cloned into a pcDNA5/FRT/TO vector for *in vivo* glycosylation assays. All constructs were confirmed by DNA sequencing.

5.1.3 Cell Lines

Flp-In T-Rex 293 cells (Invitrogen) were maintained in DMEM supplemented with 10% FBS (Gemini Foundation), and 10,000 U/mL penicillin and 10 mg/mL streptomycin mixture (Invitrogen and Gemini). Cells were checked approximately every 6 months for mycoplasma contamination using the Universal Mycoplasma Detection Kit (ATCC), and were found to be negative. Single- and double-knockout (TMCO1, nicalin and CCDC47) HEK293 cell lines were generated by CRISPR–Cas9 as previously described (Anghel et

al., 2017; McGilvray et al., 2020). An STT3A-knockout cell line was generated similarly. Briefly, Cas9 expression was induced by addition of 10 ng/mL doxycycline followed by transfection of single guide RNA targeting STT3A (5′-TCGACATTCGGAATGTCTGT-3′). Cells were grown for 48 h, followed by single-cell sorting into 96-well plates for clonal isolation. Clones were verified by both western blot and genomic sequencing. Stable cell lines expressing N-terminally Flag-tagged TMCO1 and nicalin in the corresponding knockout background were described previously (McGilvray et al., 2020). A stable cell line expressing N-terminally Flag-tagged CCDC47 was generated similarly. Briefly, a CCDC47-knockout cell line was transfected with a modified pEGFP-n1 plasmid (Addgene) encoding N-terminally Flag-tagged CCDC47 (tag inserted after the signal peptide), under the control of a CMV promoter. Cells were transfected using TransIT-293 (Mirus) and selected in 0.7 mg/mL G418 (Invitrogen) for 2 weeks, changing the medium every 3 days. After selection, cells were maintained in medium supplemented with 0.3 mg/mL G418. Expression was verified by western blot. Stably integrated doxycycline-inducible ASGR1 and AGTR2 reporter lines for flow cytometry analysis were described previously (Chitwood et al., 2018). Other reporter lines were generated similarly. Briefly, pcDNA5-based reporter constructs were co-transfected with pOG44 into Flp-In T-Rex 293 cells with TransIT-293, according to the manufacturer's protocol (Invitrogen), and cells were selected in 100 µg/mL hygromycin B for 2 weeks.

5.1.4 Preparation of Rough Microsomes

HEK293 cells were grown to about 80% confluency in 15-cm dishes, washed once with 5 mL ice-cold PBS (per plate) and collected by scraping in 2 × 5 ml of PBS. Cells were

collected by centrifugation for 5 minutes at 500*g* and lysed in three volumes of hypotonic homogenization buffer (10 mM HEPES-KOH pH 7.5, 10 mM KOAc, 1 mM $MgCl_2$) for 15 minutes on ice, with gentle agitation every few minutes. Cells were then homogenized by 15 strokes (up and down) in a chilled dounce tissue grinder. Sucrose was added to a final concentration of 250 mM and mixed gently. Nuclei and cell debris were removed by centrifugation at 700*g* for 3 minutes at 4 °C and the supernatant was collected. The pellet was resuspended in 5 mL of insertion buffer (50 mM HEPES-KOH pH 7.5, 250 mM sucrose, 250 mM KOAc, 10 mM $MgCl_2$) and centrifuged again. The pooled supernatant fractions were centrifuged at 10,000*g* for 10 minutes at 4 °C. The supernatant was discarded, and the resulting membrane pellet was resuspended in insertion buffer (approximately 1 mL for about four plates). Microsomes (1-mL aliquots) were treated for 10 minutes at 37 °C with 4,000 U micrococcal nuclease (NEB), 2 U RNase-Free DNase (Promega), 1 mM $CaCl_2$ and 0.5 mM phenylmethylsulfonyl fluoride (PMSF), followed by quenching with 2 mM EGTA. Microsomes were pelleted at 10,000*g* for 10 minutes at 4 °C and resuspended in 1 mL insertion buffer, 40 U SUPERaseIn and 0.1 mM EGTA, followed by centrifugation at 10,000*g* for 10 minutes at 4 °C. The supernatant was discarded, and the membrane pellet was resuspended in insertion buffer supplemented with 50 U SUPERaseIn (per four plates). The preparation was finally adjusted with insertion buffer to an absorbance at 260 nm (A260 nm) of about 50, and 50-µL aliquots were flash frozen in liquid nitrogen and stored at −80 °C for further use.

5.1.5 Interaction Analysis in Stably Integrated Cells

Microsomes from wild-type cells and cells encoding Flag-tagged versions of TMCO1, CCDC47 or Nicalin were prepared as above, except that the micrococcal nuclease digestion was performed with 10,000 U of micrococcal nuclease (NEB), 3 U DNAse (Promega), 1 mM $CaCl_2$ and 0.6 mM PMSF, and incubated at room temperature for 20 minutes before quenching with 2.5 mM EGTA. Microsomes (1 mL at A260 nm = 50) were solubilized in insertion buffer supplemented with 2.5% digitonin and 1X protease inhibitor cocktail (Roche, 11836170001) for 45 minutes on ice and then diluted twice with 150 mM KOAc insertion buffer. Digitonin-solubilized microsomes were cleared by centrifugation at 12,500*g* for 15 minutes at 4 °C. The cleared supernatant (A260 nm of about 3.5) was immunoprecipitated in batch format using 50 µL M2 Flag affinity beads (Sigma, A2220) and gentle agitation overnight at 4 °C. Flow-through was removed and beads were washed three times with eight column volumes of insertion buffer supplemented with 0.4% digitonin. Bound material was eluted twice, for 30 minutes on ice, with two column volumes of 200 mM KOAc insertion buffer supplemented with 0.5 mg/mL Flag peptide (ApexBio, A6001) and 0.4% digitonin. The eluate was collected using a pre-equilibrated spin filter column (Thermo Fisher, 69725). Ribosome-free and ribosome-bound fractions were obtained by pelleting the eluate through a 300-µL sucrose cushion (50 mM HEPES pH 7.4, 10 mM $MgCl_2$, 150 mM KCl, 500 mM sucrose and 0.4% digitonin) at 355,000*g* for 1 hour at 4 °C in a TLA120.1 rotor.

5.1.6 *In vitro* Transcription and Translation

In vitro transcription reactions utilized PCR-based templates containing an SP6 promoter, and were carried out at 40 °C for 1 hour (Sharma et al., 2010). Unless otherwise noted, reactions contained 5–10 ng/µL PCR product, 40 mM HEPES pH 7.6, 6 mM $MgCl_2$, 2 mM spermidine, 10 mM dithiothreitol, 500 µM ATP, 500 µM UTP, 500 µM CTP, 100 µM GTP, 0.5 mM m7G(5′)ppp(5′) G RNA Cap, 0.4 U/µL SUPERaseIn and 0.4 U/µL SP6 RNA Polymerase. IVT reactions were performed using a RRL system (Green Hectares). Translation reactions contained 20% (*v/v*) of the unpurified transcription reaction, 33% (*v/v*) hemin- and micrococcal nuclease-treated RRL, 0.2 µCi/µL [35S]methionine (or 40 µM methionine for non-radioactive IVT reactions), 0.1 mg/mL bovine liver transfer RNA, 13 mM HEPES, 10 mM creatine phosphate, 1 mM ATP, 1 mM GTP, 9 mM KOH, 25 mM KOAc, 1 mM $MgCl_2$, 40 µM of the remaining 19 amino acids and 10% (*v/v*) HEK293-derived microsomes (typically A260 nm of about 50). Translation reactions were carried out for 45 minutes at 32 °C, unless otherwise noted.

5.1.7 Interaction Analysis of Stalled Ribosome–Nascent Chain Complexes *In Vitro*

Templates for the synthesis of stalled N-terminally Flag-tagged substrates were PCR amplified using reverse primers encoding a terminal Met-Leu-Lys-Val (5′-CACCTTGAGCAT-3′) sequence and lacking a stop codon. *In vitro* transcription and translation reactions were performed essentially as described above. Briefly, 100 µL of *in vitro* transcription mix containing 500 ng of purified PCR template was incubated for 1 hour at 40 °C. Translation reactions of 500 µL contained 60 µL microsomes (A260 nm of about 50) and 100 µL of the unpurified transcription reaction, and were carried out for 50

minutes at 32 °C. The translation reactions were stopped by diluting them with 500 µL IVT stop buffer, and microsomes were pelleted at 12,500*g* for 10 minutes. Microsomes were washed again with 1 mL IVT stop buffer, centrifuged at 12,500*g* for 10 minutes, and resuspended with 500 µL IVT stop buffer. The resuspension was then treated with 5,000 U micrococcal nuclease (NEB), 1 mM $CaCl_2$ and 0.6 mM PMSF at room temperature for 20 minutes. The reaction was stopped with 2.5 mM EGTA, and centrifuged at 12,500*g* for 10 minutes. The resulting membrane pellet was solubilized with 200 µL insertion buffer supplemented with 2.5% digitonin and 1X Protease Inhibitor for 45 minutes on ice, then diluted 2X with 150 mM KOAc insertion buffer, and cleared by centrifugation at 12,500*g* for 15 minutes. The cleared supernatant (A260 nm of about 1.0) was incubated overnight at 4 °C with 20 µL M2 Flag affinity beads. Flow-through was removed and beads were washed 3 times with 18 column volumes of insertion buffer containing 0.4% digitonin and 200 mM KOAc. Bound material was eluted twice with two column volumes of 200 mM KOAc insertion buffer supplemented with 0.5 mg/mL Flag peptide and 0.4% digitonin, by incubating for 30 minutes each on ice. The eluate was collected using a pre-equilibrated spin filter column. Eluted material was layered over a 300-µL sucrose cushion (50 mM HEPES pH 7.4, 10 mM $MgCl_2$, 150 mM KCl, 500 mM sucrose and 0.4% digitonin) and pelleted at 355,000*g* for 1 hour at 4 °C in a TLA120.1 rotor. The ribosomal pellet was resuspended in 35 µL of sucrose cushion buffer, normalized by A260 nm, and then analyzed by SDS–PAGE and immunoblotting.

5.1.8 Carbonate Extraction

IVT reactions (150 µL) synthesizing Flag–YIPF1 were diluted tenfold with IVT stop buffer and membranes were centrifuged for 10 minutes at 10,000*g*. The membrane pellets were resuspended with 150 µL IVT stop buffer, and one-third of the reaction was reserved as the input fraction. The remaining material was incubated with 100 volumes of 100 mM Na_2CO_3 (pH 11.5) for 30 minutes on ice. The sample was centrifuged at 214,000*g* for 40 minutes in a TLA100.3 rotor to isolate membranes, and the supernatant was discarded. This was repeated once to remove contaminating proteins. The resulting carbonate-extracted membranes were resuspended with 1X LDS sample buffer for analysis.

5.1.9 Protease Protection Assays

YIPF1–HA was synthesized in three 150-µL IVT reactions either lacking or containing microsomes. Immediately following synthesis, the samples were diluted with ten volumes of IVT stop buffer. Microsome-containing samples were centrifuged at 10,000*g* for 10 minutes to pellet membranes and remove hemoglobin, and then resuspended to 150 µL with IVT stop buffer. All three samples were then split into three equal fractions for PK analysis. The untreated fractions (−PK) were set aside, and PK was added to the other samples (+PK) to a final concentration of 0.5 mg/mL and incubated on ice for 45 minutes. The digestion was quenched with 5 mM PMSF and incubated on ice for 5 minutes, followed by addition of ten volumes of boiling 1% SDS, 100 mM Tris pH 8 and 1X Roche cOmplete Protease inhibitor cocktail. For analysis of the total PK-treated fraction, samples containing microsomes were TCA-precipitated to concentrate membranes before SDS–PAGE analysis. For HA immunoprecipitations, samples were diluted tenfold with

immunoprecipitation buffer (1X PBS, 250 mM NaCl, 0.5% (*v/v*) Triton X-100) and 30 µL HA agarose resin (Pierce, 26181) was added. Samples were incubated for 2 hours at 4 °C with gentle agitation, washed three times with 1 mL of immunoprecipitation buffer, and eluted by adding 50 µL 1X LDS sample buffer and incubating at 70 °C for 10 minutes.

5.1.10 Glycosylation Analysis *In Vitro*

IVT reactions (35 µL) synthesizing HA–YIPF1, HA–ASGR1 or TMED2–HA were carried out for 50 minutes at 32 °C. Immediately following translation, microsomes were washed twice with 15 volumes of IVT stop buffer (50 mM HEPES pH 7.5, 200 mM NaCl, 10 mM $MgCl_2$) and then collected by centrifugation at 13,000*g* for 10 minutes. Membrane pellets were lysed with 35 µL IVT stop buffer containing 1.5% DDM for 30 minutes on ice, and centrifuged at 13,000*g* for 10 minutes. A 30 µL volume of lysed material was diluted with 75 µL of 3X LDS sample buffer containing 2% β-ME, heated at 65 °C for 10 minutes, and then analyzed by SDS–PAGE and immunoblotting. Reactions without microsomes (30 µL) were supplemented with 1.5% DDM, diluted with 100 µL of 3X LDS sample buffer containing 2% β-ME, and loaded at one-tenth the amount relative to the microsome samples.

5.1.11 Glycosylation Analysis in Cells

At 24 hours before transfection, wild-type, ΔTMCO1, Δnicalin and ΔCCDC47 HEK293 cells were seeded at 400,000 cells per well onto a poly-lysine-coated 6-well plate, in triplicate. A transfection mixture containing 1 µg pcDNA5 Flag–YIPF1, 150 µL Opti-MEM and 3 µL TransIT-293 was incubated at room temperature for 25 minutes before being

added dropwise to each well. A final concentration of 1 ng/mL doxycycline was added to induce Flag–YIPF1. Following 12 hours of induction, cells were collected by scraping with chilled 1X PBS. Cells were pelleted at 500*g* for 5 minutes and resuspended in 100 µL RIPA buffer (50 mM Tris pH 7.4, 150 mM NaCl, 1% NP-40, 0.5% sodium deoxycholate, 0.1% SDS, 1 mM PMSF, 1X Roche cOmplete Protease Inhibitor Cocktail). RIPA lysis samples were incubated on ice for 15 minutes and gently vortexed every 5 minutes. The samples were centrifuged at 15,000*g* for 10 minutes, and the supernatant was collected for SDS–PAGE and western blot analysis.

5.1.12 Flow Cytometry Analysis of Reporter Cell Lines

The effect of different siRNAs on stably expressed reporter cell lines was analyzed using flow cytometry as described previously (Chitwood & Hegde, 2020). siRNA depletion was performed over a period of about 72 hours using the Lipofectamine RNAiMAX reagent (Thermo Fisher) according to the manufacturer's instructions. Briefly, a first round of siRNA treatment was performed in the presence of DMEM and 10% tetracycline-free FCS. Cells were incubated for 48 hours, and then a second round of siRNA treatment was performed. After a second incubation of about 24 hours, expression of fluorescent reporter constructs was induced with 1,000 ng/mL doxycycline for 6 hours before analysis by flow cytometry. In all experiments the cells were collected by trypsinization, washed once in ice-cold PBS, and then resuspended 1 mL of PBS. Cells were passed through a 70-µm filter before flow cytometry analysis using a Becton Dickinson LSRII instrument. Live cells were gated by forward and side scatter. Additional gating for relatively high levels of the soluble fluorescent protein reporter was used to focus on the population of

cells with productive translation of reporter constructs. Between 15,000 and 30,000 GFP-positive (EAAT1 and AGTR2) or RFP-positive (ASGR1 and YIPF1) cells were collected. Data were analyzed using FlowJo (version 10.8).

5.1.13 Statistics and Reproducibility

Biochemical experiments *in vitro* and functional assays in cells were repeated in part or in full on separate and independent occasions with similar results. Fully replicated experiments include each of the following (with the number of repeats in parentheses): Figures 3a (n = 2), 4f (n = 5), 6b (n = 2), 7a (n = 3), 8b (n = 2), 9a–d,f,i,j (n = 5, 3, 5, 3 (for YIPF1) 5, 2 and 2, respectively) and 10c (n = 2). Other experiments were partially replicated in pilot experiments not shown, or as part of other experiments. These include: Figures 2b,c, 4b,c, 5b,c, 6c, 8c and 9d (ASGR1 and TMED2), and 10a,d,e. For example, the interaction analysis in Figure 4b was performed once as shown, but it was first piloted by monitoring recruitment of a subset of components by several key ASGR1 and YIPF1 intermediates; in addition, the YIPF1 intermediate series was repeated once in its entirety with identical results. In other instances, parts of one experiment were validated by replication in another experiment (for example, Figure 4b,c, 5b,c and 6b,c). Therefore, these experiments can be considered to have been reproduced at least once, even when the experiment shown was not formally repeated. Statistical analysis of replicates of the data shown in Figure 9d,f (n = 3 and 5, respectively) was performed by ordinary one-way ANOVA with Dunnett's multiple comparison test (single pooled variance) in GraphPad Prism 9.4.0. Statistical analysis of replicates of the data shown in Figure 4f (n = 5) was performed by repeated measures one-way ANOVA with the Geisser–Greenhouse

correction and Tukey's multiple comparison test. The bar graphs in Figure 7b and Figure 9e,g show the individual data points, mean and s.d. *P < 0.0332; **P < 0.0021; ***P < 0.0002; ****P < 0.0001. The source data can be found in Supplementary Tables 1 and 2.

5.2 Protocols Related to CHAPTER 3. Progress Toward a Cryo-EM Structure of a YIPF1-programmed Multipass Translocon

5.2.1 Cryo-EM Sample Preparation and Data Acquisition

Notably, while the YIPF1-Terminal-Valine grid (described below) was prepared using *in vitro* transcription mix lacking DTT, optimization experiments have shown that the replacement of 10 mM DTT with 10 mM glutathione helps to prevent ribosomes from aggregating on grids. The transcription reaction is not purified prior to addition into the translation reaction, so the translation reaction will contain 2 mM glutathione in the final reaction. Other optimization experiments seemed to indicate that the addition of freshly prepared 1 mM glutathione to all immunoprecipitation buffers and that micrococcal nuclease treating the sample following *in vitro* translation and adding also helps with particle distribution on the grid. To ensure that all the micrococcal nuclease is quenched following the incubation, the digitonin solubilization buffer is supplemented with 5 µL (100 U) of SUPERaseIn RNase inhibitor per mL. In an effort to increase the final concentration of the sample and ultimately the number of particles on the grid, the sample is eluted from the Flag resin in small volumes (For 60 µL M2 Flag Resin, Elution 1 = 16 µL, Elution 2 = 24 µL, and Elution 3 = 30 µL) and placed on a nutator at room temperature for 15 minutes for each elution. Importantly, prior to elution, any residual wash buffer is removed with a 20 µL pipette. Yield varies depending on the *in vitro* translation substrate; however, the

second elution is typically the highest concentration and often ranges from about 15-50 nM ribosomes (A260 = 0.75 to 2.5; $\varepsilon_{A260} = 5 \times 10^7\ M^{-1}\ cm^{-1}$) (Matasova et al., 1991). To limit the extent to which particles fall apart, the sample is prepared as quickly as possible. Do not incubate the sample on the Flag resin overnight for cryo-EM sample preparation! From start to finish (including grid freezing on the vitrobot), the preparation takes about 6 hours total. Another modification that is recommended for cryo-EM samples is to decrease the amount of digitonin used. It's possible that higher levels of digitonin could wash away lipids that may be important for function of the Multipass Translocon (Frenkel et al., 2014), so by lowering the digitonin concentration we hope to minimize those effects. Optimization experiments have shown that 0.5% digitonin is sufficient for the solubilization buffer and that 0.1% digitonin is sufficient for the wash and elution buffers.

For the YIPF1-Terminal-Valine(306) cryo-EM sample, *in vitro* transcription and translation reactions were performed similarly to those as described above. One major modification to the transcription reaction included the absence of DTT in the transcription reaction. A 2 mL translation reaction was carried out using 4xFlag-YIPF1-Terminal-Valine stalled at amino acid 306 as the substrate in combination with WT Cas9 Hek293 microsomes. Following *in vitro* translation, micrococcal nuclease treatment, digitonin solubilization, and Flag immunoprecipitation were carried out as described above. A couple of modifications included the use of 60 µL M2 Flag Resin, the addition of 1 mM DTT to all immunoprecipitation buffers, and elution in smaller volumes at 30 °C to maximize concentration for loading onto grids.

Quantifoil R1.2/1.3 200 mesh gold grids coated with 2 nm amorphous carbon were glow dischared for 25 s at 5 W immediately before use. Using a Thermo Vitrobot Mark IV

system, 3 µL of 16 nM (A260 = 0.8; ε_{A260} = 5 × 10^7 M^{-1} cm^{-1}) programmed ribosomes containing the Multipass Translocon (Matasova et al., 1991). Grids were incubated for 60 seconds at room temperature (22 °C) and 100% humidity before blotting for 7 seconds with Whatman filter paper at a force of −1, draining for 0.5 seconds, and being plunged into liquid nitrogen-cooled ethane.

Data was collected on a FEI Titan Krios at 300 KV with EPU software, using a defocus range from -1.9 to -0.9 µm. Super-resolution movies (pixel size = 0.84 Å) were recorded at 53,000X magnification using a Gatan K3 energy filter and direct electron detector and a total electron exposure of 60 $e^-/Å^2$ over 52 frames.

5.2.2 Cryo-EM Image Processing

All data processing was performed in RELION-4.0.1. Following Topaz particle picking and 2D classification, the initial 3D refinement contained 1,113,500 particles. Initial 3D classification on the entire complex produced 7 similar classes (83.6%) that contained density for the Multipass Translocon, one class (5.7%) that lacked the small 40S ribosomal subunit, and one poorly-aligned class (10.7%). Careful refinement on 928,794 particles was done in four rounds of 3D refinement, post-processing, and CTF-refinement, followed by a final Bayesian polishing step once the estimated final resolution had stabilized. Focused classification with signal subtraction on the Multipass Translocon (excluding significant ribosome density) identified a subset of 232,563 particles containing the Multipass Translocon. Further focused classification with signal subtraction on the BOS complex resulted in a class with 145,202 particles. This class was reverted to its original, ribosome-containing state and refined again, focused on the translocon region.

DeepEMhancer was also used for the final map volumes with the wide target deep learning model (Sanchez-Garcia et al., 2021).

5.2.3 Generation of Puromycin-Selected Knockout Line

A TRAPα (SSR1) knockout cell line was generated using a pSpCas9(BB)-2A-Puro (pX459) plasmid containing a puromycin resistance gene. The guide RNA sequence (5'-AUCAUUAGGCUUGUUAGCAG-3') was chosen based on Synthego's knockout guide design tool. Briefly, 400,000 WT FlpIn HEK293 cells were seeded into a 6-well plate 24 h before transfection. At the time of the transfection, cells were approximately 80% confluent. A transfection mixture was prepared with 250 µL Opti-MEM, 2.5 µg pX459-TRAPα(SSR1)-gRNA, and 7.5 µL TransIT-293. The transfection mixture was incubated at room temperature for 15 minutes before being added dropwise to the plated cells. After 24 hours, puromycin was added to a final concentration of 1 µg/mL and the cells were selected for 1 week. Following puromycin selection, cells were single cell sorted by light scatter into a 96-well plate using a BD FACSAria Fusion cell sorter. Cells were expanded and single clonal knockout lines were verified by both immunoblotting and genomic sequencing.

Genomic DNA was isolated from cells in a 6-well plate using the Lucigen QuickExtract DNA Extraction Solution. For genomic DNA sequencing, primers were designed to amplify a 500-700 bp fragment, with the guide RNA cut site in the middle. To maximize success rates, it is recommended to design at least three pairs of primers, ranging in both primer length and melting temperature. For this knockout line, the melting temperature of the three primer sets was varied from 60-65 °C. New England Biolabs T_m

Calculator was used for calculating the annealing temperature during PCR, and a touchdown PCR program was successful at amplifying a single band from the genomic DNA. Herein, the annealing temperature started higher (72 °C) for the first cycle and 1 °C was subtracted from the annealing temperature until a final annealing temperature of 67 °C (suggested by the New England Biolabs T_m calculator) was reached. Another modification that has helped with genomic DNA amplification success rates is the addition of 3% (*v/v*) DMSO.

5.3 Other Protocols

5.3.1 Digitonin Recrystallization

Digitonin is the most widely-used detergent for cryo-EM and used in up to a third of all sample preparations (Choy et al., 2021). Digitonin is a natural product isolated from the foxglove plant and is useful because it preserves the native lipid environment of membrane protein complexes. However, each batch must be further purified from other contaminating molecules to limit precipitation during use and batch-to-batch variation. A simple ethanol recrystallization procedure is used for purification, which was developed by Ben Zalisko in the lab. As an alternative to digitonin recrystallization, some labs have begun to use the digitonin synthetic analog glycol-diosgenin (GDN) (Guo et al., 2017; Velazhahan et al., 2021). However, it is advised to proceed with caution when using GDN. Therefore, our lab has continued to use digitonin to limit potential extraneous effects.

Digitonin (Millipore Sigma, 300410) was added to a 100 mL Pyrex bottle and weighed before starting the recrystallization procedure. Then, 40 mL of 200 proof ethanol and a stir bar were added to the container. The initial 5 g vial of digitonin was washed with 750 µL of 200 proof ethanol four times to ensure a quantitative transfer to the 100

mL bottle, with the final wash being clear and colorless after the fourth wash. The bottle was placed into a water bath just deep enough to come up to the level of ethanol in the bottle. The digitonin and ethanol mixture was slowly heated to 80 °C, at which point the ethanol was completely dissolved. Then, the digitonin was removed from the water bath and wrapped in a thick layer of aluminum foil to slowly cool. Once cooled, the digitonin will settle to the bottom of the bottle. The supernatant was transferred to a falcon tube and centrifuged at 3220*g* for 20 minutes to isolate any digitonin that did not pellet. The ethanol supernatant was discarded and the digitonin pellet was transferred bath to the 100 mL bottle with 200 proof ethanol. This ethanol recrystallization procedure was repeated a second time to remove any other impurities. Following the second round of recrystallization, the ethanol was evaporated overnight under reduced pressure using an Edwards RV3 vacuum pump. After drying, the bottle with digitonin was again weighed to calculate percent yield, which is typically around 70-75%. Solubility was tested by preparing a small amount of 2.5% (*w/v*) digitonin and placing in the cold room at 4 °C. Many digitonin recrystallization preparations remain soluble at 4 °C for at least a week, but as long as it is soluble for more than 24 hours, it should be sufficient for experimental use. For additional quality control, it is also recommended to test the new versus old digitonin batch in a side-by-side immunoprecipitation experiment.

5.3.2 Guide to Setting up a Data Collection using EPU

The following section is a guide to setting up a data collection on the Titan Krios using EPU automated software. This guide can also be used for screening sessions, where the number of holes imaged per grid square can be set to a smaller number.

Set up your Session:

If you're the first one setting up a session, Create a new session queue. Don't load presets from previous day. *If somebody has already started a queue*, load your grid and then add to the current EPU session. It is very important that you do these steps before changing any settings (magnification, exposure time, etc.) so that you don't erase the other user's settings.

General Session Settings:

Session Name: <Date>_LabName>_<YourName>_<GridName>

Acquisition Mode: Faster

Image Format: Tiff

Dose Fraction Output Form: Tiff Lzw Non-Gain Normalized

Output Folder: Leave as the default (in the root of the Dose Fractions Folder)

Import Optics Session: 53,000X from the EPU presets folder

Open the most recent optics session (Preparations Tab > Import > .sxml file). Change the square magnification based on the mesh size (470X for 200 mesh grids and 580X for 300 mesh grids is good). To save a new optics session (.sxml file), click on Export in the Preparations tab

Calibrate Image Shifts: This is recommended if the optics session is more than a few months old. It's best to do it every time. Change the exposure time to ~2 s (the loaded optics session may have an exposure time of ~ 16 s for the actual data collection). Move over a chunk of ice or other recognizable feature and center it in the data acquisition magnification. Click on Autofunctions > Autoeucentric by Beam Tilt > Hole/Eucentric

Height > Start. Then, click on Calibrate Image Shifts in (Preparations tab) and follow the directions on the right hand side of the screen to calibrate the image shift.

EPU Tab:

Square Selection:

When you first go to this tab, all the squares will be highlighted > Unselect All > Select squares (Right Click > Select)

Select Holes:

Select a square that is thicker and with more ice chunks in it (it will have a white border so that you know it is selected)

Autoeucentric > Aquire

Measure the hole size > Find Holes

Note: If you're screening, there's a drop-down menu to limit the number of holes to ~5 per square

Right Click on a hole with ice chunk in it > set lower bound > Manually type a number slightly higher than that and click Apply.

Click on "Remove holes close to grid bar."

The total number of exposures will be shown on the right hand side. Add more squares if you want more data collected. A typical 24 h data collection will take ~4000-5000 movies, so I usually ask for ~ 5500.

Template Definition:

Load Data Collection template (Import > EPUPresets/2022_07_21_Basic_Data_25to09.epuTemplate)

Line up templates (autofocus area should lie in between the four holes)

Click on template > Change defocus list (-1.9 Å and above is good for large ribosome particles)

Note for Screening and Pilot Data Collections:

Create an extra session ("dummy") with 1 exposure if there is somebody after you. This is to prevent somebody from accidentally erasing your optics settings. Make sure that the session is last in the queue and that it is highlighted (double click on it) before you leave.

Automated Acquisition:

Set the zero loss to "yes."

Set Exposure Time:

Move over a square with a tear in it

EF-CCD camera (righthand computer) should be on Counted 1X mode

Take a picture at Data Acquisition magnification (preparations tab) > Click on SET button (middle of the upper tab) > Capture (computer on the right)

A dose rate of ~10-14 e-/s/pixel is good. You may need to adjust the beam area (µm) size in Preparations tab, but the beam size is often ~ 1.7-1.9 µm.

To calculate exposure time from dose rate: Record these numbers – they are needed for the motion correction job in Relion.

Use a total dose of 60 e-/Å^2 over 52 frames (1.15 e-/Å^2 per frame)

Say the dose rate is 11 e-/s for example

Pixel size will depend on magnification. For 53,000X, it's 1.68 Å

$$\frac{60\ \mathrm{e^-}}{\mathrm{Å^2}} \times \frac{\mathrm{pixel}}{11\ \mathrm{e^-s}} \times \frac{(1.68\ \mathrm{Å})^2}{\mathrm{pixel}} = 15.4\ \mathrm{s}$$

Other Notes:

For a good grid with ribosomes, a pilot dataset with 500 micrographs will be sufficient to produce nice 2D classes. It's recommended to collect a small dataset before a full data collection to ensure that the frozen sample is good. *Save the atlas image with the squares collected on*! This is necessary if you want to do another data collection on the same grid. Make sure there is storage space so that the run doesn't stop. If somebody is screening after you, ask them or somebody in the core facility to start the session. Close the column valves if you need to leave at any point.

5.3.3 Canine Pancreatic Microsome Preparation

This protocol was adapted from Susan Shao's lab, which was adapted from the Lingappa lab. Other protocols that were referenced during this canine microsome prep include the following: (Bernstein, 1998; Sabatini, 2014). To obtain the pancreas material, a veterinarian from the University of Illinois Chicago (Lisa Halliday, DVM) was contacted. The pancreas was harvested around 1:45 pm and placed in a plastic bag placed on ice. The microsome prep was started around 2:15 and took approximately 5 hours to complete from that point on.

Canine pancreas was isolated from a 35 kg hound and kept cold the entire time. Half of the harvested pancreas was immediately used for a microsome prep while the other half was frozen in liquid nitrogen and stored at –80 °C for a future preparation. The pancreas was broken up into small pieces (~0.5-1 cm) on a glass plate and blood vessels and connective tissue were removed with forceps. The isolated pancreas was weighed, and 4 mL Buffer A (50 mM HEPES pH 7.4, 50 mM KOAc, 6 mM $Mg(OAc)_2$, 1 mM EDTA,

1X Roche cOmplete EDTA-free Protease Inhibitor Cocktail) was added per gram of tissue. The tissue was blended and pulsed about 5 times for a few seconds each time until the solution became smooth and pink. Another 15 mL of Buffer A was used to collect all the tissue. The homogenate was filtered through a few layers of cheese cloth to remove any non-homogenized tissue, followed by dounce-homogenizing with 5 strokes up and down. Homogenate was transferred to 85 mL Nalgene tubes and centrifuged for 10 minutes at 10000*g*. The supernatant was decanted (and the pellet was discarded) into a new beaker, and the sample was again centrifuged for 10 minutes at 10000*g* in new 85 mL tubes. The sample was carefully decanted from the same edge of the tube as the pellet, being careful not to contaminate it with parts of the pellet which contain other organelles. A total of four sucrose cushions were set up with 15.5 mL supernatant each, and 8 mL Buffer B (50 mM HEPES pH 7.4, 50 mM KOAc, 6 mM $Mg(OAc)_2$, 1 mM EDTA, 1 M sucrose) was underlaid using a syringe. The sample was centrifuged in a Ti70 rotor for 1 h at 60,000 rpm at 4 °C. Following centrifugation, the supernatant was removed by aspirating from top to bottom to avoid contamination of the pellet with the supernatant. Each of the four pellets were gently resuspended with 2 mL Buffer C (50 mM HEPES pH 7.4, 250 mM sucrose, 0.5 mM $Mg(OAc)_2$), avoiding air bubbles. The resuspended pellet was transferred to a fresh cell douncer and the pellet was further homogenized with 5 gentle and slow passes with the pestle by hand. Total yield was approximately 9 mL of canine microsomes, which were aliquoted into 50 µL fractions, flash frozen in liquid nitrogen, and stored at −80 °C. To measure the absorbance of the final sample, the canine microsomes were diluted 1:20 in 1% SDS. Final absorbance values were A260 = 124.48 and A280 = 64.18.

5.3.4 Immunoblotting Whole Cell Lysate Samples

The day before harvesting, 400,000 cells are seeded onto a 6-well plate. The following day, the media is aspirated, and the cells are harvested with 1 mL of cold PBS. The cells are pelleted at 500*g* for 5 minutes at 4 °C and the supernatant is discarded. The cells are lysed with 100 µL RIPA buffer (50 mM Tris pH 7.4, 150 mM NaCl, 1% NP-40, 0.5% sodium deoxycholate, 0.1% SDS, 1 mM PMSF, 0.25X Roche cOmplete Protease Inhibitor Cocktail) and incubated on ice for 15 minutes, vortexing the sample every few minutes. The sample is then pelleted at 20,000*g* for 15 minutes and the supernatant is harvested.

If the samples are not normalized by cell-counting, they can be normalized by A260. Importantly, this normalization method is only accurate when a small amount (for example, 0.25X) protease inhibitor cocktail is added. Once normalized, 1 µL of the whole cell lysate sample can be run per lane on the gel. It is also recommended to obtain a stain free image prior to western blot transferring.

REFERENCES

Almagro Armenteros, J. J., Tsirigos, K. D., Sønderby, C. K., Petersen, T. N., Winther, O., Brunak, S., Von Heijne, G., & Nielsen, H. (2019). SignalP 5.0 improves signal peptide predictions using deep neural networks. *Nature Biotechnology*, *37*(4), 420–423. https://doi.org/10.1038/s41587-019-0036-z

Anghel, S. A., McGilvray, P. T., Hegde, R. S., & Keenan, R. J. (2017). Identification of Oxa1 Homologs Operating in the Eukaryotic Endoplasmic Reticulum. *Cell Reports*, *21*(13), 3708–3716. https://doi.org/10.1016/j.celrep.2017.12.006

Arthur, L. L., Pavlovic-Djuranovic, S., Koutmou, K. S., Green, R., Szczesny, P., & Djuranovic, S. (2015). Translational control by lysine-encoding A-rich sequences. *Science Advances*, *1*(6), e1500154. https://doi.org/10.1126/sciadv.1500154

Attwood, M. M., Krishnan, A., Almén, M. S., & Schiöth, H. B. (2017). Highly diversified expansions shaped the evolution of membrane bound proteins in metazoans. *Scientific Reports*, *7*(1), 12387. https://doi.org/10.1038/s41598-017-11543-z

Bai, L., You, Q., Feng, X., Kovach, A., & Li, H. (2020). Structure of the ER membrane complex, a transmembrane-domain insertase. *Nature*, *584*(7821), 475–478. https://doi.org/10.1038/s41586-020-2389-3

Bernstein, H. D. (1998). Cotranslational Translocation of Proteins into Canine Rough Microsomes. *Current Protocols in Cell Biology*, *00*(1). https://doi.org/10.1002/0471143030.cb1104s00

Blobel, G. (1980). Intracellular protein topogenesis. *Proceedings of the National Academy of Sciences*, *77*(3), 1496–1500. https://doi.org/10.1073/pnas.77.3.1496

Borowska, M. T., Dominik, P. K., Anghel, S. A., Kossiakoff, A. A., & Keenan, R. J. (2015). A YidC-like Protein in the Archaeal Plasma Membrane. *Structure*, *23*(9), 1715–1724. https://doi.org/10.1016/j.str.2015.06.025

Braunger, K., Pfeffer, S., Shrimal, S., Gilmore, R., Berninghausen, O., Mandon, E. C., Becker, T., Förster, F., & Beckmann, R. (2018). Structural basis for coupling protein transport and N-glycosylation at the mammalian endoplasmic reticulum. *Science*, *360*(6385), 215–219. https://doi.org/10.1126/science.aar7899

Brodsky, J. L., Goeckeler, J., & Schekman, R. (1995). BiP and Sec63p are required for both co- and posttranslational protein translocation into the yeast endoplasmic reticulum. *Proceedings of the National Academy of Sciences*, *92*(21), 9643–9646. https://doi.org/10.1073/pnas.92.21.9643

Canul-Tec, J. C., Assal, R., Cirri, E., Legrand, P., Brier, S., Chamot-Rooke, J., & Reyes, N. (2017). Structure and allosteric inhibition of excitatory amino acid transporter 1. *Nature*, *544*(7651), 446–451. https://doi.org/10.1038/nature22064

Chacinska, A., Koehler, C. M., Milenkovic, D., Lithgow, T., & Pfanner, N. (2009). Importing Mitochondrial Proteins: Machineries and Mechanisms. *Cell*, *138*(4), 628–644. https://doi.org/10.1016/j.cell.2009.08.005

Chavent, M., Karia, D., Kalli, A. C., Domański, J., Duncan, A. L., Hedger, G., Stansfeld, P. J., Seiradake, E., Jones, E. Y., & Sansom, M. S. P. (2018). Interactions of the EphA2 Kinase Domain with PIPs in Membranes: Implications for Receptor Function. *Structure*, *26*(7), 1025-1034.e2. https://doi.org/10.1016/j.str.2018.05.003

Cherepanova, N. A., & Gilmore, R. (2016). Mammalian cells lacking either the cotranslational or posttranslocational oligosaccharyltransferase complex display substrate-dependent defects in asparagine linked glycosylation. *Scientific Reports*, *6*(1), 20946. https://doi.org/10.1038/srep20946

Cherepanova, N. A., Venev, S. V., Leszyk, J. D., Shaffer, S. A., & Gilmore, R. (2019). Quantitative glycoproteomics reveals new classes of STT3A- and STT3B-dependent N-glycosylation sites. *Journal of Cell Biology*, *218*(8), 2782–2796. https://doi.org/10.1083/jcb.201904004

Chevet, E., Wong, H. N., Gerber, D., Cochet, C., Fazel, A., Cameron, P. H., Gushue, J. N., Thomas, D. Y., & Bergeron, J. J. M. (1999). Phosphorylation by CK2 and MAPK enhances calnexin association with ribosomes. *The EMBO Journal*, *18*(13), 3655–3666. https://doi.org/10.1093/emboj/18.13.3655

Chiti, F., & Dobson, C. M. (2006). Protein Misfolding, Functional Amyloid, and Human Disease. *Annual Review of Biochemistry*, *75*(1), 333–366. https://doi.org/10.1146/annurev.biochem.75.101304.123901

Chitwood, P. J., & Hegde, R. S. (2019). The Role of EMC during Membrane Protein Biogenesis. *Trends in Cell Biology*, *29*(5), 371–384. https://doi.org/10.1016/j.tcb.2019.01.007

Chitwood, P. J., & Hegde, R. S. (2020). An intramembrane chaperone complex facilitates membrane protein biogenesis. *Nature*, *584*(7822), 630–634. https://doi.org/10.1038/s41586-020-2624-y

Chitwood, P. J., Juszkiewicz, S., Guna, A., Shao, S., & Hegde, R. S. (2018). EMC Is Required to Initiate Accurate Membrane Protein Topogenesis. *Cell*, *175*(6), 1507-1519.e16. https://doi.org/10.1016/j.cell.2018.10.009

Choy, B. C., Cater, R. J., Mancia, F., & Pryor, E. E. (2021). A 10-year meta-analysis of membrane protein structural biology: Detergents, membrane mimetics, and structure determination techniques. *Biochimica et Biophysica Acta (BBA) - Biomembranes*, *1863*(3), 183533. https://doi.org/10.1016/j.bbamem.2020.183533

Christodoulou, A., Maimaris, G., Makrigiorgi, A., Charidemou, E., Lüchtenborg, C., Ververis, A., Georgiou, R., Lederer, C. W., Haffner, C., Brügger, B., & Santama, N. (2020). TMEM147 interacts with Lamin B Receptor, regulates its localization and levels, and affects cholesterol homeostasis. *Journal of Cell Science*, jcs.245357. https://doi.org/10.1242/jcs.245357

Conti, B. J., Devaraneni, P. K., Yang, Z., David, L. L., & Skach, W. R. (2015). Cotranslational Stabilization of Sec62/63 within the ER Sec61 Translocon Is Controlled by Distinct Substrate-Driven Translocation Events. *Molecular Cell*, *58*(2), 269–283. https://doi.org/10.1016/j.molcel.2015.02.018

Costello, J. L., Castro, I. G., Camões, F., Schrader, T. A., McNeall, D., Yang, J., Giannopoulou, E.-A., Gomes, S., Pogenberg, V., Bonekamp, N. A., Ribeiro, D., Wilmanns, M., Jedd, G., Islinger, M., & Schrader, M. (2017). Predicting the targeting of tail-anchored proteins to subcellular compartments in mammalian cells. *Journal of Cell Science*, jcs.200204. https://doi.org/10.1242/jcs.200204

Cui, X. A., Zhang, H., & Palazzo, A. F. (2012). P180 Promotes the Ribosome-Independent Localization of a Subset of mRNA to the Endoplasmic Reticulum. *PLoS Biology*, *10*(5), e1001336. https://doi.org/10.1371/journal.pbio.1001336

Dalbey, R. E., Kuhn, A., Zhu, L., & Kiefer, D. (2014). The membrane insertase YidC. *Biochimica et Biophysica Acta (BBA) - Molecular Cell Research*, *1843*(8), 1489–1496. https://doi.org/10.1016/j.bbamcr.2013.12.022

Deshaies, R. J., Sanders, S. L., Feldheim, D. A., & Schekman, R. (1991). Assembly of yeast Sec proteins involved in translocation into the endoplasmic reticulum into a membrane-bound multisubunit complex. *Nature*, *349*(6312), 806–808. https://doi.org/10.1038/349806a0

Dettmer, U., Kuhn, P.-H., Abou-Ajram, C., Lichtenthaler, S. F., Krüger, M., Kremmer, E., Haass, C., & Haffner, C. (2010). Transmembrane Protein 147 (TMEM147) Is a Novel Component of the Nicalin-NOMO Protein Complex. *Journal of Biological Chemistry*, *285*(34), 26174–26181. https://doi.org/10.1074/jbc.M110.132548

Do, H., Falcone, D., Lin, J., Andrews, D. W., & Johnson, A. E. (1996). The Cotranslational Integration of Membrane Proteins into the Phospholipid Bilayer Is a Multistep Process. *Cell*, *85*(3), 369–378. https://doi.org/10.1016/S0092-8674(00)81115-0

Doma, M. K., & Parker, R. (2006). Endonucleolytic cleavage of eukaryotic mRNAs with stalls in translation elongation. *Nature*, *440*(7083), 561–564. https://doi.org/10.1038/nature04530

Dudek, J., Greiner, M., Müller, A., Hendershot, L. M., Kopsch, K., Nastainczyk, W., & Zimmermann, R. (2005). ERj1p has a basic role in protein biogenesis at the

endoplasmic reticulum. *Nature Structural & Molecular Biology*, *12*(11), 1008–1014. https://doi.org/10.1038/nsmb1007

Evans, E. A., Gilmore, R., & Blobel, G. (1986). Purification of microsomal signal peptidase as a complex. *Proceedings of the National Academy of Sciences*, *83*(3), 581–585. https://doi.org/10.1073/pnas.83.3.581

Fagerberg, L., Jonasson, K., Von Heijne, G., Uhlén, M., & Berglund, L. (2010). Prediction of the human membrane proteome. *PROTEOMICS*, *10*(6), 1141–1149. https://doi.org/10.1002/pmic.200900258

Ferguson, M. A. J. (1991). Lipid anchors on membrane proteins. *Current Opinion in Structural Biology*, *1*(4), 522–529. https://doi.org/10.1016/S0959-440X(05)80072-7

Fons, R. D., Bogert, B. A., & Hegde, R. S. (2003). Substrate-specific function of the translocon-associated protein complex during translocation across the ER membrane. *The Journal of Cell Biology*, *160*(4), 529–539. https://doi.org/10.1083/jcb.200210095

Fredriksson, R., & Schiöth, H. B. (2005). The Repertoire of G-Protein–Coupled Receptors in Fully Sequenced Genomes. *Molecular Pharmacology*, *67*(5), 1414–1425. https://doi.org/10.1124/mol.104.009001

Frenkel, N., Makky, A., Sudji, I. R., Wink, M., & Tanaka, M. (2014). Mechanistic Investigation of Interactions between Steroidal Saponin Digitonin and Cell Membrane Models. *The Journal of Physical Chemistry B*, *118*(50), 14632–14639. https://doi.org/10.1021/jp5074939

Gemmer, M., & Förster, F. (2020). A clearer picture of the ER translocon complex. *Journal of Cell Science*, *133*(3), jcs231340. https://doi.org/10.1242/jcs.231340

Görlich, D., Hartmann, E., Prehn, S., & Rapoport, T. A. (1992). A protein of the endoplasmic reticulum involved early in polypeptide translocation. *Nature*, *357*(6373), 47–52. https://doi.org/10.1038/357047a0

Görlich, D., & Rapoport, T. A. (1993). Protein translocation into proteoliposomes reconstituted from purified components of the endoplasmic reticulum membrane. *Cell*, *75*(4), 615–630. https://doi.org/10.1016/0092-8674(93)90483-7

Gouaux, E. (1997). Channel-forming toxins: Tales of transformation. *Current Opinion in Structural Biology*, *7*(4), 566–573. https://doi.org/10.1016/S0959-440X(97)80123-6

Guna, A., Volkmar, N., Christianson, J. C., & Hegde, R. S. (2018). The ER membrane protein complex is a transmembrane domain insertase. *Science*, *359*(6374), 470–473. https://doi.org/10.1126/science.aao3099

Guo, H., Bueler, S. A., & Rubinstein, J. L. (2017). Atomic model for the dimeric F $_{O}$ region of mitochondrial ATP synthase. *Science*, *358*(6365), 936–940. https://doi.org/10.1126/science.aao4815

Halic, M., Becker, T., Pool, M. R., Spahn, C. M. T., Grassucci, R. A., Frank, J., & Beckmann, R. (2004). Structure of the signal recognition particle interacting with the elongation-arrested ribosome. *Nature*, *427*(6977), 808–814. https://doi.org/10.1038/nature02342

Hanover, J. A., & Lennarz, W. J. (1980). N-Linked glycoprotein assembly. Evidence that oligosaccharide attachment occurs within the lumen of the endoplasmic

reticulum. *Journal of Biological Chemistry*, *255*(8), 3600–3604. https://doi.org/10.1016/S0021-9258(19)85745-9

Hartmann, E., Gorlich, D., Kostka, S., Otto, A., Kraft, R., Knespel, S., Burger, E., Rapoport, T. A., & Prehn, S. (1993). A tetrameric complex of membrane proteins in the endoplasmic reticulum. *European Journal of Biochemistry*, *214*(2), 375–381. https://doi.org/10.1111/j.1432-1033.1993.tb17933.x

Hegde, R. S., & Keenan, R. J. (2022). The mechanisms of integral membrane protein biogenesis. *Nature Reviews Molecular Cell Biology*, *23*(2), 107–124. https://doi.org/10.1038/s41580-021-00413-2

Hegde, R. S., & Lingappa, V. R. (1997). Membrane Protein Biogenesis: Regulated Complexity at the Endoplasmic Reticulum. *Cell*, *91*(5), 575–582. https://doi.org/10.1016/S0092-8674(00)80445-6

Heijne, G., & Gavel, Y. (1988). Topogenic signals in integral membrane proteins. *European Journal of Biochemistry*, *174*(4), 671–678. https://doi.org/10.1111/j.1432-1033.1988.tb14150.x

Heinrich, S. U., Mothes, W., Brunner, J., & Rapoport, T. A. (2000). The Sec61p Complex Mediates the Integration of a Membrane Protein by Allowing Lipid Partitioning of the Transmembrane Domain. *Cell*, *102*(2), 233–244. https://doi.org/10.1016/S0092-8674(00)00028-3

Helenius, A., & Aebi, M. (2004). Roles of N-Linked Glycans in the Endoplasmic Reticulum. *Annual Review of Biochemistry*, *73*(1), 1019–1049. https://doi.org/10.1146/annurev.biochem.73.011303.073752

Hell, K., Neupert, W., & Stuart, R. A. (2001). Oxa1p acts as a general membrane insertion machinery for proteins encoded by mitochondrial DNA. *The EMBO Journal*, *20*(6), 1281–1288. https://doi.org/10.1093/emboj/20.6.1281

Hessa, T., Meindl-Beinker, N. M., Bernsel, A., Kim, H., Sato, Y., Lerch-Bader, M., Nilsson, I., White, S. H., & Von Heijne, G. (2007). Molecular code for transmembrane-helix recognition by the Sec61 translocon. *Nature*, *450*(7172), 1026–1030. https://doi.org/10.1038/nature06387

Hessa, T., White, S. H., & Von Heijne, G. (2005). Membrane Insertion of a Potassium-Channel Voltage Sensor. *Science*, *307*(5714), 1427–1427. https://doi.org/10.1126/science.1109176

Hori, O., Miyazaki, M., Tamatani, T., Ozawa, K., Takano, K., Okabe, M., Ikawa, M., Hartmann, E., Mai, P., Stern, D. M., Kitao, Y., & Ogawa, S. (2006). Deletion of SERP1/RAMP4, a Component of the Endoplasmic Reticulum (ER) Translocation Sites, Leads to ER Stress. *Molecular and Cellular Biology*, *26*(11), 4257–4267. https://doi.org/10.1128/MCB.02055-05

Horie, C., Suzuki, H., Sakaguchi, M., & Mihara, K. (2002). Characterization of Signal That Directs C-Tail–anchored Proteins to Mammalian Mitochondrial Outer Membrane. *Molecular Biology of the Cell*, *13*(5), 1615–1625. https://doi.org/10.1091/mbc.01-12-0570

Hwang Fu, Y.-H., Huang, W. Y. C., Shen, K., Groves, J. T., Miller, T., & Shan, S. (2017). Two-step membrane binding by the bacterial SRP receptor enable efficient and accurate Co-translational protein targeting. *eLife*, *6*, e25885. https://doi.org/10.7554/eLife.25885

Itskanov, S., Kuo, K. M., Gumbart, J. C., & Park, E. (2021). Stepwise gating of the Sec61 protein-conducting channel by Sec63 and Sec62. *Nature Structural & Molecular Biology*, *28*(2), 162–172. https://doi.org/10.1038/s41594-020-00541-x

Itskanov, S., & Park, E. (2019). Structure of the posttranslational Sec protein-translocation channel complex from yeast. *Science*, *363*(6422), 84–87. https://doi.org/10.1126/science.aav6740

Itskanov, S., Wang, L., Junne, T., Sherriff, R., Xiao, L., Blanchard, N., Shi, W. Q., Forsyth, C., Hoepfner, D., Spiess, M., & Park, E. (2023). A common mechanism of Sec61 translocon inhibition by small molecules. *Nature Chemical Biology*, *19*(9), 1063–1071. https://doi.org/10.1038/s41589-023-01337-y

Jaskolowski, M., Jomaa, A., Gamerdinger, M., Shrestha, S., Leibundgut, M., Deuerling, E., & Ban, N. (2023). Molecular basis of the TRAP complex function in ER protein biogenesis. *Nature Structural & Molecular Biology*, *30*(6), 770–777. https://doi.org/10.1038/s41594-023-00990-0

Jayaprakash, N. G., & Surolia, A. (2017). Role of glycosylation in nucleating protein folding and stability. *Biochemical Journal*, *474*(14), 2333–2347. https://doi.org/10.1042/BCJ20170111

Jiang, X.-C., & Li, Z. (2022). Sphingolipids and Cholesterol. In X.-C. Jiang (Ed.), *Sphingolipid Metabolism and Metabolic Disease* (Vol. 1372, pp. 1–14). Springer Nature Singapore. https://doi.org/10.1007/978-981-19-0394-6_1

Jonikas, M. C., Collins, S. R., Denic, V., Oh, E., Quan, E. M., Schmid, V., Weibezahn, J., Schwappach, B., Walter, P., Weissman, J. S., & Schuldiner, M. (2009). Comprehensive Characterization of Genes Required for Protein Folding in the

Endoplasmic Reticulum. *Science*, *323*(5922), 1693–1697. https://doi.org/10.1126/science.1167983

Keenan, R. J., Freymann, D. M., Walter, P., & Stroud, R. M. (1998). Crystal Structure of the Signal Sequence Binding Subunit of the Signal Recognition Particle. *Cell*, *94*(2), 181–191. https://doi.org/10.1016/S0092-8674(00)81418-X

Kelleher, D. J., Karaoglu, D., Mandon, E. C., & Gilmore, R. (2003). Oligosaccharyltransferase Isoforms that Contain Different Catalytic STT3 Subunits Have Distinct Enzymatic Properties. *Molecular Cell*, *12*(1), 101–111. https://doi.org/10.1016/S1097-2765(03)00243-0

Knorr, A. G., Schmidt, C., Tesina, P., Berninghausen, O., Becker, T., Beatrix, B., & Beckmann, R. (2019). Ribosome–NatA architecture reveals that rRNA expansion segments coordinate N-terminal acetylation. *Nature Structural & Molecular Biology*, *26*(1), 35–39. https://doi.org/10.1038/s41594-018-0165-y

Kopito, R. R. (2000). Aggresomes, inclusion bodies and protein aggregation. *Trends in Cell Biology*, *10*(12), 524–530. https://doi.org/10.1016/S0962-8924(00)01852-3

Kramer, G., Shiber, A., & Bukau, B. (2019). Mechanisms of Cotranslational Maturation of Newly Synthesized Proteins. *Annual Review of Biochemistry*, *88*(1), 337–364. https://doi.org/10.1146/annurev-biochem-013118-111717

Krieg, U. C., Johnson, A. E., & Walter, P. (1989). Protein translocation across the endoplasmic reticulum membrane: Identification by photocross-linking of a 39-kD integral membrane glycoprotein as part of a putative translocation tunnel. *The Journal of Cell Biology*, *109*(5), 2033–2043. https://doi.org/10.1083/jcb.109.5.2033

Krogh, A., Larsson, B., Von Heijne, G., & Sonnhammer, E. L. L. (2001). Predicting transmembrane protein topology with a hidden markov model: Application to complete genomes11Edited by F. Cohen. *Journal of Molecular Biology*, *305*(3), 567–580. https://doi.org/10.1006/jmbi.2000.4315

Kutay, U., Hartmann, E., & Rapoport, T. (1993). A class of membrane proteins with a C-terminal anchor. *Trends in Cell Biology*, *3*(3), 72–75. https://doi.org/10.1016/0962-8924(93)90066-A

Lee, H. S., Qi, Y., & Im, W. (2015). Effects of N-glycosylation on protein conformation and dynamics: Protein Data Bank analysis and molecular dynamics simulation study. *Scientific Reports*, *5*(1), 8926. https://doi.org/10.1038/srep08926

Letzring, D. P., Wolf, A. S., Brule, C. E., & Grayhack, E. J. (2013). Translation of CGA codon repeats in yeast involves quality control components and ribosomal protein L1. *RNA*, *19*(9), 1208–1217. https://doi.org/10.1261/rna.039446.113

Lewis, A. J. O., & Hegde, R. S. (2021). A unified evolutionary origin for the ubiquitous protein transporters SecY and YidC. *BMC Biology*, *19*(1), 266. https://doi.org/10.1186/s12915-021-01171-5

Li, L., Park, E., Ling, J., Ingram, J., Ploegh, H., & Rapoport, T. A. (2016). Crystal structure of a substrate-engaged SecY protein-translocation channel. *Nature*, *531*(7594), 395–399. https://doi.org/10.1038/nature17163

Liaci, A. M., Steigenberger, B., Telles De Souza, P. C., Tamara, S., Gröllers-Mulderij, M., Ogrissek, P., Marrink, S. J., Scheltema, R. A., & Förster, F. (2021). Structure of the human signal peptidase complex reveals the determinants for signal

peptide cleavage. *Molecular Cell*, *81*(19), 3934-3948.e11. https://doi.org/10.1016/j.molcel.2021.07.031

Luirink, J. (2004). SRP-mediated protein targeting: Structure and function revisited. *Biochimica et Biophysica Acta (BBA) - Molecular Cell Research*. https://doi.org/10.1016/j.bbamcr.2004.03.013

Mandon, E. C., Trueman, S. F., & Gilmore, R. (2009). Translocation of proteins through the Sec61 and SecYEG channels. *Current Opinion in Cell Biology*, *21*(4), 501–507. https://doi.org/10.1016/j.ceb.2009.04.010

Mariappan, M., Li, X., Stefanovic, S., Sharma, A., Mateja, A., Keenan, R. J., & Hegde, R. S. (2010). A ribosome-associating factor chaperones tail-anchored membrane proteins. *Nature*, *466*(7310), 1120–1124. https://doi.org/10.1038/nature09296

Mariappan, M., Mateja, A., Dobosz, M., Bove, E., Hegde, R. S., & Keenan, R. J. (2011). The mechanism of membrane-associated steps in tail-anchored protein insertion. *Nature*, *477*(7362), 61–66. https://doi.org/10.1038/nature10362

Matasova, N. B., Myltseva, S. V., Zenkova, M. A., Graifer, D. M., Vladimirov, S. N., & Karpova, G. G. (1991). Isolation of ribosomal subunits containing intact rRNA from human placenta: Estimation of functional activity of 80S ribosomes. *Analytical Biochemistry*, *198*(2), 219–223. https://doi.org/10.1016/0003-2697(91)90416-Q

Mateja, A., Paduch, M., Chang, H.-Y., Szydlowska, A., Kossiakoff, A. A., Hegde, R. S., & Keenan, R. J. (2015). Structure of the Get3 targeting factor in complex with its membrane protein cargo. *Science*, *347*(6226), 1152–1155. https://doi.org/10.1126/science.1261671

McCormick, P. J., Miao, Y., Shao, Y., Lin, J., & Johnson, A. E. (2003). Cotranslational Protein Integration into the ER Membrane Is Mediated by the Binding of Nascent Chains to Translocon Proteins. *Molecular Cell*, *12*(2), 329–341. https://doi.org/10.1016/S1097-2765(03)00304-6

McDowell, M. A., Heimes, M., Fiorentino, F., Mehmood, S., Farkas, Á., Coy-Vergara, J., Wu, D., Bolla, J. R., Schmid, V., Heinze, R., Wild, K., Flemming, D., Pfeffer, S., Schwappach, B., Robinson, C. V., & Sinning, I. (2020). Structural Basis of Tail-Anchored Membrane Protein Biogenesis by the GET Insertase Complex. *Molecular Cell*, *80*(1), 72-86.e7. https://doi.org/10.1016/j.molcel.2020.08.012

McGilvray, P. T., Anghel, S. A., Sundaram, A., Zhong, F., Trnka, M. J., Fuller, J. R., Hu, H., Burlingame, A. L., & Keenan, R. J. (2020). An ER translocon for multi-pass membrane protein biogenesis. *eLife*, *9*, e56889. https://doi.org/10.7554/eLife.56889

Meacock, S. L., Lecomte, F. J. L., Crawshaw, S. G., & High, S. (2002). Different Transmembrane Domains Associate with Distinct Endoplasmic Reticulum Components during Membrane Integration of a Polytopic Protein. *Molecular Biology of the Cell*, *13*(12), 4114–4129. https://doi.org/10.1091/mbc.e02-04-0198

Miller-Vedam, L. E., Bräuning, B., Popova, K. D., Schirle Oakdale, N. T., Bonnar, J. L., Prabu, J. R., Boydston, E. A., Sevillano, N., Shurtleff, M. J., Stroud, R. M., Craik, C. S., Schulman, B. A., Frost, A., & Weissman, J. S. (2020). Structural and mechanistic basis of the EMC-dependent biogenesis of distinct transmembrane clients. *eLife*, *9*, e62611. https://doi.org/10.7554/eLife.62611

Mock, J.-Y., Chartron, J. W., Zaslaver, M., Xu, Y., Ye, Y., & Clemons, W. M. (2015). Bag6 complex contains a minimal tail-anchor–targeting module and a mock BAG domain. *Proceedings of the National Academy of Sciences*, *112*(1), 106–111. https://doi.org/10.1073/pnas.1402745112

Mohorko, E., Glockshuber, R., & Aebi, M. (2011). Oligosaccharyltransferase: The central enzyme of N-linked protein glycosylation. *Journal of Inherited Metabolic Disease*, *34*(4), 869–878. https://doi.org/10.1007/s10545-011-9337-1

Moore, M., Harrison, M. S., Peterson, E. C., & Henry, R. (2000). Chloroplast Oxa1p Homolog Albino3 Is Required for Post-translational Integration of the Light Harvesting Chlorophyll-binding Protein into Thylakoid Membranes. *Journal of Biological Chemistry*, *275*(3), 1529–1532. https://doi.org/10.1074/jbc.275.3.1529

Moraleva, A. A., Deryabin, A. S., Rubtsov, Y. P., Rubtsova, M. P., & Dontsova, O. A. (2022). Eukaryotic Ribosome Biogenesis: The 40S Subunit. *Acta Naturae*, *14*(1), 14–30. https://doi.org/10.32607/actanaturae.11540

Müller, L., De Escauriaza, M. D., Lajoie, P., Theis, M., Jung, M., Müller, A., Burgard, C., Greiner, M., Snapp, E. L., Dudek, J., & Zimmermann, R. (2010). Evolutionary Gain of Function for the ER Membrane Protein Sec62 from Yeast to Humans. *Molecular Biology of the Cell*, *21*(5), 691–703. https://doi.org/10.1091/mbc.e09-08-0730

Murata, K., & Wolf, M. (2018). Cryo-electron microscopy for structural analysis of dynamic biological macromolecules. *Biochimica et Biophysica Acta (BBA) - General Subjects*, *1862*(2), 324–334. https://doi.org/10.1016/j.bbagen.2017.07.020

Nagamori, S., Smirnova, I. N., & Kaback, H. R. (2004). Role of YidC in folding of polytopic membrane proteins. *The Journal of Cell Biology*, *165*(1), 53–62. https://doi.org/10.1083/jcb.200402067

Nicolson, G. L. (2014). The Fluid—Mosaic Model of Membrane Structure: Still relevant to understanding the structure, function and dynamics of biological membranes after more than 40years. *Biochimica et Biophysica Acta (BBA) - Biomembranes*, *1838*(6), 1451–1466. https://doi.org/10.1016/j.bbamem.2013.10.019

Nishiyama, K., Mizushima, S., & Tokuda, H. (1993). A novel membrane protein involved in protein translocation across the cytoplasmic membrane of Escherichia coli. *The EMBO Journal*, *12*(9), 3409–3415. https://doi.org/10.1002/j.1460-2075.1993.tb06015.x

O'Donnell, J. P., Phillips, B. P., Yagita, Y., Juszkiewicz, S., Wagner, A., Malinverni, D., Keenan, R. J., Miller, E. A., & Hegde, R. S. (2020). The architecture of EMC reveals a path for membrane protein insertion. *eLife*, *9*, e57887. https://doi.org/10.7554/eLife.57887

O'Keefe, S., Zong, G., Duah, K. B., Andrews, L. E., Shi, W. Q., & High, S. (2021). An alternative pathway for membrane protein biogenesis at the endoplasmic reticulum. *Communications Biology*, *4*(1), 828. https://doi.org/10.1038/s42003-021-02363-z

Osborne, A. R., Rapoport, T. A., & Van Den Berg, B. (2005). PROTEIN TRANSLOCATION BY THE SEC61/SECY CHANNEL. *Annual Review of Cell and Developmental Biology*, *21*(1), 529–550. https://doi.org/10.1146/annurev.cellbio.21.012704.133214

Panzner, S., Dreier, L., Hartmann, E., Kostka, S., & Rapoport, T. A. (1995). Posttranslational protein transport in yeast reconstituted with a purified complex of Sec proteins and Kar2p. *Cell*, *81*(4), 561–570. https://doi.org/10.1016/0092-8674(95)90077-2

Park, E., Ménétret, J.-F., Gumbart, J. C., Ludtke, S. J., Li, W., Whynot, A., Rapoport, T. A., & Akey, C. W. (2014). Structure of the SecY channel during initiation of protein translocation. *Nature*, *506*(7486), 102–106. https://doi.org/10.1038/nature12720

Patterson, M. A., Bandyopadhyay, A., Devaraneni, P. K., Woodward, J., Rooney, L., Yang, Z., & Skach, W. R. (2015). The Ribosome-Sec61 Translocon Complex Forms a Cytosolically Restricted Environment for Early Polytopic Membrane Protein Folding. *Journal of Biological Chemistry*, *290*(48), 28944–28952. https://doi.org/10.1074/jbc.M115.672261

Paulick, M. G., & Bertozzi, C. R. (2008). The Glycosylphosphatidylinositol Anchor: A Complex Membrane-Anchoring Structure for Proteins. *Biochemistry*, *47*(27), 6991–7000. https://doi.org/10.1021/bi8006324

Pfanner, N., & Geissler, A. (2001). Versatility of the mitochondrial protein import machinery. *Nature Reviews Molecular Cell Biology*, *2*(5), 339–349. https://doi.org/10.1038/35073006

Pfeffer, S., Burbaum, L., Unverdorben, P., Pech, M., Chen, Y., Zimmermann, R., Beckmann, R., & Förster, F. (2015). Structure of the native Sec61 protein-conducting channel. *Nature Communications*, *6*(1), 8403. https://doi.org/10.1038/ncomms9403

Pfeffer, S., Dudek, J., Gogala, M., Schorr, S., Linxweiler, J., Lang, S., Becker, T., Beckmann, R., Zimmermann, R., & Förster, F. (2014). Structure of the mammalian oligosaccharyl-transferase complex in the native ER protein translocon. *Nature Communications*, *5*(1), 3072. https://doi.org/10.1038/ncomms4072

Pleiner, T., Hazu, M., Pinton Tomaleri, G., Nguyen, V. N., Januszyk, K., & Voorhees, R. M. (2023). A selectivity filter in the ER membrane protein complex limits protein misinsertion at the ER. *Journal of Cell Biology*, *222*(8), e202212007. https://doi.org/10.1083/jcb.202212007

Pleiner, T., Tomaleri, G. P., Januszyk, K., Inglis, A. J., Hazu, M., & Voorhees, R. M. (2020). Structural basis for membrane insertion by the human ER membrane protein complex. *Science*, *369*(6502), 433–436. https://doi.org/10.1126/science.abb5008

Pohlschröder, M., Prinz, W. A., Hartmann, E., & Beckwith, J. (1997). Protein Translocation in the Three Domains of Life: Variations on a Theme. *Cell*, *91*(5), 563–566. https://doi.org/10.1016/S0092-8674(00)80443-2

Pool, M. R. (2009). A trans-membrane segment inside the ribosome exit tunnel triggers RAMP4 recruitment to the Sec61p translocase. *Journal of Cell Biology*, *185*(5), 889–902. https://doi.org/10.1083/jcb.200807066

Pross, E., Soussoula, L., Seitl, I., Lupo, D., & Kuhn, A. (2016). Membrane Targeting and Insertion of the C-Tail Protein SciP. *Journal of Molecular Biology*, *428*(20), 4218–4227. https://doi.org/10.1016/j.jmb.2016.09.001

Ramesh, M., & Woolford, J. L. (2016). Eukaryote-specific rRNA expansion segments function in ribosome biogenesis. *RNA*, *22*(8), 1153–1162. https://doi.org/10.1261/rna.056705.116

Rao, M., Okreglak, V., Chio, U. S., Cho, H., Walter, P., & Shan, S. (2016). Multiple selection filters ensure accurate tail-anchored membrane protein targeting. *eLife*, *5*, e21301. https://doi.org/10.7554/eLife.21301

Rapoport, T. A., Li, L., & Park, E. (2017). Structural and Mechanistic Insights into Protein Translocation. *Annual Review of Cell and Developmental Biology*, *33*(1), 369–390. https://doi.org/10.1146/annurev-cellbio-100616-060439

Rosemond, E., Rossi, M., McMillin, S. M., Scarselli, M., Donaldson, J. G., & Wess, J. (2011). Regulation of M_3 Muscarinic Receptor Expression and Function by Transmembrane Protein 147. *Molecular Pharmacology*, *79*(2), 251–261. https://doi.org/10.1124/mol.110.067363

Ruiz-Canada, C., Kelleher, D. J., & Gilmore, R. (2009). Cotranslational and Posttranslational N-Glycosylation of Polypeptides by Distinct Mammalian OST Isoforms. *Cell*, *136*(2), 272–283. https://doi.org/10.1016/j.cell.2008.11.047

Sabatini, D. D. (2014). Preparation of Crude Rough Microsomes from Dog Pancreas. *Cold Spring Harbor Protocols*, *2014*(8), pdb.prot079988. https://doi.org/10.1101/pdb.prot079988

Sadlish, H., Pitonzo, D., Johnson, A. E., & Skach, W. R. (2005). Sequential triage of transmembrane segments by Sec61α during biogenesis of a native multispanning membrane protein. *Nature Structural & Molecular Biology*, *12*(10), 870–878. https://doi.org/10.1038/nsmb994

Samuelson, J. C., Chen, M., Jiang, F., Möller, I., Wiedmann, M., Kuhn, A., Phillips, G. J., & Dalbey, R. E. (2000). YidC mediates membrane protein insertion in bacteria. *Nature*, *406*(6796), 637–641. https://doi.org/10.1038/35020586

Sanchez-Garcia, R., Gomez-Blanco, J., Cuervo, A., Carazo, J. M., Sorzano, C. O. S., & Vargas, J. (2021). DeepEMhancer: A deep learning solution for cryo-EM volume post-processing. *Communications Biology*, *4*(1), 874. https://doi.org/10.1038/s42003-021-02399-1

Saurí, A., McCormick, P. J., Johnson, A. E., & Mingarro, I. (2007). Sec61α and TRAM are Sequentially Adjacent to a Nascent Viral Membrane Protein during its ER Integration. *Journal of Molecular Biology*, *366*(2), 366–374. https://doi.org/10.1016/j.jmb.2006.11.052

Schlenstedt, G., Gudmundsson, G. H., Boman, H. G., & Zimmermann, R. (1990). A large presecretory protein translocates both cotranslationally, using signal recognition particle and ribosome, and post-translationally, without these ribonucleoparticles, when synthesized in the presence of mammalian microsomes. *Journal of Biological Chemistry*, *265*(23), 13960–13968. https://doi.org/10.1016/S0021-9258(18)77442-5

Schroder, K. (1999). Control of glycosylation of MHC class II-associated invariant chain by translocon-associated RAMP4. *The EMBO Journal*, *18*(17), 4804–4815. https://doi.org/10.1093/emboj/18.17.4804

Schuldiner, M., Metz, J., Schmid, V., Denic, V., Rakwalska, M., Schmitt, H. D., Schwappach, B., & Weissman, J. S. (2008). The GET Complex Mediates

Insertion of Tail-Anchored Proteins into the ER Membrane. *Cell*, *134*(4), 634–645. https://doi.org/10.1016/j.cell.2008.06.025

Schulz, G. (1996). Porins: General to specific, native to engineered passive pores. *Current Opinion in Structural Biology*, *6*(4), 485–490. https://doi.org/10.1016/S0959-440X(96)80113-8

Serdiuk, T., Steudle, A., Mari, S. A., Manioglu, S., Kaback, H. R., Kuhn, A., & Müller, D. J. (2019). Insertion and folding pathways of single membrane proteins guided by translocases and insertases. *Science Advances*, *5*(1), eaau6824. https://doi.org/10.1126/sciadv.aau6824

Shakoori, A., Fujii, G., Yoshimura, S., Kitamura, M., Nakayama, K., Ito, T., Ohno, H., & Nakamura, N. (2003). Identification of a five-pass transmembrane protein family localizing in the Golgi apparatus and the ER. *Biochemical and Biophysical Research Communications*, *312*(3), 850–857. https://doi.org/10.1016/j.bbrc.2003.10.197

Shao, S., & Hegde, R. S. (2011). Membrane Protein Insertion at the Endoplasmic Reticulum. *Annual Review of Cell and Developmental Biology*, *27*(1), 25–56. https://doi.org/10.1146/annurev-cellbio-092910-154125

Shao, S., & Hegde, R. S. (2014). Reconstitution of a Minimal Ribosome-Associated Ubiquitination Pathway with Purified Factors. *Molecular Cell*, *55*(6), 880–890. https://doi.org/10.1016/j.molcel.2014.07.006

Shao, S., Rodrigo-Brenni, M. C., Kivlen, M. H., & Hegde, R. S. (2017). Mechanistic basis for a molecular triage reaction. *Science*, *355*(6322), 298–302. https://doi.org/10.1126/science.aah6130

Shao, S., von der Malsburg, K., & Hegde, R. S. (2013). Listerin-Dependent Nascent Protein Ubiquitination Relies on Ribosome Subunit Dissociation. *Molecular Cell*, *50*(5), 637–648. https://doi.org/10.1016/j.molcel.2013.04.015

Sharma, A., Mariappan, M., Appathurai, S., & Hegde, R. S. (2010). In Vitro Dissection of Protein Translocation into the Mammalian Endoplasmic Reticulum. In A. Economou (Ed.), *Protein Secretion* (Vol. 619, pp. 339–363). Humana Press. https://doi.org/10.1007/978-1-60327-412-8_20

Shrimal, S., Cherepanova, N. A., & Gilmore, R. (2015). Cotranslational and posttranslocational N-glycosylation of proteins in the endoplasmic reticulum. *Seminars in Cell & Developmental Biology*, *41*, 71–78. https://doi.org/10.1016/j.semcdb.2014.11.005

Shrimal, S., Ng, B. G., Losfeld, M.-E., Gilmore, R., & Freeze, H. H. (2013). Mutations in STT3A and STT3B cause two congenital disorders of glycosylation. *Human Molecular Genetics*, *22*(22), 4638–4645. https://doi.org/10.1093/hmg/ddt312

Shurtleff, M. J., Itzhak, D. N., Hussmann, J. A., Schirle Oakdale, N. T., Costa, E. A., Jonikas, M., Weibezahn, J., Popova, K. D., Jan, C. H., Sinitcyn, P., Vembar, S. S., Hernandez, H., Cox, J., Burlingame, A. L., Brodsky, J. L., Frost, A., Borner, G. H., & Weissman, J. S. (2018). The ER membrane protein complex interacts cotranslationally to enable biogenesis of multipass membrane proteins. *eLife*, *7*, e37018. https://doi.org/10.7554/eLife.37018

Singer, S. J., & Nicolson, G. L. (1972). The Fluid Mosaic Model of the Structure of Cell Membranes: Cell membranes are viewed as two-dimensional solutions of

oriented globular proteins and lipids. *Science*, *175*(4023), 720–731. https://doi.org/10.1126/science.175.4023.720

Smalinskaitė, L., Kim, M. K., Lewis, A. J. O., Keenan, R. J., & Hegde, R. S. (2022). Mechanism of an intramembrane chaperone for multipass membrane proteins. *Nature*, *611*(7934), Article 7934. https://doi.org/10.1038/s41586-022-05336-2

Stefer, S., Reitz, S., Wang, F., Wild, K., Pang, Y.-Y., Schwarz, D., Bomke, J., Hein, C., Löhr, F., Bernhard, F., Denic, V., Dötsch, V., & Sinning, I. (2011). Structural Basis for Tail-Anchored Membrane Protein Biogenesis by the Get3-Receptor Complex. *Science*, *333*(6043), 758–762. https://doi.org/10.1126/science.1207125

Sundaram, A.[#], Yamsek, M.[#], Zhong, F.[#], Hooda, Y., Hegde, R. S., & Keenan, R. J. (2022). Substrate-driven assembly of a translocon for multipass membrane proteins. *Nature*, *611*(7934), Article 7934. ([#] = Equal Contribution, Listed Alphabetically) https://doi.org/10.1038/s41586-022-05330-8

Sych, T., Levental, K. R., & Sezgin, E. (2022). Lipid–Protein Interactions in Plasma Membrane Organization and Function. *Annual Review of Biophysics*, *51*(1), 135–156. https://doi.org/10.1146/annurev-biophys-090721-072718

Tai, V. W.-F., & Imperiali, B. (2001). Substrate Specificity of the Glycosyl Donor for Oligosaccharyl Transferase. *The Journal of Organic Chemistry*, *66*(19), 6217–6228. https://doi.org/10.1021/jo0100345

Tamborero, S., Vilar, M., Martínez-Gil, L., Johnson, A. E., & Mingarro, I. (2011). Membrane Insertion and Topology of the Translocating Chain-Associating Membrane Protein (TRAM). *Journal of Molecular Biology*, *406*(4), 571–582. https://doi.org/10.1016/j.jmb.2011.01.009

Tanaka, Y., Sugano, Y., Takemoto, M., Mori, T., Furukawa, A., Kusakizako, T., Kumazaki, K., Kashima, A., Ishitani, R., Sugita, Y., Nureki, O., & Tsukazaki, T. (2015). Crystal Structures of SecYEG in Lipidic Cubic Phase Elucidate a Precise Resting and a Peptide-Bound State. *Cell Reports*, *13*(8), 1561–1568. https://doi.org/10.1016/j.celrep.2015.10.025

Tian, S., Wu, Q., Zhou, B., Choi, M. Y., Ding, B., Yang, W., & Dong, M. (2019). Proteomic Analysis Identifies Membrane Proteins Dependent on the ER Membrane Protein Complex. *Cell Reports*, *28*(10), 2517-2526.e5. https://doi.org/10.1016/j.celrep.2019.08.006

Tsuboi, T., Kuroha, K., Kudo, K., Makino, S., Inoue, E., Kashima, I., & Inada, T. (2012). Dom34:Hbs1 Plays a General Role in Quality-Control Systems by Dissociation of a Stalled Ribosome at the 3′ End of Aberrant mRNA. *Molecular Cell*, *46*(4), 518–529. https://doi.org/10.1016/j.molcel.2012.03.013

Van den Berg, B., Clemons, W. M., Collinson, I., Modis, Y., Hartmann, E., Harrison, S. C., & Rapoport, T. A. (2004). X-ray structure of a protein-conducting channel. *Nature*, *427*(6969), 36–44. https://doi.org/10.1038/nature02218

Velazhahan, V., Ma, N., Pándy-Szekeres, G., Kooistra, A. J., Lee, Y., Gloriam, D. E., Vaidehi, N., & Tate, C. G. (2021). Structure of the class D GPCR Ste2 dimer coupled to two G proteins. *Nature*, *589*(7840), 148–153. https://doi.org/10.1038/s41586-020-2994-1

Voigt, S., Jungnickel, B., Hartmann, E., & Rapoport, T. A. (1996). Signal sequence-dependent function of the TRAM protein during early phases of protein transport

across the endoplasmic reticulum membrane. *The Journal of Cell Biology*, *134*(1), 25–35. https://doi.org/10.1083/jcb.134.1.25

Volkmar, N., & Christianson, J. C. (2020). Squaring the EMC – how promoting membrane protein biogenesis impacts cellular functions and organismal homeostasis. *Journal of Cell Science*, *133*(8), jcs243519. https://doi.org/10.1242/jcs.243519

Von Heijne, G. (1985). Signal sequences. The limits of Variation. *Journal of Molecular Biology*, *184*(1), 99–105. https://doi.org/10.1016/0022-2836(85)90046-4

Von Heijne, G. (2007). The membrane protein universe: What's out there and why bother? *Journal of Internal Medicine*, *261*(6), 543–557. https://doi.org/10.1111/j.1365-2796.2007.01792.x

Voorhees, R. M., Fernández, I. S., Scheres, S. H. W., & Hegde, R. S. (2014). Structure of the Mammalian Ribosome-Sec61 Complex to 3.4 Å Resolution. *Cell*, *157*(7), 1632–1643. https://doi.org/10.1016/j.cell.2014.05.024

Voorhees, R. M., & Hegde, R. S. (2015). Structures of the scanning and engaged states of the mammalian SRP-ribosome complex. *eLife*, *4*, e07975. https://doi.org/10.7554/eLife.07975

Voorhees, R. M., & Hegde, R. S. (2016). Structure of the Sec61 channel opened by a signal sequence. *Science*, *351*(6268), 88–91. https://doi.org/10.1126/science.aad4992

Voss, N. R., Gerstein, M., Steitz, T. A., & Moore, P. B. (2006). The Geometry of the Ribosomal Polypeptide Exit Tunnel. *Journal of Molecular Biology*, *360*(4), 893–906. https://doi.org/10.1016/j.jmb.2006.05.023

Wallin, E., & Heijne, G. V. (1998). Genome-wide analysis of integral membrane proteins from eubacterial, archaean, and eukaryotic organisms: Membrane protein topology. *Protein Science*, *7*(4), 1029–1038. https://doi.org/10.1002/pro.5560070420

Wang, F., Brown, E. C., Mak, G., Zhuang, J., & Denic, V. (2010). A Chaperone Cascade Sorts Proteins for Posttranslational Membrane Insertion into the Endoplasmic Reticulum. *Molecular Cell*, *40*(1), 159–171. https://doi.org/10.1016/j.molcel.2010.08.038

Wang, F., Chan, C., Weir, N. R., & Denic, V. (2014). The Get1/2 transmembrane complex is an endoplasmic-reticulum membrane protein insertase. *Nature*, *512*(7515), 441–444. https://doi.org/10.1038/nature13471

Wang, L., & Dobberstein, B. (1999). Oligomeric complexes involved in translocation of proteins across the membrane of the endoplasmic reticulum. *FEBS Letters*, *457*(3), 316–322. https://doi.org/10.1016/S0014-5793(99)01075-3

Wang, P., & Dalbey, R. E. (2011). Inserting membrane proteins: The YidC/Oxa1/Alb3 machinery in bacteria, mitochondria, and chloroplasts. *Biochimica et Biophysica Acta (BBA) - Biomembranes*, *1808*(3), 866–875. https://doi.org/10.1016/j.bbamem.2010.08.014

Welply, J. K., Shenbagamurthi, P., Lennarz, W. J., & Naider, F. (1983). Substrate recognition by oligosaccharyltransferase. Studies on glycosylation of modified Asn-X-Thr/Ser tripeptides. *Journal of Biological Chemistry*, *258*(19), 11856–11863. https://doi.org/10.1016/S0021-9258(17)44311-0

White, S., & Vonheijne, G. (2005). Transmembrane helices before, during, and after insertion. *Current Opinion in Structural Biology*, *15*(4), 378–386. https://doi.org/10.1016/j.sbi.2005.07.004

Wideman, J. G. (2015). The ubiquitous and ancient ER membrane protein complex (EMC): Tether or not? *F1000Research*, *4*, 624. https://doi.org/10.12688/f1000research.6944.2

Wu, X., Cabanos, C., & Rapoport, T. A. (2019). Structure of the post-translational protein translocation machinery of the ER membrane. *Nature*, *566*(7742), 136–139. https://doi.org/10.1038/s41586-018-0856-x

Wu, X., & Rapoport, T. A. (2021). Translocation of Proteins through a Distorted Lipid Bilayer. *Trends in Cell Biology*, *31*(6), 473–484. https://doi.org/10.1016/j.tcb.2021.01.002

Xin, B., Puffenberger, E. G., Turben, S., Tan, H., Zhou, A., & Wang, H. (2010). Homozygous frameshift mutation in *TMCO1* causes a syndrome with craniofacial dysmorphism, skeletal anomalies, and mental retardation. *Proceedings of the National Academy of Sciences*, *107*(1), 258–263. https://doi.org/10.1073/pnas.0908457107

Yamaguchi, A., Hori, O., Stern, D. M., Hartmann, E., Ogawa, S., & Tohyama, M. (1999). Stress-Associated Endoplasmic Reticulum Protein 1 (Serp1)/Ribosome-Associated Membrane Protein 4 (Ramp4) Stabilizes Membrane Proteins during Stress and Facilitates Subsequent Glycosylation. *The Journal of Cell Biology*, *147*(6), 1195–1204. https://doi.org/10.1083/jcb.147.6.1195

Yen, H.-Y., Hoi, K. K., Liko, I., Hedger, G., Horrell, M. R., Song, W., Wu, D., Heine, P., Warne, T., Lee, Y., Carpenter, B., Plückthun, A., Tate, C. G., Sansom, M. S. P., & Robinson, C. V. (2018). PtdIns(4,5)P2 stabilizes active states of GPCRs and enhances selectivity of G-protein coupling. *Nature*, *559*(7714), 423–427. https://doi.org/10.1038/s41586-018-0325-6

Zafar, S., Nasir, A., & Bokhari, H. B. (2011). Computational analysis reveals abundance of potential glycoproteins in Archaea, Bacteria and Eukarya. *Bioinformation*, *6*(9), 352–355. https://doi.org/10.6026/97320630006352

Zalisko, B. E., Chan, C., Denic, V., Rock, R. S., & Keenan, R. J. (2017). Tail-Anchored Protein Insertion by a Single Get1/2 Heterodimer. *Cell Reports*, *20*(10), 2287–2293. https://doi.org/10.1016/j.celrep.2017.08.035

Zhu, L., Kaback, H. R., & Dalbey, R. E. (2013). YidC Protein, a Molecular Chaperone for LacY Protein Folding via the SecYEG Protein Machinery. *Journal of Biological Chemistry*, *288*(39), 28180–28194. https://doi.org/10.1074/jbc.M113.491613